High-Resolution Spectroscopy of Cluster Ions

Evan J. Bieske*,†

School of Chemistry, The University of Melbourne, Parkville 3052, Australia

Otto Dopfer*,‡

Physical Chemistry, University of Basel, Klingelbergstrasse 80, CH-4056 Basel, Switzerland

Received January 10, 2000

Contents

I. Introduction

Over the past 15 years the high-resolution spectroscopic study of ionic complexes has grown into an active field with relevance to significant physical, chemical, and biological phenomena. Progress has involved the application of traditional experimental techniques, akin to those used for neutral van der Waals and radical molecule spectroscopy,[1−19] along with development of specialized approaches that are particularly suitable for the study of weakly bound charged species. High-resolution studies have encompassed intermediates in fundamental ion−neutral reactions, elementary solvation complexes, and charged complexes that exist in the terrestrial atmosphere. Although the focus has largely been on cation systems, during the past few years high-resolution spectra have also been obtained for several anion complexes. The advances over the past 15 years are apparent when it is realized that in 1986, when an article by Castleman and Keesee on ionic clusters appeared in *Chemical Reviews*,[20] no rotationally resolved spectrum had been published. The situation changed soon thereafter, with publication of the microwave (MW) spectrum of H_3^+−Ar[21] and the infrared (IR) spectrum of FHF^-.[22] Since then rotationally resolved spectra have been obtained for more than 50 different cation and anion complexes (Table 1). A goal of much of the work has been to complement the vast wealth of information on neutral van der Waals molecules accrued over the last 25 years with comparable data on ionic complexes. High-resolution electronic, mid-IR, and MW spectra provide direct information on structures, binding energies, and inter- and intramolecular vibrations and thus promise a more intimate understanding of the manner in which charged and neutral species interact at close range.

The focus of this review is on ionic complexes (larger than diatomics) for which rotationally resolved spectra have been obtained, and for the most part we refrain from considering species for which spectra have been recorded with only vibrational resolution. Nor do we discuss complexes involving metal ions. By limiting the article's range in this fashion, we do not intend to discount the importance of the many spectroscopic studies conducted at the vibrational level of resolution or of ones on metal-containing systems. The reasons for imposing the limitation are rather ones of manageability, along with a recognition that much of the excluded work has been covered by other excellent reviews. For example, the spectroscopy of metal cation−ligand systems has recently been reviewed.[23−30] Other general reviews of cluster ion spectroscopy that include descriptions of lower resolution studies can be found in refs 29−42. There are also several excellent

† Phone: ++61 3 8344 7082. Fax: ++61 3 9347 5180. E-mail: e.bieske@chemistry.unimelb.edu.au.
‡ Phone: ++41 61 267 3823. Fax: ++41 61 267 3855. E-mail: otto.dopfer@unibas.ch.

10.1021/cr990064w CCC: $35.00
Published on Web 09/19/2000

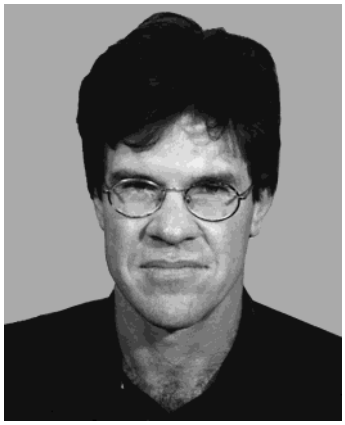

Evan Bieske was born in Mackay, Australia. He succumbed to the thrall of ions and ion clusters while undertaking his Ph.D. degree under the supervision of A. E. W. Knight at Griffith University. In 1990 he began work as a postdoctoral fellow with J. P. Maier in Basel, Switzerland. There, when not climbing in the Basler Jura, he focused on exploring the properties of mass-selected ion complexes and clusters through their electronic and infrared spectra. In 1996, after completing his habilitation, he returned to Australia to begin life as an antipodean academic in the School of Chemistry, University of Melbourne. His main concerns remain connected with the spectroscopic investigations of charged complexes and clusters in the gas phase.

Otto Dopfer was born in Memmingen, Germany, in 1965. His research interests focus on the spectroscopic and quantum chemical characterization of unstable species relevant in physical, chemical, and biological contexts (radicals, ions, and clusters). He received his Diploma in Physics in 1991 and his Ph.D. degree in Physical Chemistry from the Technische Universität München in 1994, under the supervision of K. Müller-Dethlefs and E. W. Schlag, for the application of REMPI, ZEKE, and MATI spectroscopy to hydrogen-bonded phenol complexes. In 1995, he joined the research group of J. P. Maier as a postdoctoral fellow at the Universität Basel, Switzerland, to develop a photodetachment spectrometer for the study of hydrocarbon anions. In 2000, he received his Habilitation in Physical Chemistry from the Universität Basel for spectroscopic and theoretical work on intermolecular forces and microsolvation processes in charged complexes.

articles discussing the formation, energetics, and reactivity of ionic complexes and clusters.[20,43−52]

The motivations for spectroscopically characterizing ionic complexes and clusters are diverse. Ionic complexes, $A^{\pm}-L_n$, serve as model systems to investigate the interaction between ions, $A^{\pm}$, and neutral ligands, L, from a microscopic point of view. Both positively and negatively charged complexes are known to be important in the ion−molecule chemistry of the upper atmosphere.[53] Ion−molecule reactions dominate the chemistry of low-density media (e.g., interstellar media) due to the long range of the interaction.[54,55] Ionic complexes are often intermediates of such reactions (e.g., proton transfer, S_N2 reactions), and their characterization improves our understanding of the fundamental reaction mechanisms. The characterization of proton-bound complexes is of importance in understanding the microscopic details of proton-transfer reactions and exploring the nature of ionic hydrogen bonds.[56−58] The transfer of a proton from one base to another is a fundamental chemical event, playing a role not only in solution chemistry but also in more rarefied gas-phase environments. Ion−ligand interactions are relevant for solvation processes, e.g., in electrolytic media (salt solutions, oceans) and industrial processes (hydrometallurgic processes).[59] The solvated proton is of fundamental importance in liquid-phase chemistry, proton transfer, and proton mobility in aqueous solutions (proton wires).

Ion−neutral interactions bridge the gap between weak bonds in neutral clusters (van der Waals and hydrogen bonds) and strong chemical bonds (Figure 1). The interaction in ionic complexes is usually

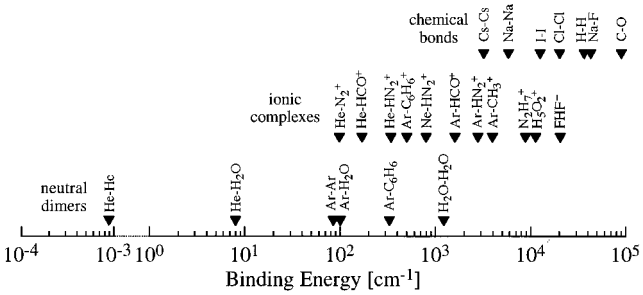

Figure 1. Binding energies of selected neutral dimers, ionic complexes, and chemically bound species (Reprinted with permission from ref 364. The values cover 8 orders of magnitude, ranging from the weakest van der Waals interaction (He−He, $\sim 10^{-3}$ cm^{-1}) to the strongest covalent bonds (e.g., C−O, $\sim 10^{5}$ cm^{-1}). Forces in ionic complexes ($10^{2}-10^{4}$ cm^{-1}) bridge the gap between weak interactions in neutral dimers ($10^{-3}-10^{3}$ cm^{-1}) and strong chemical bonds ($10^{3}-10^{5}$ cm^{-1}).

stronger than in their neutral counterparts, owing to additional stabilization from electrostatic and induction forces, charge transfer, and covalent contributions. The ultimate goal of high-resolution spectroscopic studies is the development of accurate potential energy surfaces (PES). From the analysis of the spectra employing appropriate model Hamiltonians, properties relating to the PES can be extracted: rotational and centrifugal distortion constants, inter- and intramolecular vibrational frequencies and their IR intensities, line widths, splittings due to tunneling motions (e.g., internal rotation or inversion), hyperfine interactions, and in cases of open-shell complexes also spectroscopic parameters related to the electron spin. These data can then be related to other properties of the complexes, e.g., equilibrium geometries, force constants, binding energies, potential barriers, anharmonicities, relaxation dynamics, and vibrational coupling strengths.

Relating the spectroscopic data to the PES can be a nontrivial and sometimes ambiguous task as the experimental spectrum is usually sensitive to only a limited part of the multidimensional PES. Conse-

Table 1. List of Ionic Complexes for Which Spectra at the Level of Rotational or Higher Resolution Have Been Obtained[a]

	spectral range	spectroscopy	ion source	refs
cations				
proton-bound				
N_2H^+-He	IR	PD	EI/SS	98, 122
N_2H^+-Ne	IR	PD	EI/SS	99
N_2H^+-Ar	IR	PD	EI/SS	100, 123
	IR	DA	EI/SS	113, 124
$N_2H^+-N_2$	IR	DA	EI/SS	125
OCH^+-He	IR	PD	EI/SS	94
OCH^+-Ne	IR	PD	EI/SS	95
OCH^+-Ar	IR	PD	EI/SS	96, 126
	IR	DA	EI/SS	112
	MW	FT	Dis/SS	108
OCH^+-H_2	IR	PD	EI/SS	97, 127
$SiOH^+-Ar$	IR	PD	EI/SS	101
OH^+-He	IR	PD	EI/SS	102
OH^+-Ne	IR	PD	EI/SS	102
$CH_3CNH^+-H_2$	IR	PD	EI/SS	128
H_2^+-He	MW	EFD	EI	109, 110, 129
HNH^+-He	IR	PD	EI/SS	103
HNH^+-Ar	IR	PD	EI/SS	104
H_3^+-Ar	MM/MW	DA	HCDis/cell	21,130−132
	MW	FT	Dis/SS	107
$H_3O^+-H_2$	IR	PD	CorDis/SS	88
$H_3O^+-H_2O$	IR	PD	CorDis/SS	88, 89
$H_3O^+-(H_2O)_2$	IR	PD	CorDis/SS	89
NH_4^+-He	IR	PD	EI/SS	133
NH_4^+-Ar	IR	PD	EI/SS	134−136
$NH_4^+-(NH_3)_n$	IR	PD	CorDis/SS	87, 137
$CH_5^+-H_2$	IR	PD	CorDis/SS	138
p/π-bound				
CH_3^+-He	IR	PD	EI/SS	139
CH_3^+-Ne	IR	PD	EI/SS	106
$CH_3^+-Ne_2$	IR	PD	EI/SS	106
CH_3^+-Ar	IR	PD	EI/SS	105
$CH_3^+-Ar_2$	IR	PD	EI/SS	105
$CH_3^+-Ar_3$	IR	PD	EI/SS	105
$CH_3^+-H_2 (=CH_5^+)$	IR	DA	HCDis/cell	140
$SiH_3^+-H_2$	IR	PD	CorDis/SS	141
$C_6H_6^+-Ne$		Rydberg-PFI	neutral/SS	142
$C_6H_6^+-Ar$		Rydberg-PFI	neutral/SS	143, 144
$C_6H_6^+-Kr$		Rydberg-PFI	neutral/SS	143
miscellaneous				
$N_2^+-He_n$	UV	PD	EI/SS	90, 145, 146
$N_2^+-N_2$	IR	DA	EI/SS	111, 147
Ar_3^+		RDCS	sputter	119
metal-bearing				
Na^+-H_2O		ZEKE	neutral/SS	120, 121
Al^+-H_2O		ZEKE	neutral/SS	148
Mg^+-H_2O	UV	PD	LV/SS	91
Mg^+-H_2	UV	PD	LV/SS	92
Ca^+-N_2	VIS	PD	LV/SS	149
Ca^+-D_2O	VIS	PD	LV/SS	93
$Ca^+-C_2H_2$	VIS	PD	LV/SS	150, 151
Ca^+-CH_4	VIS	PD	LV/SS	152
Co^+-OCO	VIS	PD	LV/SS	153
anions				
proton-bound				
FHF^-	IR	DA	HCDis/cell	22, 154
$ClHCl^-$	IR	DA	HCDis/cell	155
I^--H_2O	IR	PD	EI/SS	115
$Br^--C_2H_2$	IR	PD	EI/SS	118
I^--CH_3	IR	PD	EI/SS	117
S_N2				
Cl^--CH_3Br	IR	PD	EI/SS	116

[a] Abbreviations: MW (microwave), MM (millimeter wave), IR (infrared), VIS (visible), UV (ultraviolet), PD (photodissociation), DA (direct absorption), FT (Fourier transform), EFD (electric field dissociation), PFI (pulsed field ionization), RDCS (rotational depletion coherence spectroscopy), ZEKE (zero kinetic energy photoelectron spectroscopy), EI (electron impact), Dis (discharge), CorDis (corona discharge), HCDis (hollow cathode discharge), LV (laser vaporization), SS (supersonic expansion), neutral (neutral precursor).

quently, the interpretation of the results can strongly depend on the model Hamiltonian employed for the analysis. In strongly bound and semirigid systems, the traditional concepts developed for molecular species can be applied (e.g., anharmonic oscillator, semirigid rotor). However, in weakly bound or fluxional systems with shallow minima and low barriers for internal motions, theoretical information concerning the PES is required for a secure interpretation of the experimental data, as the wave functions are more delocalized and probe larger parts of the PES. In these cases the theoretical PES can be iteratively refined until agreement between theoretical and experimental data is achieved. In some cases PESs have been constructed by combining the empirically determined potential near the equilibrium geometry with a theoretical long-range potential. These issues have been extensively discussed with regard to the analysis of neutral van der Waals molecule spectra,[16,60−68] where fruitful interplay between experiment and theory has led to the construction of accurate PESs for a number of small dimers and trimers.[8,16,62,69−72]

The spectroscopic study of ionic complexes has often been preceded by their formation and characterization by other means. Of particular importance has been the use of high-pressure mass spectrometry to determine association enthalpies and entropies for a vast number of $A^{\pm}-L_n$ combinations (see refs 20, 73−75 for details). More recently, ion−ligand binding energies have been ascertained through the analysis of metastable decay fractions and fragment kinetic energy releases within the framework of evaporative ensemble theory.[48,76−81] For anion systems, photoelectron spectra provide comparable ligand binding energy data.[45,82,83] In some cases there are discontinuities in the binding enthalpies or entropies that signal the closure of the first solvation shell or the establishment of a central structural unit.[20,43,45] The predominance of particular cluster sizes in mass spectra (magic numbers) are also often associated with particularly stable structures or solvent shell closure. Although these data provide insights into cluster structures, particularly the formation of solvation shells and the existence of isomers, many details of the PES remain obscure.

The first high-resolution studies of ionic complexes were reported in 1987 with a MW absorption spectrum of H_3^+-Ar and a diode laser IR absorption spectrum of FHF^-. While in both cases the studies used traditional techniques with the complexes being formed in gas discharge cells, several factors contributed to their success. H_3^+-Ar has a large dipole moment and consequently strong MW absorptions, and FHF^- is strongly bound and thus can be generated in high abundances. At around the same time, IR spectra of several chemically significant protonated cluster ions (e.g., H_5^+,[84] $H_9O_4^+-H_2$ and $H_7O_3^+-H_2$,[85] $H_3O^+-(H_2O)_{1-3}$,[86] $NH_4^+-(NH_3)_4$[87]) were obtained using a strategy that involved vibrational predissociation in a tandem mass spectrometer, with the cluster ions being formed in a corona discharge supersonic expansion. In some cases the spectra contained features due to internal rotation of ligands (e.g., $NH_4^+-(NH_3)_4$),[87] while in others (e.g., $H_3O^+-H_2$,[88] $H_5O_2^+$ [86,89]) features due to the overall rotation of the complex where resolved. The techniques employed in these investigations (vibrational predissociation, laser excitation in a tandem mass spectrometer, ionic complex formation in a supersonic expansion) played an important role in later studies and were adopted (with variations) by other groups. Mass spectrometric and laser techniques were combined to explore the properties of $N_2^+-He_n$ complexes through their B←X electronic absorptions.[35,90] Rotationally resolved electronic transitions of metal−ligand ionic complexes formed in laser vaporization sources (e.g., Mg^+-H_2O,[91] Mg^+-H_2,[92] Ca^+-H_2O[93]) were probed by exciting metal-centered electronic absorptions in the visible (VIS) or ultraviolet (UV) and monitoring the fragmentation products.

In the mid-1990s, the mid-IR spectra of a series of simple linear or T-shaped closed-shell complexes (OCH^+-L,[94−97] N_2H^+-L,[98−100] $SiOH^+-L$,[101] L = He, Ne, Ar, H_2) were recorded. The spectra were distinguished by their simplicity and interpretability and allowed the exploration of systematic changes in the intermolecular bond as the attached ligand was varied. Rotationally resolved combination and overtone bands were also observed. The same approach was used to obtain rotationally resolved spectra of open-shell complexes (OH^+-He, OH^+ Ne,[102] HNH^+-He,[103] HNH^+-Ar[104]) and trimer complexes ($CH_3^+-Rg_2$, Rg = Ne,Ar).[105,106] Other developments occurred in the same period: FTMW spectra of OCH^+-Ar and H_3^+-Ar were recorded in a pulsed discharge expansion,[107,108] near dissociation spectra of H_2^+-He were obtained in a fast ion beam,[109,110] and direct IR absorption spectra of cation complexes (N_4^+,[111] OCH^+-Ar,[112] N_2H^+-Ar[113]) were recorded in an electron crossed slit jet source.[114] The first rotationally resolved spectra of weakly bound anion complexes were reported with spectra of I^-H_2O,[115] Cl^-CH_3Br,[116] I^-HCH_2[117] (K structure), and $Br^-C_2H_2$ [118] (J structure). Novel approaches to the high-resolution study of ionic complexes in this period included the rotational depletion coherence (RDCS) studies of Ar_3^+ [119] and the zero kinetic energy photoelectron (ZEKE) studies of Na^+-H_2O.[120,121]

Table 1 provides a list of complexes for which rotationally resolved spectra have been obtained, along with the experimental method that was utilized. Included in the table are complexes for which spectral structure relating to internal rotation has been observed. The complexes can be divided into several general classes. Cation systems include (i) proton-bound complexes $AH_{(k)}^+-L_n$ with one or k equivalent protons for which mid-IR and MW spectra have been measured; (ii) p/π-bound complexes of the type $CH_3^+-L_n$, $SiH_3^+-(H_2)_n$ and $C_6H_6^+-Rg$ (Rg = rare gas); (iii) complexes containing a charged metal atom, Me^+-L, that have generally been studied either by exciting strong electronic transitions centered on the Me^+ cation or by ZEKE spectroscopy; and (iv) miscellaneous complexes (N_4^+, Ar_3^+, $N_2^+-He_n$). The anion complexes are either proton-bound or S_N2-type complexes.

The outline of this review is as follows. After a short description of the experimental techniques which have been used to obtain high-resolution spectra of ionic complexes, the details of individual systems are discussed. For each complex attention is given to structures, binding energies, force constants, potential barriers, frequency shifts, and intermolecular frequencies derived from spectroscopy, thermochemistry, and calculations. The outlook sheds some light on prospective developments in the field.

II. Experimental Strategies

Characterization of cluster ions requires sensitive spectroscopic detection techniques owing to low concentrations usually achieved in cluster ion sources. The most frequently applied spectroscopic approach has been resonance-enhanced photodissociation (PD) spectroscopy conducted in a tandem mass spectrometer. The concept and experimental realization of this technique have been extensively described and reviewed.[23−29,31,32,35,84,156] Briefly, parent ions ($A^{\pm}-L_n$) are mass selected by a mass spectrometer (MS) prior to resonant excitation by tunable laser radiation (IR, VIS, UV) into metastable rovibrational or rovibronic states lying above the dissociation limit. Subsequent redistribution of the internal energy causes rupture of the weak intermolecular bond(s) to yield ionic and neutral fragments:

$$A^{\pm}-L_n + h\nu \rightarrow (A^{\pm}-L_n) \rightarrow A^{\pm}-L_m + (n - m)L \quad (1)$$

The photofragment ions ($A^{\pm}-L_m$) are selected by a second MS and monitored as a function of the laser frequency to obtain a PD spectrum. This type of PD spectroscopy features high selectivity and sensitivity: (i) it is a (nearly) background-free consequence technique, as absorption is monitored by fragmentation; (ii) ion detection is very sensitive owing to the possibility of single-ion counting with nearly 100% detection efficiency (leading to detection limits of <10 cm^{-3}); (iii) high selectivity is achieved through mass selection of both parent and daughter ions. The main disadvantage of PD spectroscopy is that it can only be used to detect transitions terminating at levels above the cluster's dissociation threshold, and thus, it is more suitable for complexes with lower binding energies. Nevertheless, in several cases it has been possible to spectroscopically probe more strongly bound ions either by exciting overtone transitions[105] or using multiphoton dissociation schemes.[86] It is worthwhile remarking that upper levels accessed in PD spectroscopy can be homogeneously broadened due to short lifetimes. This is obviously a nuisance if it results in obscuration of rotational structure. On the other hand, the line widths furnish information on the vibrational predissociation rate, allowing dynamical effects to be explored (see section III.A.1.a for an illustration).

A variant of PD spectroscopy involves using an electric field to dissociate molecules that have been photoexcited to near dissociation states. This approach has been employed to detect rovibronic transitions induced by IR or MW radiation between levels close to the dissociation limit (long-range complexes). A number of diatomic and triatomic ions including the weakly bound H_2^+-He complex have been studied by this technique.[109,110,129]

Instruments employed for mass selection include quadrupole mass filters (QMS), time-of-flight MS (sometimes in combination with mass gates), magnetic and electric sectors, and Wien filters. The ions have been irradiated in quadrupole and octopole ion guides, field-free flight tubes, and ion traps. Narrow band tunable radiation in the mid-IR spectral range is usually provided by optical parametric oscillators (OPO), difference frequency generation, or color center lasers, while dye lasers (in combination with second-harmonic generation) are commonly employed to investigate the spectrum in the VIS and UV spectral range.

There have also been a number of non-mass-selective studies by way of direct MW and millimeter wave absorption,[21,131] FTMW spectroscopy,[107,108] and direct IR absorption[22,114,140,155] in either supersonic expansions or hollow cathode discharge cells (Table 1). The sensitivity of these techniques is often enhanced by modulation techniques (e.g., velocity modulation, frequency and/or intensity modulation, ion production modulation, etc.) and various ways of increasing the effective path lengths (e.g., slit jets, multipass arrangements). Due to the lack of mass selection, the carrier of the observed spectrum must be identified by alternative means (e.g., rotational analysis of the spectrum, isotopic substitution, plasma chemical arguments, Doppler profiles, etc.).

Sources for the production of ionic complexes must reconcile the somewhat conflicting requirements of high ion current and low effective temperatures. Low temperatures are desirable both for maximizing the concentration of weakly bound complexes and also to ensure the preferential population of the lowest few energy levels so that the spectra are not unduly congested. The majority of ionic complexes subject to high-resolution characterization have been generated by ion sources that generate a plasma in a supersonic expansion (Table 1). Formation of the plasma usually involves either a corona discharge,[85] electron impact ionization using an electron gun,[116] thermionic filaments adjacent to the nozzle orifice,[35] a pulsed discharge,[107,108] or laser ablation (in the case of complexes containing metal ions).[23,28] Some control over the formation and cooling of the ionic species can be achieved by varying the electron energy, moving the nozzle back and forth with respect to the ionization zone, and by altering the composition of the expansion gas (Figure 2). Slit jet expansions have been employed in conjunction with electron impact ionization for direct IR absorption studies.[111,114]

There are several possible mechanisms for cluster ion formation in the expansion. If the plasma is initiated close to the nozzle orifice, ligands are able to accrete about a seed ion (which is produced by ionization of the expanding gas mixture and possibly subsequent ion−molecule reactions) via three-body association reactions. Subsequent collisions then serve to effectively cool the nascent clusters to relatively low temperatures (10−50 K). Rotationally resolved spectra show that the complexes are usually

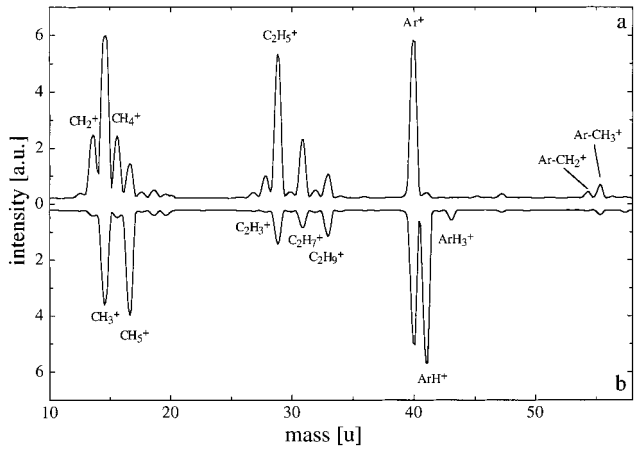

Figure 2. Mass spectra obtained in a supersonic expansion coupled to electron impact ionization using the mixtures CH_4/He/Ar = 1/100/500 (a) and CH_4/H_2/He/Ar = 1/25/100/500 (b) at 5 bar stagnation pressure (Reprinted with permission from ref 105. Copyright 1998 American Institute of Physics). Due to saturation effects, relative intensities can only be compared for peaks with intensities of less than 5 au. The spectra are dominated by ions of the form CH_n^+, $C_2H_n^+$ and/or $C_2H_n^+-(H_2)_m$ and/or $CH_n^+-CH_4$, Ar-H_n^+ and CH_n^+-Ar. Though the addition of H_2 increases the relative abundance of CH_3^+ versus other CH_n^+ ions, it does not enhance the absolute ion currents of either CH_3^+ or CH_3^+-Ar.

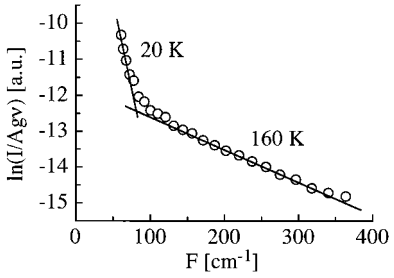

Figure 3. Boltzmann plot for the Π−Π band of the parallel transition of the H−H stretch fundamental of OCH^+-H_2 (Reprinted with permission from ref 127. Copyright 1997 American Institute of Physics). The complex was produced in a supersonic expansion of a CO/H_2/He mixture (with a ratio 1/50/50, backing pressure 5 bar) exposed to electron impact ionization. Plotted is the relative population of ground-state rotational levels as a function of their energy. The distribution is nonthermal: the population of the lowest J levels corresponds to a temperature $T = 20$ K, while higher J levels are best characterized by $T = 160$ K.

not in thermal equilibrium, with ineffective cooling of the complexes in higher rotational energy levels due to large gaps between the rotational energy levels. A Boltzmann plot demonstrating this effect in OCH^+-H_2 is shown in Figure 3.[127]

Positive cluster ions can also be formed by bombarding neutral clusters with electrons downstream in the collision-free part the expansion. In this case the nascent complexes are usually highly energized owing to substantial changes in the intermolecular potential accompanying ionization. The only agency for dissipation of the excess energy is through evaporation of neutral ligands, so that the resulting clusters can have substantial internal energies. Negative cluster ions can also be formed downstream in the expansion through the dissociative attachment of an electron to a molecular constituent (intracluster dissociative attachment).[157] For example, $Cl^-(H_2O)_n$ complexes can be formed through dissociative electron attachment to neutral $CCl_4-(H_2O)_n$ clusters followed by loss of CCl_3 and H_2O ligands.[158] Again, the clusters are cooled through evaporation.

High-resolution spectra of a few cation dimers have been obtained by photoionization of the corresponding neutral precursors produced in supersonic expansions (Table 1). The applicable techniques are ZEKE spectroscopy[159] and mass-analyzed threshold ionization (MATI) spectroscopy[160] and rely on pulsed field ionization (PFI) of highly excited Rydberg states of the neutral species ($n > 150$) with subsequent detection of electrons (ZEKE) and/or ions (MATI). Mass selectivity in these experiments is achieved either via resonance-enhanced multiphoton excitation (ZEKE) and/or the detection of the parent or fragment ions (MATI). The application of ZEKE and MATI spectroscopy to clusters has been extensively reviewed.[36−39,161,162] Only a few spectra of ionic complexes have been obtained with rotational resolution using ZEKE or MATI (Table 1), due to the limited resolution achieved so far (>0.1 cm^{-1}). Recently, high-resolution spectra of lower lying Rydberg states ($40 < n < 120$) were recorded for C_6H_6-Rg dimers and yielded, via extrapolation to the series limit ($n \rightarrow \infty$), rotational constants of the cationic ground states.[142,143,163] In general, high-resolution spectra of ionic complexes are difficult to obtain by means of photoionization of the neutral species if (i) the neutral precursor is unstable or (ii) neutral and cationic species have very different equilibrium geometries (unfavorable Franck−Condon factors).

Rotational depletion coherence spectroscopy (RDCS) is a time domain technique suitable for furnishing structural information on cluster ions that possess directly dissociative excited electronic states.[119] Its application to the Ar_3^+ ion is described in section III.C.3. The technique depends on the preparation and subsequent detection of rotational coherences using short (ps) polarized laser pulses. The preparation laser pulse (Z polarization) serves to preferentially dissociate ions with transition moments aligned along the polarization vector (for a parallel transition). The remaining subassembly of ions with transition moments preferentially aligned toward the XY plane continues to rotate, but the transition moments are periodically realigned in the XY plane at times $t_n - t_0 = n/(4B)$. A measure of the realignment is provided by the ratio of the population dissociated by a time delayed probe laser pulse whose polarization is aligned along the Y or Z axes. Although the technique has only been applied to Ar_3^+, it appears to have much wider potential application.

Valuable spectral information on ionic complexes has been obtained by several other techniques, including laser-induced fluorescence (LIF),[164,165] various variants of photoelectron spectroscopy (X-ray-PES,[40] UV−PES,[41,42] REMPI−PES[166,167]), photoionization efficiency measurements (REMPI−PIE),[168,169] and REMPI−IR ion dip spectroscopy.[170] There have also been several spectroscopic studies in which the cluster ions have been formed by REMPI of neutral complexes followed by electronic excitation and pho-

todissociation (e.g., $C_8H_{10}^+-Ar$,[171] $C_6H_4F_2^+-Ar$[35,172]). As the spectra were not at the level of rotational (or higher) resolution, the techniques are not discussed in detail in this review.

III. Cation Complexes

A. Proton-Bound Complexes

1. AH^+–L

In proton-bound $A-H^+-L$ dimers, two bases A and L share an intermediate proton (Figure 4). Part of

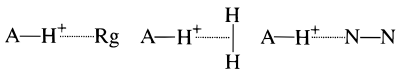

Figure 4. Equilibrium structures of selected proton-bound dimers.

the interest in such complexes arises from the fact that they are stabilized intermediates of proton-transfer reactions, which play a key role in a broad range of chemical and biological contexts. The proton-bound complexes feature properties that are characteristic for hydrogen bonding:[57,58,173] (i) the separation between A and L is smaller than the sum of their van der Waals radii; (ii) the intermolecular bond is strongly directional and rarely deviates significantly from linearity; (iii) the formation of the intermolecular bond between the proton donor, $A-H^+$, and the proton acceptor, L, leads to a destabilization of the A−H bond. The partial proton transfer from A to L results in a red shift of the A−H stretching fundamental, ν_{A-H}, which is accompanied by an increase in its IR oscillator strength. Moreover, anharmonic coupling between the intra- and intermolecular bonds activates combination bands involving the A−H stretch and the intermolecular stretch modes ($\nu_{A-H} + \nu_s$). IR spectroscopy is thus an ideal tool for the investigation of proton bonds, and most high-resolution spectra have been obtained in this spectral range.

a. N_2H^+-He,Ne,Ar,H_2,N_2. Complexes consisting of He, Ne, Ar, H_2, and N_2 ligands attached to the linear closed-shell N_2H^+ ion have been extensively examined using IR spectroscopy and theoretical techniques. The N_2H^+-L complexes can be viewed as ones where a proton is shared between two Lewis bases (N_2 and L) and serve as prototypical examples of proton-bound species. As the proton affinity (PA) of N_2 (118.2 kcal/mol) exceeds the ones of He, Ne, Ar, and H_2 (42.5, 48.1, 88.6, and 101 kcal/mol),[174] complexes containing these ligands essentially consist of an N_2H^+ core to which the perturbing ligand is attached. The IR spectra along with ab initio calculations show that the complexes possess structures in which the proton is shared most effectively with the ligand. Thus, the rare gas (Rg) containing complexes are linear, $N_2H^+-H_2$ is T-shaped with the shared proton attached to the midpoint of the H−H bond, and the $N_2-H^+-N_2$ complex is linear and centrosymmetric, with the intermediate proton shared by equivalent N_2 ligands (Figure 4).

Vibrational predissociation investigations (N_2H^+-He,[98,122] N_2H^+-Ne,[99] N_2H^+-Ar,[100,123,126] and $N_2H^+-H_2$[175]) using a pulsed OPO light source (0.02 cm^{-1} bandwidth) have been directed principally in the region of the chromphore ν_1 band (N−H stretch) in the 3000 cm^{-1} region, although combination and overtone bands have also been observed. The N_2H^+-Rg species were among the first complexes to display fully rotationally resolved vibrational predissociation spectra, demonstrating the effectiveness of the strategy for sensitively recording high-resolution IR spectra. The limitations of this approach are also apparent. For example, due to rapid vibrational predissociation and consequent lifetime broadening, rotational structure has not been observed in the predissociating bands of $N_2H^+-H_2$. Direct diode laser IR absorption spectroscopy in a slit jet plasma has also been employed to provide complementary information on nondissociative levels of N_2H^+-Ar[113,124] and new information on the strongly bound $N_2-H^+-N_2$ complex.[125]

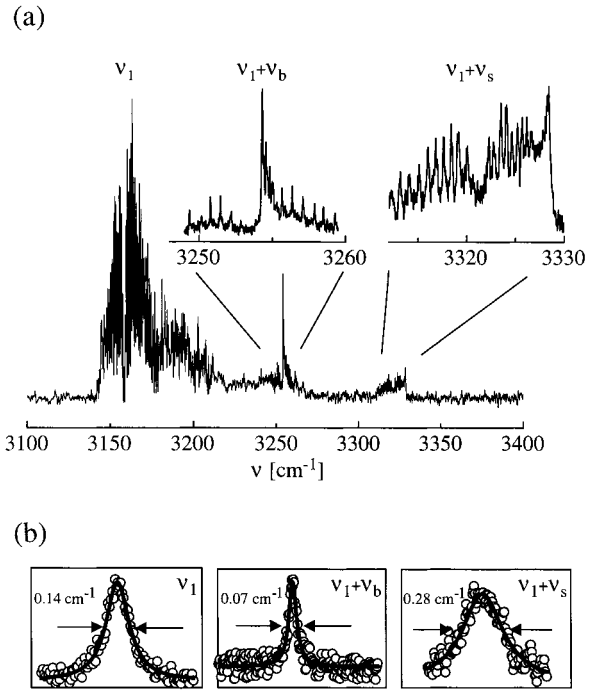

Figure 5. (a) IRPD spectrum of N_2H^+-He between 3100 and 3400 cm^{-1}. The rotationally resolved transitions correspond to the N−H stretch fundamental (ν_1, $\Sigma-\Sigma$) and its combination bands with the intermolecular bend ($\nu_1 + \nu_b$, $\Pi-\Sigma$) and stretch ($\nu_1 + \nu_s$, $\Sigma-\Sigma$) modes. (b) Line profiles of individual rotational transitions of the ν_1, $\nu_1 + \nu_b$, and $\nu_1 + \nu_s$ bands of N_2H^+-He. The line widths of the fitted Lorentian curves (0.14, 0.07, 0.28 cm^{-1}) correspond to lifetimes of 38, 76, and 19 ps, respectively. (Reprinted with permission from ref 98. Copyright 1996 American Institute of Physics.)

To illustrate the sort of spectroscopic information that is obtained for the N_2H^+-Rg dimers, the IRPD spectrum of N_2H^+-He is shown in Figure 5. Conspicuous in the spectrum are rotationally resolved bands that correspond to the N−H stretch fundamental (ν_1, $\Sigma-\Sigma$) and its combination bands with the intermolecular bend ($\nu_1 + \nu_b$, $\Pi-\Sigma$) and stretch ($\nu_1 + \nu_s$, $\Sigma-\Sigma$) modes. The three bands can be analyzed in terms of standard pseudodiatomic energy level expressions to yield lower- and upper-state rotational and centrifugal distortion constants that deliver

information on the vibrationally averaged bond length, R_{cm}, and radial flexibility of the intermolecular bond, k_s. Information on the angular flexibility of the intermolecular bond, k_b, is provided by the spacing between ν_1 and $\nu_1 + \nu_b$. Corresponding IRPD spectra to the one shown for N_2H^+-He (Figure 5) have been recorded for N_2H^+-Ne[122] and N_2H^+-Ar.[100,123,126] Generally, the rotational structure in the N_2H^+-Ne and N_2H^+-Ar bands is more complex than for N_2H^+-He due to disruptions of the upper-state rotational manifolds by interacting dark states. Besides making analysis and assignment of the higher vibrational transitions problematic, these effects mean that it is often difficult to extract excited-state constants (especially centrifugal distortion constants).[100,126]

In the case of N_2H^+-Ne, rotationally resolved bands assigned to ν_1, $\nu_2 + \nu_3 + \nu_b$ (ν_3 = N−N stretch), $\nu_1 + \nu_b$, $\nu_1 + \nu_s$, $\nu_1 + 2\nu_b$, and $2\nu_1$ have been observed.[99] The ν_1 state is found to be in resonance with a nearby level, which on the basis of $N_2H^+-{}^{22}Ne$ and $^{15}N_2H^+-Ne$ isotopomer spectra is assigned to the $l = 0$ component of $\nu_2 + \nu_3 + \nu_b$. For N_2H^+-Ar, the vibrational energy level structure is complicated by exceptionally strong interactions between the N−N and N−H stretch modes. In all, 25 different vibrational predissociation bands have been recorded between 2470 and 6000 cm^{-1}, over one-half of which display rotational resolution.[100,126] At this stage, only the few lowest lying bands have been assigned and analyzed. Initially, it was thought that a strong band with origin at 2505.5 cm^{-1} was the $\nu_1 + \nu_s$ combination band.[100] However, more recent diode laser absorption studies, along with theoretical work,[124] show that it is more likely due to the ν_1 fundamental that is displaced upward due to strong coupling with the N−N stretch level. Transitions to the latter level have been observed using diode laser spectroscopy. The rotational constants for the two levels are similar, constituting further evidence for the mixing.[124]

The degree to which the properties of the N_2H^+ core are disrupted by the attached ligand and the strength of the intermolecular interaction depend sensitively upon the difference between the PAs of N_2 and the participating ligand, ΔPA. As ΔPA diminishes, the proton becomes increasingly delocalized, resulting in a displacement to lower frequency for the N_2H^+ ν_1 absorption. Thus, the ν_1 origins for N_2H^+-He, N_2H^+-Ne, and N_2H^+-Ar are red shifted by −75.5, −180.5, −728.5 cm^{-1} with respect to the monomer band (3233.95 cm^{-1}).[176] In comparison, vibrational band shifts for analogous neutral Rg-containing van der Waals complexes are invariably small.[4] For example, the complexation-induced vibrational band shift is −2.69 cm^{-1} for the linear hydrogen-bonded NCH−Ar dimer (which is isoelectronic with N_2H^+-Ar).[177]

A diminishing ΔPA is accompanied by an increase in the radial and angular rigidity of the intermolecular bond and also in the bond dissociation energy. For example, the harmonic stretching force constants for N_2H^+-Rg are k_s = 4.8, 12.8, 37.8 N/m for Rg = He, Ne, Ar. The radial force constants reflect the strength of the charge-induced dipole interaction and are of similar magnitude to those found for strongly bound neutral hydrogen-bonded systems (e.g., $H_2O-HCCH$, k_s = 6.5 N/m).[178] The separation between the attached Rg atom and the intermediate proton is also much shorter in N_2H^+-He (1.72 Å), N_2H^+-Ne (1.76 Å), and N_2H^+-Ar (1.90 Å) than in the corresponding NCH−Ar dimer (2.721 Å).[179] The bond is even shorter in the strongly bound $N_2-H^+-N_2$ complex (1.28 Å).[125]

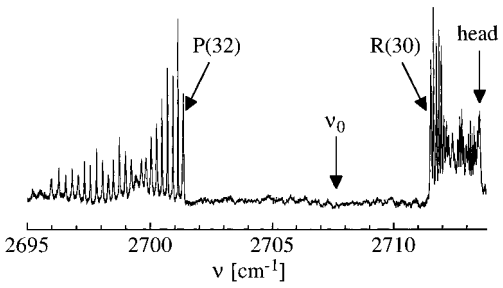

Figure 6. IRPD spectrum of N_2H^+-Ar showing the onset of dissociation at $J' = 31$ in an unassigned vibrational state with band origin ν_0 = 2707 cm^{-1} (Reprinted with permission from ref 126.

Observation of $\nu_1 + \nu_b$ combination bands for N_2H^+-He and N_2H^+-Ne furnishes information on the bending potential for the Rg interacting with vibrationally excited N_2H^+. These bands occur 96 and 128 cm^{-1} above the ν_1 transition, corresponding to harmonic force constants of $k_b = 4.5 \times 10^{-20}$ and 9.6×10^{-20} Nm. The bending frequencies are much larger than those for related neutral complexes (e.g., $k_b = 7 \times 10^{-22}$ Nm for NCH−Ar)[179] and prove that N_2H^+-Rg bonds are quite directional. It is worth noting that not all He-containing ionic complexes feature strongly directional intermolecular bonds. For example, N_2^+-He and NH_4^+-He have been shown through calculations and spectroscopic studies to have a PES where the intermolecular angular motion is almost unhindered (sections III.C.1 and III.A.2.e).[90,133,146]

Theoretical estimates for the dissociation energies of N_2H^+-He (378 cm^{-1}),[180] N_2H^+-Ne (795 cm^{-1}),[181] N_2H^+-Ar (2800 cm^{-1}),[123,124] and $N_2-H^+-N_2$ (5911 cm^{-1})[125] follow the trends expected from the ordering of the ligands' PAs (He < Ne < Ar < H_2 < N_2). The D_0 for $N_2H^+-H_2$ is calculated to be 2000 cm^{-1},[175] which is somewhat lower than might be expected. The calculated binding energies for $N_2H^+-H_2$ and $N_2-H^+-N_2$ are supported by association enthalpies measured using high-pressure mass spectrometry.[182] For N_2H^+-Ar, an accurate experimental value for the dissociation energy can be derived from the IRPD spectrum, as the onset of dissociation occurs at specific rotational levels in ν_1, $\nu_1 + \nu_s$, and a higher unidentified level.[100] Thus, the lower J lines are absent from the vibrational predissociation spectrum (Figure 6), although they are apparent in diode laser absorption spectra of the ν_1 transition.[113] By combining the charge-induced dipole and centrifugal potentials, independent assessments of the dissociation energy can be made for each of the three levels, leading to $D_0 = 2781.5 \pm 1.5$ cm^{-1}.[100] Currently, this is perhaps the most accurately determined dissociation energy for an ionic complex and accords well with recent ab initio values.

Excitation of the monomer N_2H^+ ν_1 mode causes a stiffening and shortening of the intermolecular bond. This is a characteristic of proton-bound complexes (cation and anions) and can be seen as evidence for incipient proton transfer to the base with the lower PA. For N_2H^+-He, N_2H^+-Ne, and N_2H^+-Ar, the ν_1 level is associated with H−Rg bond contractions of 0.04, 0.04, and 0.02 Å with respect to the ground state. Analysis of the $2\nu_1$ band of N_2H^+-Ne shows that the H−Ne bond for the $2\nu_1$ level is 0.05 Å shorter than in the ground state, proving that the bond continues to contract as more quanta are added to the ν_1 mode. The excited-state bond contraction is accompanied by a stiffening of the radial bond, so that, for example, in N_2H^+-He the stretching force constant increases from 4.8 to 7.5 N/m while for N_2H^+-Ar there is an increase from 37.8 to 42.2 N/m.

For N_2H^+-He, the spectroscopically determined molecular constants have been used to generate radial potential energy curves near the well minimum using a modified Rydberg−Klein−Rees (RKR) procedure.[98] These short-range potentials have been combined with long-range potentials determined by considering the interaction between the Rg atom and multipoles distributed on the N_2H^+ ion, obtained through an ab initio distributed multipole analysis (DMA). The resulting radial RKR/DMA potentials have been used to determine energies of excited intermolecular stretching states, dissociation energies, and equilibrium bond distances. On the basis of these potentials the binding energies for He interacting with the ground and ν_1 vibrational states are predicted to be $D_0 = 378$ and 431 cm^{-1}.

The ground- and excited-state properties of N_2H^+-He, N_2H^+-Ne, N_2H^+-Ar, and $N_2-H^+-N_2$ have also been explored from an entirely theoretical viewpoint. In the case of N_2H^+-He[180] and N_2H^+-Ne,[99,181] rovibrational calculations have been conducted using ab initio PESs. An important feature of this work is that the effect of the proton stretching motion on the intermolecular potential has been included in an adiabatic fashion. This is done by, first of all, calculating effective N−H stretching potentials for different angular and radial positions of the Rg atom with respect to the N_2H^+ core. Subsequently, energies for ground- and excited-state N−H stretching levels are calculated for each of the points and used to correct the intermolecular PES for the Rg atom interacting with a frozen N_2H^+. This procedure yields effective two-dimensional intermolecular PESs for N_2H^+-Rg in its ground and ν_1 states that are then used for the rovibrational calculations. Generally, the calculated ground- and excited-state rotational constants and intermolecular stretching and bending frequencies match the experimental values quite well. Distinctive features of the N_2H^+-He and N_2H^+-Ne complexes, such as the contraction and stiffening of the intermolecular bond accompanying the excitation of the ν_1 stretch, are reproduced by the approach. The ν_1 band shifts tend to be overestimated (e.g., −93 vs −75.5 cm^{-1} for N_2H^+-He, −210 vs −180.5 cm^{-1} for N_2H^+-Ne), an effect that has been attributed to the neglect of the N_2H^+ bending vibration on the intermolecular interaction.

For N_2H^+-Ar, the shared proton is far more delocalized than in N_2H^+-He and N_2H^+-Ne. This is reflected in a large reduction in the N−H stretch frequency and also a strong coupling between the intramolecular and intermolecular degrees of freedom. The first theoretical predictions of the ν_1 fundamental for N_2H^+-Ar (2330 cm^{-1}) were made on the basis of one-dimensional proton potentials developed by fixing the Ar atom in reasonable positions.[183] Subsequently, the stretching vibrational energy levels of N_2H^+-Ar have been calculated using a three-dimensional coupled oscillator model that includes all three stretching coordinates.[124] The presence of the Ar atom leads to strong anharmonic interactions between the N−N and N−H stretches, resulting in substantial mixing of the zero-order states, shifts in their energies, and a large increase in the IR intensity of the N−N stretch. Significantly, the experimentally observed frequencies for the ν_1, ν_3, and $\nu_1 + \nu_s$ modes are successfully matched by calculated vibrational energies.

Information on excited-state predissociation dynamics is provided by the rotational line widths. Line widths for the ν_1 levels of N_2H^+-Ne[99] and N_2H^+-Ar[100] are limited by the laser bandwidth (0.02 cm^{-1}), proving that dissociation ensues on time scales longer than 250 ps. Dissociation is more rapid for N_2H^+-He, where rotational line widths for the ν_1, $\nu_1 + \nu_b$, and $\nu_1 + \nu_s$ transitions (Figure 5) are consistent with upper-state lifetimes of 38, 76, and 19 ps.[122] The longer lifetime for the $\nu_1 + \nu_b$ combination level is probably due to a diminished average projection of the ν_1 stretch displacement onto the intermolecular bond (the dissociation coordinate), while the shorter lifetime of the $\nu_1 + \nu_s$ combination is consistent with a better overlap between the bound and continuum wave functions. As already mentioned, for $N_2H^+-H_2$ predissociation is sufficiently rapid for both the N−H and the H−H stretch levels for rotational structure to be obscured through lifetime broadening.[175]

b. OCH^+-He,Ne,Ar,H_2. The OCH^+-He,[94] OCH^+-Ne,[95] OCH^+-Ar,[96] and OCH^+-H_2[97,127] proton-bound complexes have been studied using IRPD spectroscopy. Additional information on OCH^+-Ar has been provided by FTMW studies of four isotopomers[108] and direct diode laser spectroscopy of the ν_3 (C−O stretch) band.[112] The OCH^+ ion is isoelectronic with N_2H^+, and the properties of the OCH^+-Rg complexes are similar in most regards to those of the N_2H^+-Rg ones. They possess linear proton-bound structures, and their ν_1 absorptions are red shifted from the ν_1 band of free OCH^+ at 3089 cm^{-1}.[184] However, because of the CO molecule's higher PA, the intermolecular interaction is weaker for the OCH^+ complexes than the N_2H^+ ones, and this is reflected in smaller ν_1 red shifts, stretching and bending force constants, longer intermolecular bonds, and lower dissociation energies. The relative interaction strengths for OCH^+-Rg and N_2H^+-Rg complexes are apparent by noting that the ν_1 band shift in OCH^+-He is only −12.4 cm^{-1} compared to −75 cm^{-1} in N_2H^+-He.

The IRPD spectra of the OCH^+-Rg complexes are generally less complicated than the corresponding N_2H^+-Rg ones. While the ν_1 band of OCH^+-He is

perturbed, with displacements and splittings of rotational lines, the corresponding OCH^+-Ne and OCH^+-Ar ν_1 spectra are relatively unperturbed. For OCH^+-He, the perturbations were tentatively ascribed to an accidental resonance between ν_1 and the combination of the intramolecular $\nu_2 + \nu_3$ vibration with quanta of intermolecular modes ($\nu_2 + \nu_3 = 3012$ cm^{-1} for OCH^+).[94] In OCH^+-Ne, the ν_1 level is depressed by roughly 30 cm^{-1} compared to OCH^+-He and it is possible that the interacting states have moved away from resonance.[95] Further support for this hypothesis arises from the apparent absence of perturbations for the OCH^+-Ar ν_1 band where the decrease in the ν_1 frequency is even more substantial.[96]

The spectroscopic data show that, as expected, the strength of the intermolecular bond of the OCH^+-Rg complexes increases in the order He < Ne < Ar, in line with PAs and polarizabilities of the attached bases. Thus, the radial force constants for OCH^+-He, OCH^+-Ne, and OCH^+-Ar are 1.6, 4.8, and 17 N/m. The ν_1 red shifts, which reflect the influence of the Rg atom on the effective proton potential, vary in the same way: −12.5, −42.5, −274 cm^{-1} for Rg = He, Ne, Ar. Interestingly, the vibrationally averaged intermolecular separation does not depend strongly upon the Rg atom: in OCH^+-He (2.00 Å) it is almost the same as in OCH^+-Ne (1.99 Å) and OCH^+-Ar (2.13 Å). The similarity is most probably due to a cancellation of competing effects. While the polarization attraction is stronger for larger Rg atoms, overlap repulsion becomes important at longer distances.

Currently, there are few empirical data concerning the effective bending potentials for the OCH^+-Rg dimers. In the case of OCH^+-Ar, the FTMW isotopomer spectra have been used to determine the average angular zero-point excursion (9.6°), effective bending force constant (7.95×10^{-20} Nm), and estimated harmonic bending frequency (110 cm^{-1}).[108] Ab initio intermolecular harmonic bending frequencies have been calculated for OCH^+-He (65 cm^{-1})[185] and OCH^+-Ar (135 or 171 cm^{-1}).[123,185]

The mid-IR spectra of OCH^+-Ne and OCH^+-Ar provide information on the interaction of the Rg atom with the vibrationally excited OCH^+ monomer. Due to perturbations in the OCH^+-He ν_1 spectrum, the upper-state rotational constants are not well defined, making it difficult to extract accurate estimates for the bond distance and stretching force constant. For OCH^+-Ne, excitation of the ν_1 mode leads to an intermolecular bond contraction of 0.01 Å and a 10% increase in k_s. For OCH^+-Ar, the contraction is somewhat larger (0.04 Å). In this case there is also an increase in k_s, although a precise determination of its magnitude is not possible due to the relatively large uncertainty in the upper state *D* value. Excitation of the ν_3 mode (principally a C−O stretch) in OCH^+-Ar also affects the intermolecular potential and results in a 0.01 Å bond contraction compared to the ground-state geometry.[112] It might be expected that the ν_3 vibration should be decoupled from the intermolecular potential. However, the ν_3 mode is not a pure C−O stretch and also involves motion of the intermediate proton. This is emphasized by the 48.2 cm^{-1} red shift of the ν_3 transition in the complex with respect to the OCH^+ ν_3 transition.

Currently there are no accurate experimental measurements of OCH^+-Rg binding energies and estimates are based upon ab initio calculations (OCH^+-He, OCH^+-Ar) and RKR/DMA potentials (OCH^+-Ne). Binding energy estimates are 130−170 cm^{-1} for OCH^+-He,[185,186] 438 cm^{-1} for OCH^+-Ne,[95] and 1470−1550 cm^{-1} for OCH^+-Ar.[123,185]

Mid-IR spectra of both OCH^+-H_2[97,127] and OCD^+-D_2[127] have been obtained using IRPD spectroscopy. Interest in the isomeric forms of H_3CO^+ followed the proposal that formaldehyde may be produced in dark interstellar clouds through a mechanism in which the primary step was the radiative association of OCH^+ and H_2.[55] The association product was presumed to be protonated formaldehyde, H_2COH^+, which produced formaldehyde after dissociative recombination with electrons. Subsequently, it was shown that H_3CO^+ ions formed in such low-energy encounters rapidly exchange H_2 for CO to form $(CO)_2H^+$, suggesting that they have an OCH^+-H_2 form, rather than the more stable H_2COH^+ structure.[187] This conjecture was given firm foundation by high-pressure mass spectrometry measurements which provided an association energy for the complex of ∼3.9 kcal/mol with respect to the $OCH^+ + H_2$ limit.[188] Theoretical studies[189−194] have identified three stable isomers of H_3CO^+, the H_2COH^+ cation (the most stable form), and the OCH^+-H_2 and COH^+-H_2 proton-bound complexes. Barriers for isomerization between the three forms exceed the $H_3^+ + CO$ and $OCH^+ + H_2$ dissociation limits, making it appropriate to think of them as distinct molecular species. Prior to the OCH^+-H_2 studies, only H_2COH^+ had received spectroscopic attention.[195]

While rotational structure is not apparent in the band corresponding to C−H excitation of OCH^+-H_2 (shifted by −249 cm^{-1} with respect to ν_1 of OCH^+) due to lifetime broadening, the H−H (D−D) stretch band (which becomes IR active due to the presence of the OCH^+) is rotationally resolved and furnishes structural information. The charge−quadrupole interaction favors a T-shaped equilibrium structure with the shared proton (deuteron) bound to the midpoint of the H−H (D−D) bond (Figure 4).[97,127] The spectra are consistent with such a T-shaped equilibrium geometry but also provide evidence of large-amplitude H_2/D_2 hindered internal rotation. For OCH^+-H_2, parallel $\Sigma-\Sigma$ and $\Pi-\Pi$ bands are observed corresponding to *para* and *ortho* H_2.[97,127] The OCD^+-D_2 spectrum features parallel $\Sigma-\Sigma$, $\Pi-\Pi$, and $\Delta-\Delta$ bands.[127] Fitting the observed line positions to a semirigid Watson A-type Hamiltonian yields anomalous rotational constants reflecting the appreciable zero-point excursions of the H_2/D_2 molecule.[127] Ab initio calculations predict that the barrier for internal rotation through a linear $C_{\infty v}$ transition state is 1153 cm^{-1},[97] a value that is consistent with the IR spectra when analyzed using a hindered rotor model. According to the model, the effective barrier for internal rotation increases by about 15% upon excitation of the H−H stretch. A crude pseudodiatomic analysis

of the spectrum yields an estimated distance between the H_2 midpoint and the intermediate proton of 1.84 Å. An increase in bond strength upon vibrational excitation is indicated by the decrease of the intermolecular separations of 0.008 and 0.005 Å for OCH^+-H_2 and OCD^+-D_2. The enhanced excited-state barrier and shorter intermolecular bond can be rationalized by the larger quadrupole moment of molecular hydrogen in the vibrationally excited state.

c. $SiOH^+-He,Ne,Ar,N_2$. SiO is isovalent with N_2 and CO and prefers protonation at the oxygen end.[196−198] IRPD spectra of linear $SiOH^+$ complexed with He, Ne, Ar, and N_2 have been recorded[101,199] in the vicinity of the O−H stretch vibration of $SiOH^+$ ($\nu_1 = 3662$ cm^{-1}).[198] The $SiOH^+$ ion was produced by electron impact ionization of a SiH_4/O_2/L mixture, and subsequent dimerization with a ligand L was achieved via three-body collisions in the expanding plasma. As for the related N_2H^+-L and OCH^+-L complexes, the mid-IR spectra of $SiOH^+-L$ dimers are dominated by red shifted ν_1 bands, indicative of linear proton-bound geometries.[101,199] The magnitude of the observed red shifts increases with the interaction strength: $\Delta\nu_1 = -8, -36, -217, -517$ cm^{-1} for L = He, Ne, Ar, N_2. Ab initio calculations confirm that the global minimum of the intermolecular PES of all investigated $SiOH^+-L$ dimers corresponds to the linear proton-bound structure ($C_{\infty v}$, Figure 4).[101,199] The major effects of complexation on the $SiOH^+$ properties are a lengthening of the O−H bond, accompanied by a red shift and intensity enhancement of the O−H stretch fundamental, $\Delta\nu_1$ and ΔI_1. These effects are typical for hydrogen-bonded systems and become more pronounced as the interaction strength increases: $\Delta r_{O-H} = 0.0011, 0.0022, 0.0114, 0.0276$ Å, $\Delta\nu_1 = -23, -52, -246, -566$ cm^{-1}, $\Delta I_1 = 29, 53, 206, 386\%$, $D_e = 190, 332, 1117, 2642$ cm^{-1} for L = He, Ne, Ar, N_2.[199]

As an example, the spectrum of the $SiOH^+-Ar$ dimer is reproduced in Figure 7.[101] Three rotationally resolved $\Sigma-\Sigma$-type bands were observed and assigned to ν_1 (3445.0 cm^{-1}) and its combination bands with the intermolecular stretch ($\nu_1 + \nu_s$, 3554.6 cm^{-1}) and bend vibrations ($\nu_1 + 2\nu_b$, 3581.5 cm^{-1}) of linear $SiOH^+-Ar$.[101] From the rotational constants, the interatomic bond length in the ground vibrational state is found to be $R_{H-Ar} = 2.19$ Å. Excitation of ν_1 results in a stabilization of the intermolecular bond, indicated by the ν_1 red shift ($\Delta\nu_1 = -217$ cm^{-1}) and a contraction of the bond (~0.05 Å). Excitation of ν_s in combination with ν_1 elongates the bond by 0.03 Å, while excitation of $2\nu_b$ reduces the bond length by 0.014 Å. These observations are typical for a proton-bound rod-and-ball complex. As the PAs decrease in the order SiO > CO > N_2, the intermolecular interaction strengths in complexes composed of their protonated ions with Rg or N_2 increase in the same order. This trend is reflected in the intermolecular binding energies, bond lengths, stretching force constants, and complexation-induced ν_1 red shifts.[101]

The topologies of the calculated PESs of $SiOH^+-Ar$, N_2H^+-Ar, and OCH^+-Ar are qualitatively different owing to differences in the charge distributions and molecular shapes of the protonated core ions.[101,123]

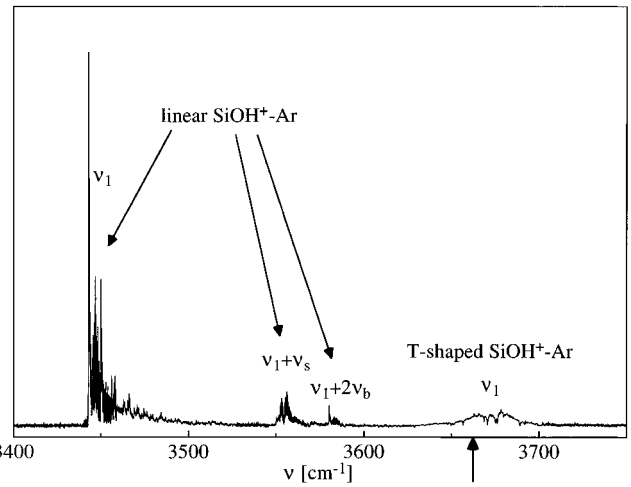

Figure 7. IRPD spectrum of $SiOH^+-Ar$ in the vicinity of the O−H stretch (ν_1) vibration (Reprinted with permission from ref 101. Copyright 1998 Elsevier Science). Three rotationally resolved $\Sigma-\Sigma$ bands are assigned to ν_1 and combination bands with intermolecular modes of the linear proton-bound isomer, while the broad band near 3670 cm^{-1} is attributed to a less stable T-shaped isomer. The ν_1 band of the linear isomer is 217 cm^{-1} shifted to the red from the monomer absorption (3662 cm^{-1}, indicated by the arrow), while the ν_1 band of the T-shaped isomer exhibits a small blue shift of 11 ± 5 cm^{-1}.

All PESs feature a deep global minimum at the proton-bound site, and for N_2H^+-Ar and OCH^+-Ar this structure is the only minimum.[123] In contrast, due to significant charge density on Si, the PES of $SiOH^+-Ar$ has an additional local minimum at the T-shaped configuration ($D_e = 938$ cm^{-1}, $R_{Ar-Si} = 3.099$ Å, ∠Ar−Si−O = 94.1°) which is separated by a high barrier (~500 cm^{-1}) from the slightly more stable proton-bound minimum ($D_e = 1117$ cm^{-1}, $R_{H-Ar} = 2.099$ Å). As the two isomers have similar binding energies, they are both produced in the cluster ion source and observed in the IR spectrum (Figure 7).[101] They can easily be identified by their characteristic ν_1 frequency shifts: the calculated values of −246 and +16 cm^{-1} for the proton-bound and T-shaped isomers are in good agreement with the observed shifts of −217 and +11 ± 5 cm^{-1}. The analysis of photofragmentation branching ratios of larger $SiOH^+-Ar_n$ complexes provides rough experimental estimates for the binding energies of the T-shaped ($700 < D_0 < 875$ cm^{-1}) and proton-bound isomers ($875 < D_0 < 1400$ cm^{-1}), which are consistent with the ab initio data.[101] T-shaped local minima were also predicted for the dimers with L = He, Ne, and N_2; however, experimentally only the one for N_2 was identified.[199]

d. OH^+-He,Ne. The OH^+-Rg complexes differ in two ways from the AH^+-Rg systems discussed in the preceding sections. First, OH^+ is a diradical with a $^3\Sigma^-$ ground electronic state, and thus the spectra of OH^+-Rg complexes exhibit the effects of electron−spin interaction, providing valuable information on the angular anisotropy of the intermolecular PES.[200] Second, as they are triatomic systems, they are attractive from a theoretical point of view, because it is feasible to calculate full-dimensional PESs at high levels of theory, with subsequent solution of the rovibrational Hamiltonian. In particular, the electron-

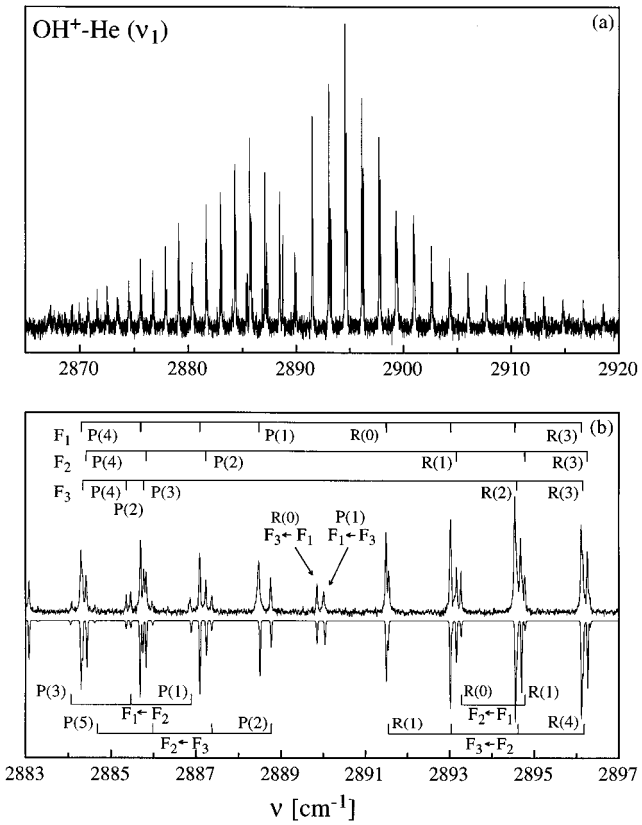

Figure 8. IRPD spectrum of the ν_1 band of OH^+-He in its $^3\Sigma^-$ electronic ground state (Reprinted with permission from ref 102. Copyright 1998 American Institute of Physics). (a) Overview spectrum of the $\Sigma-\Sigma$-type transition. (b) Comparison of experimental (top) and simulated (bottom, $T = 24$ K) spectrum near the band origin, along with assignments for allowed and forbidden transitions. The electron spin ($S = 1$) splits each rotational level in three components (F_i, $i = 1-3$), according to $J = N$, $N \pm 1$.

sparse OH^+-He complex serves as a prototype system (similar to H_2^+-He) to study intermolecular interactions in weakly bound open-shell ionic complexes.

The IRPD spectra of OH^+-He and OH^+-Ne represent the first high-resolution IR spectra of open-shell ionic dimers.[102] The clusters were produced in an electron impact ionization source by coexpanding a mixture of O_2, H_2, and He/Ne. For both dimers, the O−H stretch fundamental (ν_1) and its combination band with the intermolecular bending vibration ($\nu_1 + \nu_b$) were observed at rotational resolution. As an example, Figure 8 shows the experimental ν_1 spectrum of OH^+-He along with a simulation ($T = 24$ K) and assignments of allowed and forbidden transitions. The rovibrational analyses of the observed bands are consistent with the linear proton-bound equilibrium geometries predicted by ab initio calculations.[201,202] The rotational structure was analyzed using standard semirigid linear molecule Hamiltonians appropriate for $^3\Sigma^-$ (ground state, ν_1) and $^3\Pi$ ($\nu_1 + \nu_b$) vibronic states, including terms for rotation, centrifugal distortion, spin−spin and spin-rotation interaction arising from electron spin, and *l*-type doubling arising from the vibrational angular momentum of ν_b. Analysis of the rotational and centrifugal distortion constants yielded $R_{H-Rg} = 1.62$ and 1.67 Å, $k_s = 6$ and 16 N/m, $\omega_s = 180$ and 172 cm^{-1} for the ground states of OH^+-He and OH^+-Ne. Excitation of ν_1 leads to an increase of the interaction, indicated by bond contractions of 0.05 and 0.04 Å, and complexation-induced red shifts of $\Delta\nu_1 = -66.3$ and -169.9 cm^{-1}, respectively. Information about the angular anisotropy of the potential comes from the bending frequencies, ν_b, and the complexation-induced changes in the spin−spin interaction constants. From the latter, the zero-point angular excursion, $\langle\theta\rangle$, was estimated as 25° and 20° for the ground states of OH^+-He and OH^+-Ne, implying that the lighter He atom undergoes larger zero-point bending motion in a more isotropic potential. The smaller average angular excursions in the respective ν_1 states (21°, 17°) indicate that vibrational excitation increases not only the radial bond strength, but also the angular rigidity. As expected, the average angle increases substantially when the intermolecular bending mode is excited ($\langle\theta\rangle = 40°$ for the $\nu_1 + \nu_b$ state of OH^+-He). The smaller harmonic bending force constant in the ν_1 state of OH^+-He ($\nu_b = 203$ cm^{-1}, $k_b = 2.5 \times 10^{-20}$ Nm) compared to OH^+-Ne ($\nu_b = 327$ cm^{-1}, $k_b = 6.7 \times 10^{-20}$ Nm) also reflects a diminished angular anisotropy for the interaction in the former complex.

In general, the spectroscopic data for OH^+-He and OH^+-Ne are in good agreement with the results of rovibrational calculations employing two-dimensional ab initio intermolecular PESs for the $v_1 = 0$ and $v_1 = 1$ states, taking the intramolecular O−H coordinate into account in an adiabatic fashion.[202] These calculations predict dissociation energies of $D_0 = 416$ and 974 cm^{-1} for OH^+-He and OH^+-Ne. Comparison of the open-shell OH^+-Rg dimers with the corresponding closed-shell N_2H^+-Rg complexes reveals the influence of the diradical character on the intermolecular interaction. As the PAs of O and N_2 are similar, the characteristics of the interaction in the OH^+-Rg and N_2H^+-Rg dimers are expected to be comparable if open-shell effects are small. Indeed, both dimers feature similar intermolecular interaction properties (D_0 , $\Delta\nu_1$, k_s, R_{H-Rg}), confirming that the interaction in open-shell complexes with $^3\Sigma^-$ electronic states closely resembles the interaction in the corresponding closed-shell species.[203]

Although the interaction strengths in OH^+-He and N_2H^+-He are similar, the relaxation dynamics of the ν_1 states are rather different.[98,102] The lifetimes of ν_1 and $\nu_1 + \nu_b$ in OH^+-He (>200 ps) are much longer than the lifetimes measured for ν_1, $\nu_1 + \nu_b$, and $\nu_1 + \nu_s$ of N_2H^+-He (38, 76, 19 ps, Figure 5). The weaker coupling between intra- and intermolecular degrees of freedom in OH^+-He probably arises from the lower density of available background states compared to N_2H^+-He, owing to fewer vibrational degrees of freedom and higher intermolecular frequencies. Predissociation of OH^+-He after ν_1 excitation requires that excess energy is partitioned into either fragment translational kinetic energy or OH^+ rotational excitation. Both processes are inefficient, as they involve large changes in the effective quantum numbers of the respective degrees of freedom (energy-gap law).[204,205] In contrast, predissociation of the meta-

stable ν_1 or $\nu_1 + \nu_b/\nu_s$ levels of N_2H^+-He can result in vibrationally excited N_2H^+ fragments (e.g., ν_2), thus significantly decreasing the fragments' translational kinetic energy and N_2H^+ rotational excitation and therefore shortening the predissociation lifetime.

The ν_1 spectra of OH^+-He/Ne show the effects of small local perturbations attributed to weak interactions with dark long-lived quasibound states. These states must involve multiple quanta of the two intermolecular vibrations, lying much higher than the lowest dissociation limit! Possible candidates for such long-lived states are levels involving a high degree of bending excitation. As the barrier for internal rotation is low, these levels are likely to have practically free internal rotor character and therefore interact only weakly with the dissociation continuum and the ν_1 mode.

e. $CH_3CNH^+-H_2$. The $CH_3CNH^+-H_2$ dimer is another member of the AH^+-H_2 series studied by means of IRPD spectroscopy and ab initio calculations.[128] The rotational structure and vibrational frequency shifts of the observed ν_1 (H−H stretch) and ν_2 (N−H stretch) fundamentals are consistent with a proton-bound T-shaped equilibrium structure, where the linear $CCNH^+$ backbone of CH_3CNH^+ (C_{3v}) points toward the midpoint of H_2 (Figure 4). The calculations yield a dissociation energy of $D_e = 1102$ cm^{-1}. The H_2 unit can rotate freely around the intermolecular axis (calculated 6-fold barrier $V_6 < 0.1$ cm^{-1}), whereas internal rotation around the axis perpendicular to the intermolecular bond is strongly hindered (calculated 2-fold barrier $V_2 \sim 1050$ cm^{-1}). The major changes of the monomer structures upon complex formation are elongations of the N−H and H−H bonds. These structural changes are accompanied by red shifts in the respective frequencies, $\Delta\nu_1 \sim -64$ cm^{-1} and $\Delta\nu_2 = -183$ cm^{-1}. The relaxation dynamics of the complex are highly mode selective. The higher lying ν_1 state couples only weakly to the intermolecular degrees of freedom leading to a lifetime $\tau_1 > 130$ ps. In contrast, the coupling of the lower lying ν_2 state is more efficient, which reduces the lifetime to $\tau_2 < 30$ ps. The rotational structure of the ν_1 fundamental was analyzed assuming free internal rotation of H_2 around the intermolecular axis (molecular symmetry group G_{12}), and the rotational constants resulted in an approximate intermolecular separation, $R_{H-H_2} \sim 1.9$ Å.

2. $AH_k^+-L_n$ ($k > 1$)

a. H_2^+-He. The open-shell H_2^+-He complex is of fundamental interest as it is a few electron system for which high-quality ab initio and bound-state calculations are feasible. Laboratory-based spectroscopic studies of the complex are desirable because of its possible existence in interstellar regions and also because knowledge of its structure and dynamics should help to achieve a better understanding of the ion−molecule reactions in He- and H_2-containing plasmas (such as the interstellar medium).

Near dissociation levels of the H_2^+-He complex have been studied by subjecting a beam of highly excited complexes to tunable MW radiation with detection of H_2^+ fragment ions produced via electric field dissociation.[109,110] While the technique probes levels that lie within a few cm^{-1} of the $H_2^+ + He$ dissociation limit, because of the high resolution with which the spectra are recorded, the transition frequencies are sensitive to details of the entire PES. Several MW absorptions have been observed, and perhaps the most informative of these occurs at 15.2 GHz (Figure 9). It consists of two sets of sextets, one of which is only apparent at higher irradiation levels, and has been assigned to transitions between a parity doublet of H_2^+-He containing *ortho* H_2^+ ($i = 1$), the structure being due to nuclear hyperfine effects.

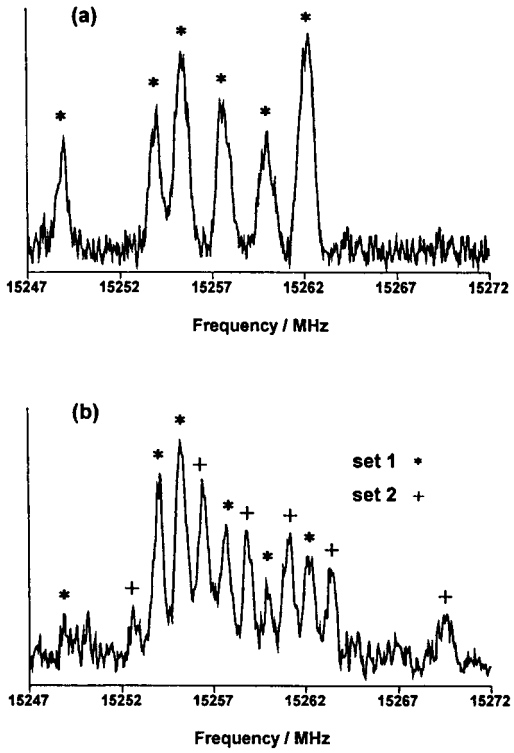

Figure 9. Near dissociation transition of H_2^+-He near 15.2 GHz (Reprinted with permission from ref 109. Copyright 1996 Elsevier Science). (a) Parallel Doppler-shifted resonances recorded with a microwave power level of 6.3 μW. (b) Parallel Doppler-shifted resonances recorded with a microwave power level of 50 μW, showing the appearance of a second sextet at higher power levels.

Several H_2^+-He PESs have been developed and used to determine bound-state levels and effective rotational constants.[109,206−215] The most recent of these was carefully constructed in an attempt to explain the near dissociation MW transitions.[215] It is fitted to ab initio points in the short to intermediate range and has the long-range form expected from induction, electrostatic, and dispersion interactions between the constituents. The surface exhibits two equivalent linear minima ($D_e = 2717$ cm^{-1}), separated by a substantial barrier (~2400 cm^{-1}) in the T-shaped configuration (Figure 10). At the potential minimum, the H_2^+-He center of mass separation is 1.5727 Å and the H−H bond length is 1.098 Å.

The bound-state energies for the low-lying levels of complexes containing *ortho* and *para* H_2^+ are very similar, a consequence of the large tunneling barrier. The intermolecular bend and stretch frequencies are predicted to be 646 and 716 cm^{-1}, respectively.[215] The excited H−H stretching state lies at approximately

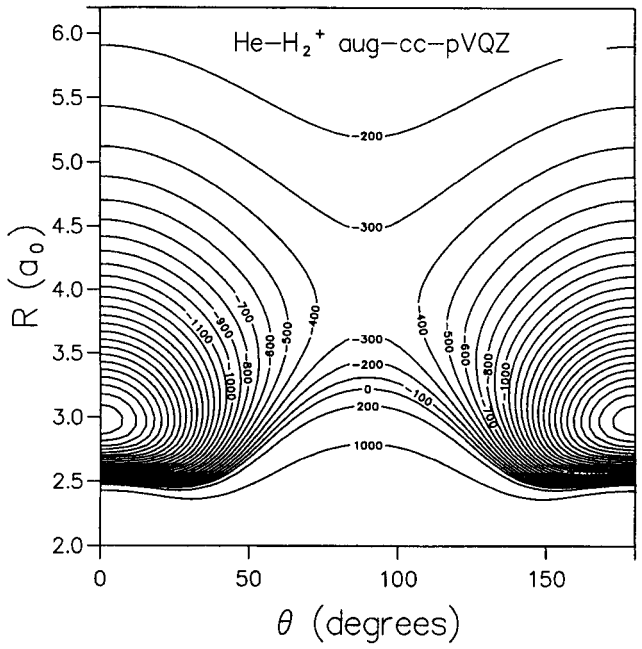

Figure 10. Contour plot of the QCISD(T) aug-cc-pVQZ potential for H_2^+−He with the H−H distance fixed at $r = 2a_0$ (Reprinted with permission from ref 215. Copyright 1999 American Institute of Physics). Contours (in cm^{-1}) are shown relative to H_2^+ ($r = 2a_0$) + He at $R = \infty$.

1830 cm^{-1}, slightly above the H_2^+ + He dissociation limit (D_0 = 1754 cm^{-1}), and is predicted to be substantially broadened by predissociation.[213,215]

While the bound-state calculations predict the existence of near dissociation levels suitable for explaining the MW lines, there are currently no definite assignments. The discrepancy between the experimental and calculated transition frequencies may arise from several sources. The bound-state calculations show that small changes in the PES result in significant shifts in the absolute and relative energies of near dissociation states.[215] Adequate treatment of the near dissociation levels may also require consideration of non-Born−Oppenheimer effects that are known to be important in H_2^+ [216] and H_3^+.[217]

b. HNH^+−He,Ar. The nitrenium ion, HNH^+, is a bent diradical in its $^3B_1$ electronic ground state (C_{2v}).[218] It can, however, be treated as a quasilinear species ($^3\Sigma_g^-$, $D_{\infty h}$) owing to its low barrier to linearity ($V_b \sim 200$ cm^{-1}). Ab initio calculations and rotationally resolved IRPD spectra of HNH^+−Ar/He in the N−H stretch region revealed that the Rg ligands bind to one of the two H atoms forming linear proton bonds.[103,104] The diradical character and quasilinearity are not significantly affected upon complexation.

The relatively high binding energy of the HNH^+−Ar dimer (D_e = 1773 cm^{-1}) has a drastic effect on the composition of the N−H stretch normal coordinates.[104] In the HNH^+ monomer, symmetric (ν_1) and antisymmetric (ν_3) N−H stretch modes arise from the resonant interaction between the two degenerate local N−H oscillators. Complexation with Ar significantly reduces the frequency of the N−H oscillator involved in the intermolecular bond, leading to two normal modes in the dimer that can be described to a good approximation as bound (ν_1) and free (ν_3) N−H stretch vibrations. The changes in the N−H normal coordinates upon Ar complexation affect both their intensities and frequencies: the ν_1 mode, IR forbidden in HNH^+, becomes for HNH^+−Ar more intense than the strong IR-active ν_3 mode and shows a much larger red shift (−300 ± 50 vs −73 cm^{-1}). In addition, the relaxation dynamics are largely different for both vibrational states: as expected, the bound N−H stretch mode couples much more efficiently to the intermolecular degrees of freedom, leading to a shorter lifetime (∼25 ps) compared to the free N−H stretch (>130 ps).

Analysis of the molecular constants of HNH^+−Ar yield ground-state parameters of R_{H-Ar} = 2.06 Å, k_s = 20 N/m, ω_s = 171 cm^{-1}. From the spin−spin interaction constant, the zero-point bending excursion could be estimated as $\langle\theta\rangle = 17°$. The radial and angular properties of the intermolecular potential are almost unchanged upon excitation of the free N−H stretch. In contrast, excitation of the bound stretch leads to a significantly shorter and stronger intermolecular bond (R_{H-Ar} = 2.01 Å, $k_s \sim 28$ N/m, $\omega_s \sim 200$ cm^{-1}). The fundamental frequencies of ν_s in the ground (ν_s = 170 cm^{-1}) and ν_1 state (ν_s = 197 cm^{-1}), derived from the weak $\nu_1 + \nu_s$, $\nu_1 + \nu_s - \nu_s$, and $\nu_1 - \nu_s$ hot and sequence bands, confirm these conclusions.

In contrast to HNH^+−Ar, the interaction in HNH^+−He is weak (D_e = 273 cm^{-1}) and the effects of complexation on the properties of the N−H normal modes are small.[103] The ν_1 and ν_3 modes of this dimer are best described as symmetric and antisymmetric N−H stretch vibrations, and the intensity of ν_3 is calculated to be at least 1 order of magnitude higher than that of ν_1. Experimentally, only the ν_3 fundamental could be observed and the analysis of the molecular constants yielded ground-state parameters of R_{H-He} = 1.90 Å, k_s = 1.5 N/m, ω_s = 90 cm^{-1}, $\langle\theta\rangle$ = 24°. Severe perturbations in the ν_3 state prevented detailed analysis of its molecular constants; however, the small complexation-induced red shift, $\Delta\nu_3 = -7$ cm^{-1}, implies that the intermolecular interaction is almost unaffected by ν_3 excitation.

The ab initio calculations showed that the barrier to linearity is reduced from 152 cm^{-1} in HNH^+ to 111 and 66 cm^{-1} in HNH^+−He and HNH^+−Ar.[103,104] Apparently, the stronger intermolecular bonds to larger Rg atoms changes the electronic properties of HNH^+ such that the barrier decreases, and dimers with Xe or Kr may have linear equilibrium geometries. As the calculated barriers for internal rotation of HNH^+ within HNH^+−He (156 cm^{-1}) and HNH^+−Ar (806 cm^{-1}) are much higher than the HNH^+ rotational constant (8 cm^{-1}),[218] this motion is largely quenched and the dimers are much closer to the semirigid bender than the free internal rotor limit. Nonetheless, the weakly bound HNH^+−He dimer may serve as a suitable model system to study the intermolecular forces in an open-shell ionic dimer with low barriers for motions in both intermolecular and intramolecular degrees freedom (internal rotation, quasilinearity). As the system contains only four atoms of which only one is heavy, it should be possible to determine the interaction potential of this dimer at high levels of theory and solve the rovibra-

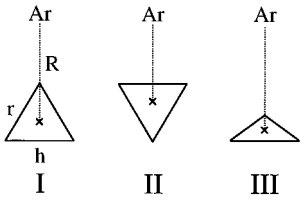

Figure 11. Several stationary points on the calculated PES of H_3^+-Ar (Reprinted with permission from ref 219. Copyright 1987 Elsevier Science): (I) proton-bound global minimum (C_{2v}); (II) side-bound transition state (C_{2v}); (III) top-bound transition state (C_{3v}).

tional Hamiltonian in all dimensions.

NH and CO have similar PAs, and the fact that the HNH^+ diradical does not form a significantly stronger bond to Rg atoms than the closed-shell OCH^+ ion confirms that the interaction of Rg atoms with linear open-shell molecules in $^3\Sigma$ electronic states resembles the interaction with related closed-shell species and does not lead to the formation of an incipient chemical bond.[203]

c. H_3^+-Ar. Absorption spectra of the H_3^+-Ar dimer and its deuterated isotopomers in the millimeter and submillimeter spectral range were obtained in a magnetically confined glow discharge of $H_2/D_2/Ar$ mixtures in a liquid N_2-cooled cell.[21,130−132] The large dipole moment of the complex (∼8−9 D)[21,219] enabled the detection of its rotational transitions despite the low concentrations achieved in the discharge cell (∼3×10^8 cm^{-3}).[21] In addition, MW spectra of the lowest rotational transition of D_3^+-Ar and D_2H^+-Ar were recorded in a FTMW spectrometer coupled to a pulsed supersonic discharge nozzle.[107] The D_3^+-Ar spectrum was the first high-resolution spectrum of an ionic complex and was recorded accidentally during a search for CH_2D^+ absorptions in a $CH_4/D_2/Ar$ discharge.[131] The carrier of the obtained spectrum was identified by considering chemical and spectroscopic arguments.[21] The D_3^+-Ar spectrum was observed in pure Ar/D_2 discharges and disappeared when species with PAs larger than D_2 were added to the discharge (because D_3^+ is depleted by the $D_3^+ + X \rightarrow D_2 + XD^+$ reaction). Moreover, the spectrum is characteristic of a near prolate symmetric top with an A rotational constant expected for a D_3^+-containing species. The small inertial defect and nuclear spin statistical weights are indicative of a planar C_{2v} geometry with two equivalent deuterons, where the Ar ligand binds either to the vertex or the side of the D_3^+ triangle (structures I and II, Figure 11). The molecular constants result in an intermolecular separation R = 2.384 Å and a harmonic stretching force constant k_s = 38 N/m.[21,130]

According to ab initio calculations, the equilibrium structure of H_3^+-Ar corresponds to the proton-bound configuration (structure I, Figure 11).[219−221] The formation of the intermolecular bond (D_e = 3150 cm^{-1}, R_e = 2.363 Å)[219] is accompanied by partial charge transfer (0.14 e) and significant deformation of the H_3^+ triangle: r increases by 0.07 Å and h decreases by 0.05 Å. In general, the structure of H_3Rg^+ dimers depends on the PA of the Rg atom and changes from H_3^+-Rg toward H_2-HRg^+ as PA_{Rg} increases.[220,221] For Rg atoms with $PA_{Rg} < PA_{H_2}$ (Rg = He, Ne, Ar), the structures of H_3Rg^+ are of the form H_3^+-Rg, while in the case $PA_{Rg} > PA_{H_2}$ (Rg = Kr, Xe), the H_3Rg^+ geometries are of the type H_2-HRg^+. The calculated binding energies for H_3^+-Ar and D_3^+-Ar, $D_0 \sim 2660$ and 2830 cm^{-1},[219] are compatible with the measured bond enthalpies, $-\Delta H° = 2340 \pm 70$ and 2430 ± 70 cm^{-1}.[222] The side- and top-bound structures of H_3^+-Ar (structures II and III, Figure 11) are calculated to be transition states for the in-plane and out-of-plane internal rotations of H_3^+ with barriers of V_b = 1370 and 1930 cm^{-1}, respectively.[219] As the intermolecular interaction is much weaker at the transition states than at the global minima, the monomer deformation is small for these configurations.

The splittings observed in the H_3^+-Ar and D_3^+-Ar spectra were attributed to tunneling between three equivalent equilibrium configurations.[21,130] Due to Coriolis coupling between the internal and the end-over-end rotation, the splittings show a strong dependence on the degree of rotational excitation.[21,107,132] So far, models employed for analysis of the tunneling splittings assume a single planar tunneling path between vertex- and side-bound structures.[130,132,223] The splittings and nuclear spin statistical weights observed for the partly deuterated species could only be rationalized assuming that the proton-bound structures are minima while the side-bound structures are transition states (in agreement with the ab initio calculations). The value derived for the 3-fold barrier, V_3, depends strongly on the details of the model.[130] For example, assuming a rigid triangle and a fixed intermolecular separation R, $V_3 \sim 1600-1700$ cm^{-1}. This is reduced to ∼1000 cm^{-1} when both the triangle structure and R are allowed to depend on the internal rotation angle.[130,132,223] The potential parameters derived from the analysis of the tunneling splittings were considered as effective parameters, as the effects of the neglected out-of-plane tunneling path (via the C_{3v} transition state, structure III) might be significant.

d. $H_3O^+-(H_2O)_n$ and $H_3O^+-(H_2)_n$. Protonated water clusters have been investigated in the gas phase to elucidate, from a microscopic point of view, the properties of proton solvation and transport in aqueous solutions. Early low-resolution (∼40 cm^{-1}) vibrational IR spectra in the O−H stretching region of $H_3O^+-(H_2O)_n$ complexes were recorded by direct absorption using pulsed radiolysis in a White cell (n = 3−5).[224] Higher resolution spectra (∼1 cm^{-1}) were obtained by IRPD spectroscopy of mass-selected complexes produced in a high-pressure corona discharge coupled to a supersonic expansion (n = 1 − 8).[31,86,88,89,225] In the latter experiments, multiphoton schemes were necessary to resonantly excite the smaller clusters to levels above the lowest dissociation threshold, corresponding to the loss of a single H_2O ligand.[86,89,225] The observed bands were assigned to O−H stretching vibrations of either the H_3O^+ core ion or H_2O ligands, by considering the observed shifts and splittings with respect to the corresponding frequencies of the H_3O^+ and H_2O monomers, symmetry considerations, IR intensities, and ab

initio calculations. The general picture of sequential proton hydration derived from spectroscopic studies,[31,86,89,224,225] thermodynamic data,[226−228] ab initio calculations,[225,229−237] and molecular dynamics simulations[238−242] is that in clusters with $n \leq 3$, equivalent H_2O ligands form strong hydrogen bonds to the protons of H_3O^+, with the completion of the first solvation shell at $n = 3$. Addition of further ligands ($n > 3$) leads to the formation of a hydrogen-bonded network with weaker intermolecular bonds. The structure of these complexes is less certain, and evidence for ring and three-dimensional structures has been presented even for small n.[225,231] The $n = 20$ complex appears to adopt a stable closed-shell clathrate structure (dodecahedron).[228,243]

According to high-level ab initio calculations,[230−236] the equilibrium geometry of $H_5O_2^+$ ($n = 1$) corresponds to a symmetric $H_2O-H^+-OH_2$ structure (C_2 symmetry) with a near linear hydrogen bond ($\angle$OHO $\sim 174°$, $R_e \sim 1.20$ Å).[235] (This is in contrast to the isoelectronic $H_7N_2^+$, for which the asymmetric $NH_4^+-NH_3$ geometry is predicted to be more stable, section III.A.2.e.) The asymmetric $H_3O^+-H_2O$ structure (C_s symmetry, $\angle$OHO $\sim 176°$, $R_{e1} \sim 1.13$ Å, $R_{e2} \sim 1.26$ Å),[235] predicted to be the global minimum at low theoretical levels,[229,232] is a transition state lying only ~0.4 kcal/mol above the C_2 structure.[232,233,235] The oxonium ion, H_3O^+, is isoelectronic with NH_3, and the positive charge is distributed throughout the molecule. The charge is further delocalized in $H_5O_2^+$, and the competition between covalent contributions (favoring $H_2O-H^+-OH_2$) and electrostatic ion−dipole forces (favoring $H_3O^+-H_2O$) leads to a flat potential for the proton motion. The calculated global minima of $H_7O_3^+$ ($n = 2$) and $H_9O_4^+$ ($n = 3$) correspond to dihydrated and trihydrated H_3O^+, respectively. The hydrogen bonds are nearly linear (deviation <5°) and mainly based upon electrostatic forces.[231,233,237] The charge delocalization and accompanying change in bonding mechanism is also evident from the decreasing hydration enthalpies (~32, ~20, ~17 kcal/mol for $n = 1 - 3$).[226,227] The reduced interaction strength increases the O−O separation, which in turn leads to the formation of a barrier for the proton motion.

The vibrational analysis of the $H_5O_2^+$ spectrum assumed a symmetric equilibrium structure (C_2).[86,88,89] A band at 3684.4 cm^{-1}, assigned to the asymmetric O−H stretch vibration of the H_2O units, displayed equidistant Q branches characteristic for a perpendicular transition of a near prolate symmetric top (Figure 12, top), with spacings $2(A - B) \sim 11.6$ cm^{-1} in good agreement with the calculated value (11.65 cm^{-1}).[86,89] In subsequent experiments, rotational fine structure of this band was observed using a color center laser, which improved the spectral resolution from ~0.5 to ~0.01 cm^{-1}.[89] In total, 12 R branches were identified in the vicinity of the $^RQ_0$ and $^RQ_1$ Q branches (Figure 12, bottom).[89] The derived $B + C$ value (0.51 cm^{-1}) is 14% smaller than the ab initio value, consistent with the anharmonicity of the intermolecular stretch. The 12 branches were thought to arise from the in-phase and out-of-phase combinations of the asymmetric O−H stretch, each of them split into six components arising from large ampli-

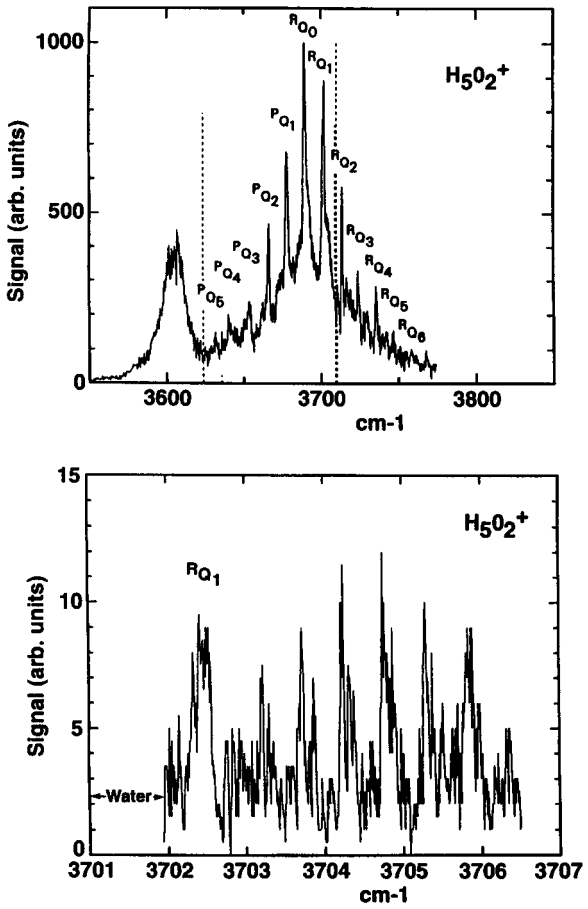

Figure 12. Multiphoton IRPD spectrum of $H_5O_2^+$ (Reprinted with permission from ref 89. Copyright 1994 Academic Press). Low-resolution scan of the symmetric (3609 cm^{-1}) and antisymmetric (3684 cm^{-1}) O−H stretch vibrations of the H_2O moieties (top). The dashed lines correspond to calculated positions and intensities. High-resolution scan in the region of the $^RQ_1$ branch of the perpendicular transition corresponding to the antisymmetric O−H stretch (bottom), showing tunneling splittings in the R branch (see text).

tude motions. For several internal motions, the calculated barriers were low enough (<1 kcal/mol) to produce the observed tunneling splittings: e.g., internal rotations of the water ligands either around the $O-H^+-O$ or their local C_2 axes, and motions involving inversion of H_2O-H^+. On the basis of group-theoretical considerations, the pattern of the splitting, nuclear spin statistical weights, and selection rules were derived for various feasible tunneling schemes.[89,236] Assuming a C_2 equilibrium structure and no scrambling of the central proton (molecular symmetry group G_{16}), a splitting into at most six components can occur. However, as not even qualitative agreement with experiment could be achieved, the interpretation of the 12 R branches remains ambiguous.[89] For example, the scenario with an asymmetric C_s equilibrium structure ($H_3O^+-H_2O$) could also produce 12 tunneling components, six from the motions feasible for the symmetric configuration, each of them doubled by the tunneling motion of the central proton.

As for $H_5O_2^+$, analyses of the $H_7O_3^+$ and $H_9O_4^+$ vibrational spectra yield only qualitative information about their geometries. The spectra are compatible

with dihydrated and trihydrated H_3O^+ ions of the form $H_3O^+-(H_2O)_{2,3}$. The water ligands are equivalent, and closure of the first solvation shell occurs at $n = 3$. The $H_7O_3^+$ spectrum was analyzed in terms of a planar H_3O^+ ion (C_{2v}),[86] while calculations predict the C_s structure with a pyramidal H_3O^+ core to be more stable.[231,237] Similarly, the interpretation of the $H_9O_4^+$ spectrum was based on either a D_{3h} or C_{3v} structure,[86] while calculations yielded a global minimum with C_3 symmetry.[231,233] Using a color center laser, a high-resolution spectrum of $H_9O_4^+$ was obtained for the band near 3730 cm^{-1}, assigned to the a_1 component of the asymmetric O−H stretch of the H_2O ligands (assuming C_{3v} symmetry for this oblate symmetric top). Analysis of the end-over-end rotational structure of the parallel band resulted in $B = 0.17$ cm^{-1}, in good agreement with the calculated value (0.175 cm^{-1}). Two types of tunneling splittings were observed with separations of 0.93 and 0.21 cm^{-1}, and possible sources include internal rotations of the H_2O ligands around their local C_2 axes as well as inversion of the central H_3O^+ ion. Vibrational spectra of clusters in the size range $n = 4-7$ provide evidence for the coexistence of $H_3O^+-(H_2O)_n$ and $H_5O_2^+-(H_2O)_{n-1}$ isomers at temperatures of 170 K, i.e., the extra proton is either localized on one H_2O molecule or shared between two molecules.[225] In addition, less stable isomers with ring structures were identified.[225]

Molecular dynamics simulations provide insight into the extent of proton delocalization in protonated water complexes as a function of cluster size and temperature.[238−242] For low temperatures, the $H_5O_2^+$ ion is always close to the symmetric $H_2O-H^+-OH_2$ configuration.[238,240] The probability for finding geometries similar to $H_3O^+-H_2O$ rises from zero at $T <$ 40 K to 9% at 225 K and 18% at 360 K.[240] The coupling of the central proton motion to other vibrational degrees of freedom increases drastically with temperature and leads to spectral broadening.[240] Simulations for $H_9O_4^+$ confirm the closure of the first hydration shell with a relatively stable H_3O^+ core even at 360 K.[241] For complexes in the size range $n = 4-6$, the number of structural isomers with energies close to the global minimum increases rapidly.[239,241] Simulations for larger clusters aim at a microscopic understanding of the high proton mobility in liquid water.[242] Early explanations[56,58,242,244] include proton diffusion (Grotthus diffusion),[245] thermal hopping,[246] and proton tunneling,[244,247] while later structural models invoked larger intermediates: (i) the Eigen $H_9O_4^+$ ion,[248] corresponding to a 3-fold hydrated oxonium ion, and (ii) the Zundel $H_5O_2^+$ cation.[56] Recent ab initio path integral simulations for the $n = 31$ cluster show, however, that at thermal temperatures the protonic defect is very fluxional and cannot be assigned to particular structures.[242] Instead, the fluxional defect is delocalized over several hydrogen bonds in the network, owing to its quantum mechanical nature, low barriers, and large zero-point effects. At thermal energies, the rate of proton migration is mainly determined by the large quantum mechanical delocalization of the defect.

Before spectra of the pure protonated water complexes were obtained, IRPD spectra of $H_3O^+-(H_2O)_n-H_2$ were recorded for $n = 1-3$.[85,86,88] It was speculated that the weakly attached H_2 ligand has only a minor effect on the $H_3O^+-(H_2O)_n$ spectra (messenger technique) and furthermore that by attaching an H_2 ligand the complicated multiphoton schemes necessary to dissociate pure $H_3O^+-(H_2O)_n$ complexes could be avoided, as resonant one-photon absorption by $H_3O^+-(H_2O)_n-H_2$ is sufficient to rupture the weak bond with H_2. Comparison of the $H_3O^+-(H_2O)_n-H_2$ spectra with those of $H_3O^+-(H_2O)_n$ revealed, however, that the H_2 ligand has a substantial influence on the structural and spectroscopic properties of the $H_3O^+-(H_2O)_n$ core.[86,88] The preferred binding site of H_2 in $H_3O^+-(H_2O)_n-H_2$ is the same as that for the $(n + 1)$th H_2O ligand in $H_3O^+-(H_2O)_{n+1}$. Thus, complexation with H_2 or H_2O has a similar effect on the properties of $H_3O^+-(H_2O)_n$, though less pronounced in the case of H_2 due to the weaker interaction. For example, attachment of H_2 to $H_5O_2^+$ reduces its symmetry from C_2 ($H_2O-H^+-OH_2$) to C_s ($H_3O^+-H_2O$) in the same manner as attachment of H_2O to $H_5O_2^+$. The spectrum of $H_7O_3^+-Ne$ closely resembles the one of $H_7O_3^+$, indicating that the interaction with the "spy" Ne is sufficiently weak for the messenger technique to work.[86] However, the signal-to-noise ratio in the $H_7O_3^+-Ne$ spectrum is significantly lower compared to the pure $H_7O_3^+$ spectrum, due to the much smaller densities of $H_7O_3^+-Ne$ achieved in the ion source. As in matrix isolation techniques, the effects of a messenger on the spectrum of a floppy parent cluster ion are difficult to predict a priori. The lighter Rg atoms (He and Ne) are generally least disruptive.

IRPD spectra of $H_3O^+-(H_2)_n$, $n = 1-3$, in the spectral region of the H−H and O−H stretch vibrations are consistent with structures in which equivalent H_2 ligands are weakly attached in a T-shaped fashion to the protons of the central H_3O^+ core.[88] The intermolecular bonds are much weaker (∼3−4 kcal/mol) than in the corresponding $H_3O^+-(H_2O)_n$ complexes. The binding energy decreases with the number of H_2 ligands, owing to larger delocalization of the charge. This trend is directly reflected in the decreasing red shift of the H−H stretch (−115, −106, −96 cm^{-1} for $n = 1-3$) and bound O−H stretch frequencies. The broad band assigned to the free O−H stretch disappears for $n = 3$, confirming closure of the first solvation shell at this cluster size. Preliminary analysis of the rotational structure of the H−H stretch band of the $H_3O^+-H_2$ dimer resulted in an approximate $B + C$ value (∼2 cm^{-1}), consistent with the calculated ab initio geometry ($R_e = 1.33$ Å, $D_e = 3.2$ kcal/mol). Observed splittings of 0.6−0.8 cm^{-1} were thought to arise either from inversion of H_3O^+ or the presence of *ortho* and *para* modifications of H_2.

e. $NH_4^+-He,Ar,(NH_3)_n$. The PESs of charged complexes often exhibit large anisotropy, even in Rg-containing systems. Consequently, the wave functions associated with the lowest few intermolecular vibrational motions (which are usually probed in spectroscopic studies) tend to be localized and theoretical calculations are required to describe the hidden regions of their PES. The high PA of NH_3

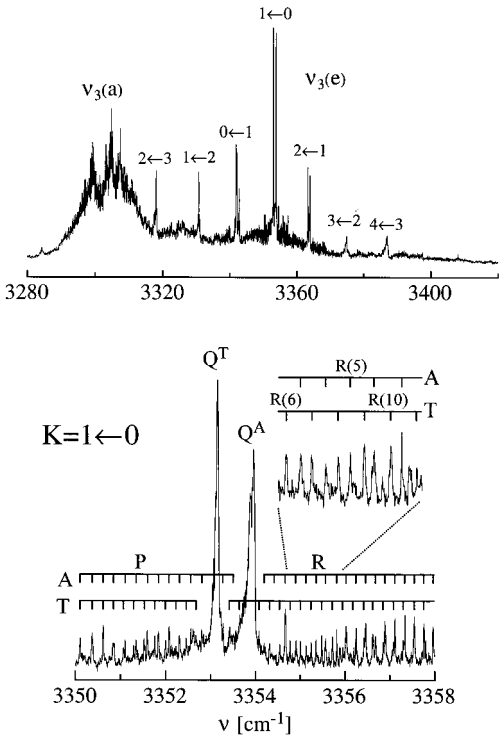

Figure 13. IRPD spectrum of NH_4^+-Ar in the vicinity of the ν_3 band of NH_4^+. The band is split into a parallel ($\Delta K = 0$) and perpendicular ($\Delta K = \pm 1$) component (top) (Reprinted with permission from ref 134. Copyright 1996 Elsevier Science). The $\Delta K = \pm 1$ subbands of the perpendicular band display further splittings due to hindered internal rotation. For example, the $K = 1 \leftarrow 0$ subband is split into two components with A and T symmetry, respectively (bottom) (Reprinted with permission from ref 136. Copyright 2000 Taylor & Francis).

leads to relatively weak interactions and low barriers for internal rotation of NH_4^+ in the NH_4^+-Rg dimers, making them favorable model systems for spectroscopically probing the potential anisotropy.[133−136,249,250]

Rotationally resolved IRPD spectra of NH_4^+-He and NH_4^+-Ar were obtained in the vicinity of the triply degenerate asymmetric N−H stretch fundamental of NH_4^+, ν_3 (t_2) = 3334 cm^{-1}.[251,252] The ν_3 band of NH_4^+-Ar shows splittings in both the vibrational and rotational structure (Figure 13), which were attributed to hindered internal rotation of NH_4^+.[134,135,250] Vibrational anisotropy splits the ν_3 band into a red-shifted (−31 cm^{-1}) parallel and a blue-shifted (+12 cm^{-1}) perpendicular component, corresponding to $\nu_3(a_1)$ and $\nu_3(e)$ modes of a symmetric top in the rigid rotor limit. Further splittings (∼0.5−1 cm^{-1}) arise from quantum mechanical tunneling through barriers on the PES separating the four equivalent minima.

The effects of hindered internal rotation on the ν_3 spectrum of NH_4^+-Ar were analyzed using a theoretical model developed for tetrahedral molecule−Rg dimers.[66,67] This model assumes that the tetrahedron is not significantly perturbed upon complexation and that the intramolecular vibrations, the end-over-end rotation, and the intermolecular stretching vibration of the complex can be separated in an adiabatic fashion from the internal rotation of the tetrahedron (these approximations were shown to be realistic for the NH_4^+-Ar system[136,250]). The intermolecular separation is kept fixed at an effective value (fixed-R model) determined from the experimental rotational constants of the dimer. The anisotropy of the interaction can then be described by a two-dimensional angular representation of the intermolecular PES containing only a few parameters: (i) a vibrational anisotropy parameter, V_2, which is correlated with the magnitude of the vibrational splitting of the ν_3 band; (ii) internal rotation anisotropy parameters, V_i (i = 3, 4, 6, etc.), which characterize the anisotropy of the PES with respect to internal rotation of the tetrahedron.

Initially, the anisotropy parameters for the NH_4^+-Ar interaction were obtained in a least-squares fit of the fixed-R model to the experimental data. The resulting PES ($V_2 \sim 90$ cm^{-1}, $|V_3| \sim 220$ cm^{-1}, $V_4 = 0$) was consistent with either vertex-bound or face-bound global minima.[134] Subsequent ab initio calculations[135,249,250] revealed that the global minima are the vertex-bound structures ($R_e = 3.338$ Å, $D_e = 927$ cm^{-1}), which are separated by barriers of about 200 cm^{-1} occurring at the edge and face-bound orientations.[250] However, the calculated rotational anisotropy parameters ($V_3 \sim -100$ cm^{-1}, $V_4 \sim 15$ cm^{-1})[250] differ considerably from the ones obtained from the fit using the fixed-R model.[134] Nonetheless, both potentials reproduce the experimental spectra reasonably well. Test calculations showed that the difference in the anisotropy of the calculated and fitted PESs does not originate from an inadequate level of theory in the ab initio calculations or invalid approximations in the fixed-R model.[136,250] Instead, the discrepancy arises mainly from a large correlation between the anisotropy parameters in the fit and their strong dependence on the truncation of the expansion of the potential.[66,250] The fixed-R model provides effective parameters which reproduce the observed spectrum but does not properly represent the true PES. This example demonstrates the difficulties and ambiguities involved with inverting limited spectral data to obtain the PES of a nonrigid complex.[63−65] It also emphasizes the fact that in such cases ab initio calculations are necessary to obtain at least a semiquantitative representation of the true PES, which can then be iteratively refined by comparison with experiment to obtain a PES of spectroscopic accuracy.

Analysis of the end-over-end rotational structure resulted in an average intermolecular separation of $R_0 \sim 3.38$ Å for NH_4^+-Ar.[136] The dissociation energy of the dimer estimated from photofragmentation branching ratios of larger $NH_4^+-Ar_n$ complexes, $D_0 \sim 825$ cm^{-1},[135] is in good agreement with the ab initio value, $D_0 = 774$ cm^{-1}.[136] In general, ν_3 excitation has only a minor influence on both the interaction strength and the rotational anisotropy. The large vibrational anisotropy suggests that the wave function of NH_4^+-Ar is mainly localized at vertex-bound configurations.[136]

Among other Ar-containing ionic dimers, H_3^+-Ar (section III.A.2.c) is most similar to NH_4^+-Ar in terms of its internal rotation dynamics. Both complexes have proton-bound equilibrium geometries;

however, partial charge transfer in H_3^+-Ar causes a stronger interaction ($D_0 \sim 2700$ cm^{-1}), accompanied by appreciable complexation-induced deformations of the H_3^+ ion.[219] The barrier for internal rotation is therefore also higher ($V_b \sim 1000-1800$ cm^{-1}).[130,219] Nevertheless, the observed tunneling splittings are similar for both complexes, as the ratios of the internal rotation barrier and the monomer rotational constant are similar, $V_b/b \sim 30-40$. Comparison of the calculated PESs of the NH_n^+-Ar series ($n = 2-4$) reveals that the relative anisotropy of the interaction, defined as the ratio V_b/D_e, diminishes with increasing separation of the equivalent hydrogen atoms: the barrier to internal rotation ($V_b \sim 800$, 300, 200 cm^{-1}) decreases faster than the interaction energy at the global minimum ($D_e \sim 1770$, 1130, 930 cm^{-1}) as n increases from 2 to 4.[104,136,253]

The ν_3 spectrum of NH_4^+-He is qualitatively different from that of NH_4^+-Ar. Apart from a small blue shift ($\sim$0.7 cm^{-1}), it closely resembles the spectrum of bare NH_4^+, indicating that neither rotational nor vibrational motions of the NH_4^+ ion are strongly affected by complexation with He.[133] This complex is thus close to the free rotor limit. The large widths of unresolved Q branches ($\sim$0.5 cm^{-1}) indicate unresolved structure due to some hindrance to internal rotation; however, the degree of anisotropy is much smaller than that for NH_4^+-Ar. For a nearly free rotor, the end-over-end rotational structure is weak and is thus not observed in the NH_4^+-He spectrum. Thus, almost all information concerning the interaction potential of NH_4^+-He comes from ab initio calculations.[133] They predict a vertex-bound minimum structure ($D_e \sim 150$ cm^{-1}, $R_e \sim 3.17$ Å) and barriers for internal rotation less than 30 cm^{-1} via both the edge- and face-bound configurations. Within the NH_4^+-Rg series, the change in interaction strength is strongly correlated with the change in the anisotropy: while NH_4^+-He is close to the limit of free internal rotation, NH_4^+-Ar is a strongly hindered rotor close to the rigid limit. Preliminary spectra and calculations reveal that NH_4^+-Ne represents an intermediate case between these two limits.[254]

In ionic NH_4^+-Rg dimers, the strength and anisotropy of the attractive interaction are dominated by inductive forces which favor vertex-bound global minima.[250,255] In contrast, in related neutral species (e.g., SiH_4-Rg, CH_4-Rg, SiF_4-Rg),[256-264] the attraction is weaker and arises almost entirely from dispersion. Hence, the intermolecular PESs of neutral dimers have lower anisotropies and face-bound global minima, as these binding sites allow closer approach of the Rg.

Vibrational spectra of $NH_4^+-(NH_3)_n$ complexes were obtained at low resolution ($\sim$25 cm^{-1}) by direct absorption spectroscopy using pulsed radiolysis in a gas cell ($n = 0-4$)[265] and at higher resolution ($\sim$1 cm^{-1}) by (multiphoton) IRPD spectroscopy in an ion trap ($n = 1-10$).[31,87,137,266] The observed bands were assigned to vibrations of both the NH_4^+ core and the NH_3 ligands. The analysis of the magnitude and direction of the observed frequency shifts and splittings, bandwidths, and IR intensities, together with symmetry considerations, provided a detailed picture of the cluster growth. The first four NH_3 ligands form strong linear N−H−N bonds to the four protons of the central NH_4^+ core, leading to highly symmetric cluster structures. The closure of the first solvation shell at $n = 4$ is strongly supported by ab initio calculations[266,267] and mass spectrometric studies, including the analysis of metastable fractions, fragmentation branching ratios following collisional or photoexcitation, and fragment kinetic energy release measurements.[48,268-270] The next four NH_3 ligands ($n = 5-8$) occupy positions in the second shell, and each of them is attached to one of the four first shell ligands, probably via hydrogen bonding.[137] Although the NH_3 ligands in the first shell are strongly bound to the NH_4^+ core via charge−dipole forces and partial charge transfer ($-\Delta H° = 25$, 17, 14, 12 kcal/mol for $n = 1-4$),[270] they can undergo nearly free internal rotation around their local C_3 axis.[87,137] The spectral signature of this internal rotation disappears for clusters with $n \geq 8$, confirming that the first four ligands in the second shell indeed bind to the four first shell ligands, thereby quenching internal rotation. The NH_3 ligands of the second shell do not undergo free internal rotation despite their weaker intermolecular bonds. This observation was taken as evidence for nonlinear hydrogen bonding between first- and second-shell ligands.[137] For $n \leq 8$, the shell structure is well defined and no isomers are evident. The spectra for $n > 8$ change little and resemble closely the spectra of ammonium salts dissolved in liquid NH_3, indicating that the onset of a liquid-like environment for the $NH_4^+-(NH_3)_4$ core occurs at $n = 8$.[31,137] This example demonstrates that IR spectroscopy of size-selected cluster ions in the gas phase can contribute significantly to our understanding of interactions in the liquid phase. Unfortunately, the details of the cluster structures remain obscure, as spectra with full rotational resolution have not yet been obtained. For example, while most of the theoretical studies predict an asymmetric $NH_4^+-NH_3$ equilibrium structure for the dimer,[266,267,271,272] its IR spectrum was interpreted in terms of a symmetric $H_3N-H^+-NH_3$ geometry.[137]

The charge−dipole interaction in $NH_4^+-NH_3$ is significantly stronger than the charge-induced dipole forces in NH_4^+-Rg dimers. Consequently, the effects of complexation on the structure and normal modes of NH_4^+ are much more pronounced upon NH_3 complexation. In addition, the anisotropy of the $NH_4^+-NH_3$ interaction is much higher and internal rotation of the NH_4^+ ion is largely quenched. Despite the significantly different ion−ligand interaction strengths, the cluster growth is similar in small $NH_4^+-Ar_n$ and $NH_4^+-(NH_3)_n$ clusters ($n \leq 4$), leading to highly symmetric structures with equivalent proton bonds.[135,137] However, after the first solvation shell is filled, differences occur for further solvation due to the different ligand−ligand interactions in $NH_4^+-Ar_n$ and $NH_4^+-(NH_3)_n$.

f. $CH_5^+-H_2$. The equilibrium geometry of methonium, CH_5^+, was calculated to be a $CH_3^+-H_2$ dimer, where H_2 and the C atom of CH_3^+ form a three-center two-electron (3c−2e) bond. Owing to substantial

charge transfer, the bond is relatively strong (~40 kcal/mol). Moreover, as the barriers for both the internal H_2 (or CH_3^+) rotation around the C_3 axis and the exchange of protons between CH_3^+ and H_2 are small, the CH_5^+ ion is fluxional even at low temperatures and all five protons are predicted to be equivalent in the vibrational ground state. As a consequence, the spectrum of CH_5^+ is rather complicated and is currently unassigned (section III.B.1.c).

Complexes of CH_5^+ with H_2 ligands were investigated spectroscopically, with the intention of revealing details of the structure and dynamics of CH_5^+.[138] Because the intermolecular bonds in $CH_5^+-(H_2)_n$ complexes mainly arise from induction and electrostatic forces, their strengths are rather small (<2 kcal/mol for $n = 1-4$).[273] It was hoped that the interaction of the H_2 ligands with the CH_5^+ ionic core would be weak enough to cause only minor perturbations to CH_5^+ but sufficiently strong to slow the scrambling motions leading to simpler spectra. These expectation were confirmed by first-principle molecular dynamic simulations of $CH_5^+-(H_2)_n$, $n = 0-3$, performed at 100 K and ab initio calculations.[273-275] The first H_2 ligand binds in a T-shaped configuration to one of the protons involved in the 3c−2e bond of CH_5^+. Although the intermolecular bond in $CH_5^+-H_2$ is very weak ($-\Delta H° = 1.88$ kcal/mol, $R_e \sim 1.9$ Å),[273,275] it is sufficient to lock this 3c−2e bond to the proton participating in the intermolecular bond. The other four protons of CH_5^+ can still undergo facile scrambling. The second H_2 ligand binds to the other proton of the CH_5^+ 3c−2e bond. As a consequence, this bond is completely localized in $CH_5^+-(H_2)_2$ and only the internal CH_3^+ rotation within CH_5^+ is still nearly free. Attachment of a third H_2 ligand to one of the CH_3^+ protons quenches this motion, leaving CH_5^+ as a semirigid ionic core within the $CH_5^+-(H_2)_3$ complex.

The IRPD spectra of $CH_5^+-(H_2)_n$ complexes ($n = 1-6$),[138] produced in a high-pressure H_2/CH_4 corona discharge source, are consistent with the theoretical and thermochemical results.[273-275] Three broad bands, attributed to C−H stretching vibrations of CH_5^+, become somewhat narrower for increasing n, as the proton scrambling in CH_5^+ is gradually switched off. In contrast to the broad C−H stretch bands of the $CH_5^+-H_2$ dimer, the H−H stretch band displays partly resolved rotational structure, confirming the small coupling between the H−H stretch mode and the nuclear motions of the CH_5^+ ion via the weak intermolecular bond. The experimental rotational constants of the dimer are consistent with the calculated proton-bound minimum. The small red shifts of the H_2 stretch frequencies in $CH_5^+-(H_2)_n$ clusters are also indicative of weak intermolecular bonds and confirm the sequential cluster growth process outlined above. In general, the structures of CH_n^+ differ qualitatively from those the corresponding SiH_n^+ species (section III.B.2).

3. Comparison

This section summarizes some of the features of the proton-bound dimers discussed above, with consideration of structures, binding energies, frequency shifts, and relaxation dynamics. Spectroscopic and theoretical studies demonstrate that AH^+-L dimers prefer equilibrium structures where the proton can be most effectively shared between the two bases A and L (Figure 4). Complexes of the type AH^+-Rg with linear or quasilinear AH^+ ions (e.g., A = H, O, OC, N_2, SiO, HN) have linear equilibrium geometries. For nonlinear AH^+ ions (e.g., A = H_2, NH_3), the global minima also feature linear or near linear proton bonds. The AH^+-H_2 dimers (e.g., A = OC, N_2, CH_3CN, H_2O, NH_3, CH_4) prefer T-shaped equilibrium structures, while AH^+-N_2 complexes have linear bonds (e.g., A = N_2, SiO). The orientation of the ligand in AH^+-H_2/N_2 is determined by the charge−quadrupole interaction, which favors a T-shaped configuration for positive values of the quadrupole moment (L = H_2) and a linear structure for negative values (L = N_2).[97,127,276-278]

Thermochemical and mass spectrometric studies show that the bond strengths in $A-H^+-B$ complexes are related to the difference in the PAs of the two bases A and B.[279] If $PA_A \gg PA_B$, the $A-H^+-B$ dimer can be considered as an $A-H^+$ ion that is slightly perturbed by the intermolecular bond to the ligand B. As PA_B is increased, the proton becomes increasingly delocalized between A and B while at the same time the proton stretching frequency drops and the intermolecular bond becomes stronger (reflected in the dissociation energy and centrifugal distortion constants). If PA_B is increased further, so that $PA_A \ll PA_B$, the complex is better viewed as an H^+-B ion perturbed by a ligand A. Examples from the preceding sections, such as OCH^+-Rg, N_2H^+-Rg, $SiOH^+-Rg$ (Rg = He, Ne, Ar), illustrate some of these effects. For a given AH^+ ion, both the shift in the proton stretching frequency, $\Delta\nu_{A-H}$, and the stretching force constant for the intermolecular bond, k_s, increase with the size of the Rg atom. Moreover, when the same Rg atom is attached to two different AH^+ ions, $\Delta\nu_{A-H}$ and k_s are larger for the monomer with smaller PA_A. The interaction in AH^+-Rg dimers with the same Rg atom but different bases A depends on the charge distribution in the AH^+ ion. For very large PA_A, the linear proton bond in AH^+-Rg is weak and other binding sites may become comparable in energy. Examples are the $SiOH^+-Rg$ dimers where two isomers with similar stability (proton-bound and T-shaped) are found both theoretically and experimentally.[101,199]

The effects of systematically varying the two bases on the $A-H^+-L$ properties have also been explored through ab initio calculations. Figure 14 displays calculated binding energies, D_e, and equilibrium intermolecular separations, R_e, for different AH^+-Rg dimers plotted as a function of the Rg polarizability, α_{Rg}. The data have been determined at the MP2/aug-cc-pVTZ# level of theory, which has been shown to yield PESs for proton-bound dimers with sufficient accuracy for the interpretation of the experimental data.[250] For a given base, the D_e values for the AH^+-Rg dimers increase with α_{Rg} (He < Ne < Ar), as the $-\alpha_{Rg} \times q^2/R^4$ induction term dominates the attraction (Figure 14a). The intermolecular separation, R_e, increases in the order He < Ne < Ar,

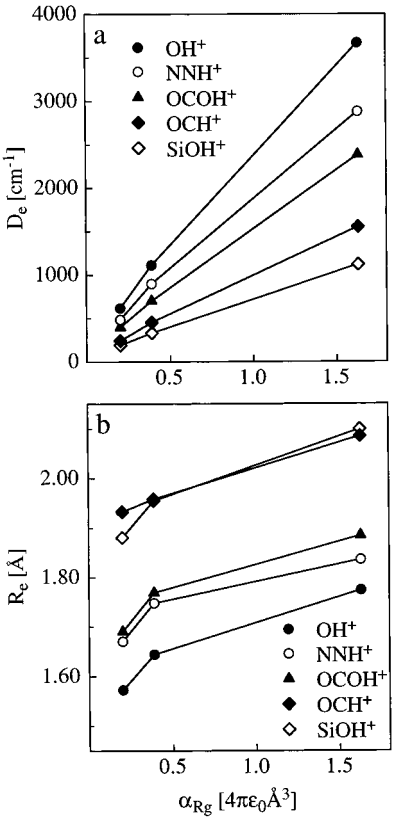

Figure 14. Binding energies, D_e (a), and intermolecular equilibrium separations, R_e (b), of selected proton-bound AH^+-L dimers calculated at the MP2/aug-cc−pVTZ# level (Reprinted with permission from ref 364. Most data are tabulated in ref 199. The values for OH^+-Ar are $D_e = 3666$ cm^{-1}, $R_e = 1.7744$ Å.[254]

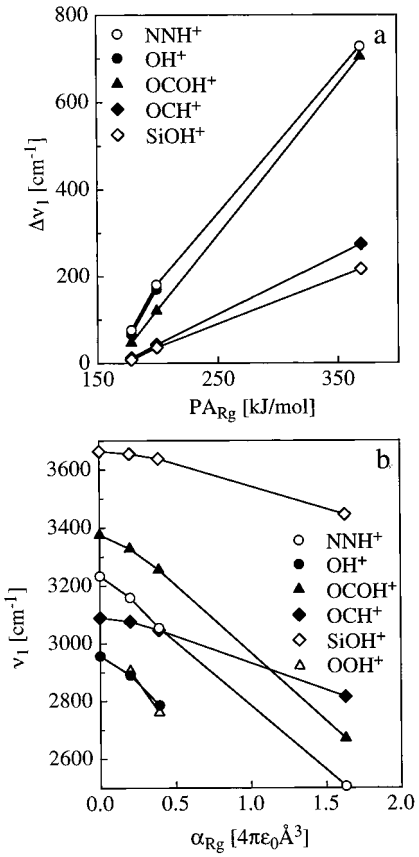

Figure 15. (a) Magnitude of the ν_{A-H} red shifts of selected proton-bound AH^+-Rg dimers as a function of the proton affinity of the Rg atom, PA_{Rg} (Reprinted with permission from ref 364. (b) ν_{A-H} frequencies of AH^+ and AH^+-Rg as a function of the polarizability of the Rg atom, α_{Rg} (Reprinted with permission from ref 364. Most data are tabulated in ref 199. For N_2H^+-Ar, $\nu_{N-H} = 2505.4$ cm^{-1} and $\Delta\nu_{N-H} = 728.6$ cm^{-1}.[100] The anomalously small $\Delta\nu_{N-H}$ shift of N_2H^+-Ar is caused by a strong interaction between the N−H and N−N stretch fundamentals (see text).PA_{Rg} = 177.8, 198.8, 369.2 kJ/mol and $\alpha_{Rg}/4\pi\epsilon_0 = 0.20$, 0.39, 1.63 $Å^3$ for Rg = He, Ne, Ar.[365,366]

although for a given base the variation is slight (Figure 14b). The vibrationally averaged intermolecular bond lengths derived from the experimental rotational constants are generally longer than the calculated ones (by up to 0.1 Å), mainly due to zero-point effects, but show the same trends as the calculated values.

As noted earlier, complexation of AH^+ with a ligand L induces a partial proton transfer from A to L and the resulting destabilization of the A−H bond is reflected in a reduction of the A−H stretching frequency, ν_{A-H}. Strong intermolecular bonds are associated with large red shifts, $\Delta\nu_{A-H}$. For AH^+-Rg dimers (Rg = He, Ne, Ar), $\Delta\nu_{A-H}$ is nearly linearly correlated with α_{Rg} or PA_{Rg} (Figure 15).[95,199,280] In cases where ν_{A-H} of the bare ion is not known (e.g., O_2H^+), it can be accurately estimated from the frequencies of the AH^+-Rg series by the extrapolation $\alpha_{Rg} \rightarrow 0$ (Figure 15b).[281] The accuracy of this method can compete with high-level ab initio calculations and provides guidance in searches for the bare ion's absorptions. The magnitude of the frequency shift can be quite substantial, even for complexation with Rg atoms (e.g., >700 cm^{-1} for N_2H^+-Ar).

For $AH_k^+-H_2$ dimers, the intensity and frequency shift for the H−H stretch vibration, $\Delta\nu_{H-H}$, also serves as an indicator for the bond strength. The H−H bond becomes weaker upon complexation and its stretching frequency decreases.[88,97,127,128,175] Perturbation of H_2 by the AH^+ ion leads to a nonvanishing transition moment for the H−H stretch (IR forbidden in free H_2) along the intermolecular axis. Again, $\Delta\nu_{H-H}$ is roughly linearly correlated with the bond strength, which in turn is controlled by PA_A (Figure 16): the larger PA_A, the smaller $\Delta\nu_{H-H}$. In general, $\Delta\nu_{H-H} \ll \Delta\nu_{A-H}$, as formation of the AH^+-H_2 dimer has a stronger effect on the A−H bond than on the H−H bond.[128] This conclusion is also valid for other molecular ligands, such as N_2, H_2O, or NH_3.[86,137]

The red shifts $\Delta\nu_{A-H}$ and $\Delta\nu_{H-H}$ in AH^+-Rg and AH^+-H_2 directly reflect the increase in the intermolecular bond strength upon vibrational excitation. Excitation of ν_{A-H} enhances the proton transfer, destabilizes the A−H bond, and increases the intermolecular interaction, leading to a shorter and more rigid bond. Excitation of ν_{H-H} leads to an increase in the quadrupole moment of H_2 (by 11%), which in turn stabilizes the intermolecular bond via the enhanced charge−quadrupole interaction.

Some of the proton-bound complexes are highly fluxional and exhibit large-amplitude zero-point motions. The usual concepts employed for the descrip-

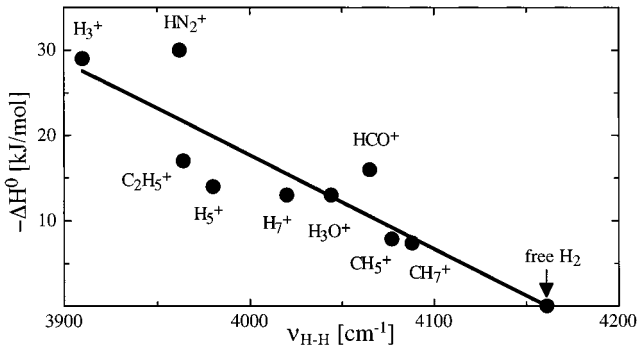

Figure 16. Correlation between ν_{H-H} frequencies and binding enthalpies of selected AH^+-H_2 dimers (Reprinted with permission from ref 127. Copyright 1997 American Institute of Physics). The frequency of the free H_2 molecule ($\Delta H° = 0$) is also included. The line results from a least-squares fit to the data points.

tion of semirigid species (e.g., anharmonic oscillator, semirigid rotor) become inadequate for very floppy systems. In the case of small angular−radial coupling, the radial and angular intermolecular degrees of freedom can be considered separately. Nonrigidity in the radial coordinate leads to centrifugal distortion and anharmonicities in the intermolecular stretching vibration. It also causes the vibrationally averaged separation, R_0, to be larger than the equilibrium separation, R_e, an effect that is typically of the order of <0.1 Å for most proton-bound dimers discussed in this review. Nonrigidity in the angular coordinates can be probed by the intermolecular bending vibrations and in the case of open-shell systems also by molecular constants related to the electron spin.

A measure of the angular rigidity is given by the ratio of the barrier for internal rotation, V_b, and the rotational constant for internal rotation, b.[61] For $V_b/b \gg 1$, i.e., large anisotropy of the PES, the intermolecular bond is directional and the system can be approximated by an anharmonic bending/torsion oscillator. For $V_b/b \ll 1$, the angular excursions are large and the system approaches the free rotor limit. In intermediate cases, the complex behaves as a hindered internal rotor and the calculation of the energy levels can be complicated, especially if the motion is coupled to other vibrations. Linear proton-bound AH^+-Rg dimers are rod-and-ball systems with relatively directional bonds and high barriers for internal rotations. The zero-point bending excursions are usually modest (<30°), even for weakly bound He-containing complexes (e.g., OCH^+-He, $D_e \sim 250$ cm^{-1}).[98,102,186,199] The situation changes for proton-bound AH_k^+-Rg dimers, where the ligand can bind to more than one equivalent proton (e.g., NH_4^+-Rg) and equivalent minima are separated by a potential barrier, V_b. For example, the weakly bound NH_4^+-He complex ($D_e \sim 150$ cm^{-1}) behaves almost as a free internal rotor, as the barrier for internal rotation is small ($V_b \sim 20$ cm^{-1}).[133] In contrast, NH_4^+-Ar ($D_e \sim 900$ cm^{-1}) is much closer to the semirigid limit where the Ar atom is locked to one proton by a large barrier ($V_b \sim 200$ cm^{-1}).[136,250] Nonetheless, there is some probability for tunneling between equivalent minima. NH_4^+-Ne is an intermediate case ($D_e \sim 280$ cm^{-1}, $V_b \sim 40$ cm^{-1}) and therefore has a complicated irregular spectrum.[254] Comparison between NH_n^+-Rg complexes with $n = 2-4$ shows that the bond strength decreases with n (as the PA of NH_{n-1} increases) while the tunneling probability increases (as V_b decreases and the tunneling path between two equivalent minima becomes shorter).[104,250,253] Comparison between OCH^+-He and NH_4^+-Ne shows that radial and angular nonrigidity are not necessarily correlated: OCH^+-He has a bond strength similar to NH_4^+-Ne ($D_e = 250$ vs 280 cm^{-1}); however, the barrier for internal rotation is much larger ($V_b \sim 200$ vs 40 cm^{-1}).[186,254]

Hindered internal rotation of the H_2 unit in AH^+-H_2 complexes constitutes another example of a large amplitude motion. Owing to the large rotational constant of H_2 ($b \sim 60$ cm^{-1}), the effects of this hindered motion on the molecular constants of the complex are significant even for substantial barriers ($V_b \sim 10^3$ cm^{-1}).[97,127,128] The choice of the Hamiltonian for analyzing the spectrum is critical for the interpretation of the data.[63,97,127] A semirigid treatment leads to molecular constants corresponding to misleading unphysical geometrical parameters, while a one-dimensional hindered rotor model provides valuable insight into the energetics of this internal motion. As V_b arises mainly from the anisotropy of the charge−quadrupole interaction, which dominates the attractive part of the intermolecular potential, V_b is also correlated with the intermolecular bond strength.[127]

Several of the AH^+-L dimers contain open-shell molecular ions with non-zero electron spin. The spectra of HNH^+-Rg and OH^+-Rg (both $^3\Sigma^-$) contain useful information about the effect of complexation on the electromagnetic properties of the electronic wave function of the monomer.[102−104] In these dimers the effects of complexation are small due to the weakness of the intermolecular bond (≤0.3 eV). Moreover, the diradical character of OH^+ and HNH^+ has little effect on the intermolecular bond strength. Nonetheless, the complexation-induced change of the spin−spin interaction constant provides valuable information on the anisotropy of the PES, as it is related to the vibrationally averaged zero-point bending excursion, $\langle\theta\rangle$, and is thus a direct probe of the angular anisotropy of the PES. For example, in OH^+-He, $\langle\theta\rangle$ was found to be ∼25°, confirming that intermolecular bonds in proton-bound AH^+-L dimers are often quite directional even in He-containing complexes.[102]

Perturbations are a common feature of the mid-IR spectra of AH^+-Rg dimers, a situation most likely due to comparatively large dissociation energies and relatively low intermolecular vibrational frequencies. Thus, any singly excited intramolecular vibration or simple combination state is likely to be nearby at least one quasibound state involving multiple quanta of the intermolecular vibrations. The strength, variety, and number of perturbations is large for N_2H^+-Ar, which has a relatively high dissociation energy and low intermolecular vibrational frequencies (due to the heavy Ar atom).[126]

Photodissociation spectroscopy probes metastable energy levels above the lowest dissociation threshold

of the complexes. In the mid-IR region, intramolecular vibrations are usually excited, sometimes in combination with intermolecular modes. The vibrational energy is subsequently redistributed into other vibrational degrees of freedom (intracomplex vibrational energy redistribution) and leads eventually to the dissociation of the complex (vibrational predissociation). The time scales for these processes can be inferred from the observed spectral line width and depend sensitively upon the coupling strength between the initially excited bright state and the available dark states and dissociation continua. For small dimers, the density of states in the mid-IR range is still rather low. The dynamical processes are therefore highly dependent on the initially excited state and cannot be described by statistical theories. For example, in $AH_k^+-H_2$ complexes, the lifetime of the lower lying ν_{A-H} stretching state is shorter than that of the higher lying ν_{H-H} stretching level, as the coupling between the dissociation coordinate and the A−H stretch mode is stronger than with the H−H stretch. In general, the coupling strength is related to the complexation-induced frequency shift of the excited intramolecular mode, which is in turn correlated with the intermolecular bond strength: the stronger the intermolecular bond, the larger the frequency shift, the stronger the coupling to intermolecular degrees of freedom, and the shorter the lifetime.[88,97,128,282,283] A similar trend is observed in AH_k^+-L dimers, e.g., H_3O^+-L or NH_k^+-L ($k = 2-4$). The A−H stretch vibrations in these complexes can be divided into bound and free stretching vibrations, depending on whether the excited A−H bond is involved in the intermolecular $A-H^+-L$ bond or not. In general, bound stretches display larger frequency shifts and shorter lifetimes than the corresponding free stretch states.[86,104,135] The different lifetimes for ν_1, $\nu_1 + \nu_s$, and $\nu_1 + \nu_b$ of N_2H^+-He demonstrate that the relaxation rate in an intramolecular excited state can depend sensitively on additional intermolecular excitation (Figure 5).[98]

B. p/π-Bound Complexes

As outlined in the preceding section, the intermolecular interaction strength in proton-bound dimers, AH^+-L, decreases as the difference in the proton affinities of the two bases, ΔPA_{A-L}, increases. Consequently, for complexes with large ΔPA_{A-L}, the proton-bound configuration features weak intermolecular bonds and other geometries may become energetically more favorable. Such a situation occurs for the complexes discussed in the present section, which all have p/π-bound global minimum structures. Here, the expression p/π-bonding is used to describe dimer geometries, where the neutral ligand is attached to a p or π orbital of the molecular ion.

1. $CH_3^+-L_n$

a. CH_3^+−He,Ne,Ar. Dimers of the methyl cation, CH_3^+, and the Rg atoms He, Ne, and Ar were investigated by IRPD spectroscopy and ab initio calculations.[105,106,139] The complexes were produced by expanding suitable CH_4/H_2/Rg mixtures in an electron impact cluster ion source (Figure 2). In the case of CH_3^+-He and CH_3^+-Ne, rotationally resolved spectra were obtained for the strong IR-active degenerate asymmetric C−H stretch fundamental (ν_3). As the dissociation energy of CH_3^+-Ar, determined as 3950 ± 700 cm^{-1} by thermochemical methods,[284] exceeds the frequencies of all CH_3^+ fundamentals, they cannot be observed in a one-photon PD spectrum. However, sequence transitions of the form $\nu_3 + \nu_x - \nu_x$ appeared as a weak, broad, and structureless band near the position of the expected ν_3 fundamental. To observe (ro)vibrational transitions of CH_3^+-Ar originating from the ground vibrational state, spectra were recorded in the first overtone region of the symmetric and asymmetric C−H stretch vibrations (ν_1 and ν_3), which lie above the dissociation limit.

The planar, closed-shell CH_3^+ ion (D_{3h} symmetry) is a strong electrophilic agent owing to the vacant $2p_z$ orbital of the central C atom.[284−286] The spectroscopic and theoretical data for the CH_3^+-Rg dimers are consistent with p-bound cluster geometries of C_{3v} symmetry, where the Rg ligands are attached to this electrophilic orbital.[105,106,139,284,287] The calculated intermolecular PESs of all three dimers have similar topologies, with the major difference being the interaction strength which increases in the order He < Ne < Ar.[105,106,139] The surfaces feature deep global minima at the p-bound sites ($D_e = 707$, 959, 6411 cm^{-1} and $R_e = 1.83$, 2.13, 1.95 Å for He, Ne, Ar) and large barriers for internal rotation of CH_3^+ around its *a* (or *b*) axis ($V_b \sim 600$, 750, 6000 cm^{-1}). This large angular anisotropy along with a small effective reduced mass for the bending motion leads to intermolecular bending frequencies of the p-bound structures which are much higher than the corresponding stretching frequencies. In all three cases, the planar vertex (local minima) and side-bound structures (transition states) with C_{2v} symmetry are significantly less stable than the global minimum ($D_e \sim$ 100, 200, 600 cm^{-1}). Their stabilities and intermolecular separations differ little, indicating that the dependencies of the PESs upon the azimuthal angle are small at long and mid range, leading to potential shapes of nearly cylindrical symmetry with respect to the C_3 axis. This behavior results in intermolecular in-plane bending frequencies for the vertex-bound structures, which are much lower than the corresponding stretching frequencies.

The long-range part of the PES is dominated in all three CH_3^+-Rg dimers by inductive interactions, arising from the multipole moments of CH_3^+ (mainly the charge) interacting with the polarizable Rg atom.[105,106,139] Formation of the intermolecular p bonds is accompanied by partial charge transfer, ΔQ, from the Rg atom into the electrophilic, positively charged $2p_z$ orbital of CH_3^+.[105,284] Although at the equilibrium geometry of CH_3^+-He and CH_3^+-Ne the transfer of electron density is small ($\Delta Q < 0.04\ e$), it is substantial in the case of CH_3^+-Ar ($\Delta Q \sim 0.3\ e$), suggesting that the contribution of charge transfer to the binding energy becomes more appreciable with increasing size of the Rg atom. This trend is directly reflected in the complexation-induced changes of the CH_3^+ properties. Most significant is the angular

deformation, which transforms the planar CH_3^+ monomer with sp^2 hybridization ($\theta_e = 90°$) toward a pyramidal structure ($\theta_e = \angle Rg-C-H = 91.4°, 91.4°, 99.6°$ for He, Ne, Ar), approaching the limit of sp^3 hybridization ($\theta_e = 109.47°$ in CH_4). The C−H bond becomes stronger and shorter upon complexation ($\Delta r_e = -0.0015, -0.0019, -0.0049$ Å; $\Delta\nu_3^{calc} \sim 13, 17, 18$ cm^{-1}; $\Delta\nu_1^{calc} \sim 13, 16, 39$ cm^{-1}). In contrast to the small degree of monomer deformation caused by He and Ne (deformation energy $E_D = 55, 58$ cm^{-1}), Ar has a much larger effect on CH_3^+ ($E_D = 2501$ cm^{-1}) due to the onset of chemical bonding.[105,106,139]

The trends derived from the ab initio PESs of the CH_3^+−Rg dimers are confirmed by the analysis of their rotationally resolved IR spectra.[105,106,139] The bands' structures are characteristic of either parallel or perpendicular transitions of prolate symmetric tops with nuclear spin statistical weights appropriate for three equivalent protons. The intermolecular separations derived from the rotational constants amount to $R_{cm} \sim 2.18, 2.30, 2.05$ Å for the dimers with He, Ne, Ar. The increase in the harmonic intermolecular stretching force constant with the size of the Rg atom ($k_s \sim 2, 9, 50$ N/m; $\omega_s \sim 110, 130, 280$ cm^{-1}) is consistent with the increase in the interaction strength. Excitation of the ν_3 vibration leads to a slight destabilization of the intermolecular bond, manifested in larger R_{cm} and lower k_s and ω_s values in the ν_3 state and blue shifts in the ν_3 frequency upon complexation. In all cases, the C−H stretch frequencies of the CH_3^+−Rg dimers are bracketed by the corresponding frequencies of CH_3^+ and CH_3, supporting the conclusion that the Rg ligands donate electron density into the $2p_z$ orbital of C. The ν_3 frequencies of CH_3^+−He and CH_3^+−Ne are closer to CH_3^+, indicating that charge transfer is small. Moreover, the ν_3 shifts of these dimers scale linearly with the polarizabities of the Rg atoms, implying that induction forces dominate the attraction. The ν_1 and ν_3 frequencies of CH_3^+−Ar are closer to those of CH_3, confirming that charge transfer is substantial.

The experimental vibrationally averaged distances are substantially larger than the corresponding calculated equilibrium values ($R_{cm}-R_e = 0.34, 0.17, 0.10$ Å for He, Ne, Ar), although the order is the same for both ($R_{C-He} < R_{C-Ar} < R_{C-Ne}$). These differences do not arise from an inadequate level of theory in the ab initio calculations but rather from large zero-point vibrational effects.[139] Analysis of the calculated intermolecular PESs reveal that the large observed differences, $R_{cm}-R_e$, are mainly due to the intermolecular bending rather than the stretching motion. Although the calculated bending frequencies are high for the p-bound equilibrium structures, the zero-point angular motions cause significant increases in the optimal intermolecular separation, which leads to vibrationally averaged R_{cm} values that are much larger than the calculated R_e values.[139] This angular−radial coupling is less significant for dimers containing heavier Rg atoms, because the bending force constants are higher and the reduced moments of inertia smaller.

The p-bound CH_3^+−Rg dimers are typical disk-and-ball complexes, as are the neutral C_6H_6−Rg or SO_3−Rg dimers.[64,139,288,289] The topology of their PESs is qualitatively different from those of linear rod-and-ball (e.g., N_2H^+−He, OCH^+−He, NCH−Ar)[10,180,186,290] and ball-and-ball complexes (e.g., NH_4^+−He, FH−Ar).[10,62,133] For ball-and-ball systems, the optimal intermolecular separation does not strongly depend on the relative orientation of the complex's constituents (though the interaction strength may do so). On the other hand, in rod-and-ball and disk-and-ball dimers, the optimal intermolecular bond length is angularly dependent causing pronounced angular−radial couplings. The difference between these two categories is that in disk-and-ball dimers the optimal separation increases as the ligand is tilted away from the equilibrium position, whereas in linear rod-and-ball complexes the separation decreases.

Comparison between H^+−Rg and CH_3^+−Rg provides useful insight into their bonding mechanism.[106] Thermodynamic studies showed that for many stable species the PA is linearly correlated to the methyl cation affinity (MCA).[291] This relation holds also for the noble gases Xe and Kr, both of which form strong bonds with H^+ and CH_3^+. However, for the smaller Rg atoms, the MCA drops much faster than the PA, indicating that the bonding mechanism in H^+−Rg and CH_3^+−Rg depends strongly on the size of the Rg atom.[106] While all Rg atoms form covalent bonds to a proton, only Xe and Kr feature such strong bonds to the methyl cation. The intermolecular interactions in CH_3^+−He and CH_3^+−Ne are weak and mainly based on inductive forces. In the case of CH_3^+−Ar, partial charge transfer provides additional stabilization, and this contribution becomes even more important for CH_3^+−Rg complexes with larger Rg atoms. Comparison of intermolecular bond properties (R_{C-Rg}, $\angle$H−C−Rg, D_0) in ionic CH_3^+−Rg dimers (Rg = He, Ne, Ar, Kr, Xe) with those in the isoelectronic neutral CH_3X molecules (X = H, F, Cl, Br, I) nicely illustrates the change in bonding mechanism in CH_3^+−Rg from mainly induction (Rg = He, Ne) to mainly covalent (Rg = Kr, Xe).[106] Clearly, for increasing Rg size, the properties of the intermolecular CH_3^+−Rg bonds converge toward those of the respective covalent intramolecular C−X bonds in CH_3X (Figure 17).

b. CH_3^+−Ne_2,$Ar_{2,3}$. The CH_3^+−Rg_2 trimers were studied with the same experimental and theoretical techniques as the CH_3^+−Rg dimers.[105,106] The IRPD spectra of the ν_3 bands of CH_3^+−Ne_2 and CH_3^+−Ar_2 are rotationally resolved, providing for the first time quantitative structural and dynamic information on ionic trimers. The CH_3^+ ion can accept Rg ligands at both sides of the electrophilic $2p_z$ orbital. Indeed, the ν_3 spectra of CH_3^+−Ne_2 and CH_3^+−Ar_2 are characteristic of symmetric prolate tops with three equivalent protons and the two Rg atoms located on opposite sites of CH_3^+ on the C_3 symmetry axis. However, the equilibrium structures of the Rg−CH_3^+−Rg trimers depend strongly on the dimer interaction strength: they have C_{3v} symmetry for Rg = Ar and D_{3h} symmetry for Rg = He and Ne.

Ab initio calculations show that the second Ar ligand in the Ar−CH_3^+−Ar trimer is only weakly attached to a strongly bound CH_3^+−Ar dimer, leading

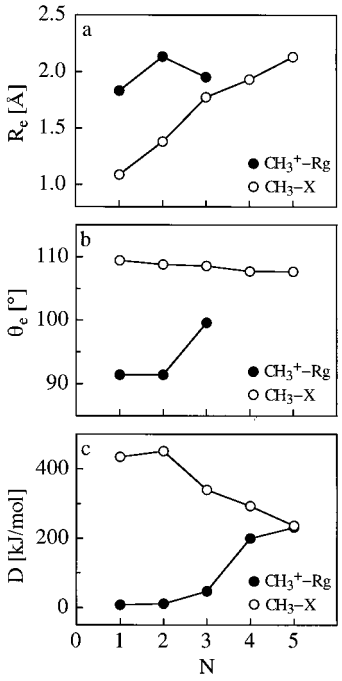

Figure 17. Comparison of the properties of the intermolecular bonds in ionic CH_3^+−Rg dimers with those of the chemical bonds in the corresponding isoelectronic neutral CH_3−X molecules (Reprinted with permission from ref 106. Copyright 2000 from American Institute of Physics): (a) interatomic separation, R_e; (b) bond angle, θ_e; (c) bond energy, D. The index N corresponds to the row of Rg/X in the periodic table: $N = 1-5$ represent Rg/X = He/H, Ne/F, Ar/Cl, Kr/Br, Xe/I.

to a C_{3v} equilibrium geometry.[105] The two C−Ar bonds have quite different bond lengths ($R_{C-Ar_1} = 2.04$ and $R_{C-Ar_2} = 2.88$ Å), and the pyramidal deformation of CH_3^+ is similar in the trimer and the dimer (θ_e = ∠H−C−Ar1 = 97.5° and 99.6°). The calculated sequential binding energies (D_e = 6411 and 768 cm^{-1}) are compatible with the experimental bond enthalpies ($-\Delta H°$ = 3950 ± 700 and 790 ± 70 cm^{-1})[284] and confirm the drastically different interaction strengths of CH_3^+ with the first and second Ar ligand. As the binding energy of the second Ar ligand is well below the ν_3 frequency of the trimer, this fundamental could be observed in a one-photon PD spectrum recorded in the dimer fragment channel (Figure 18).[105] The derived ground-state rotational constants yielded an Ar−Ar separation of 4.84 ± 0.02 Å, in good agreement with the ab initio value (4.92 Å).

Interestingly, all Q branch heads in the ν_3 band are split into two components separated by ∼0.5 cm^{-1} (Figure 18). This splitting was attributed to a tunneling motion, where the two different Ar ligands can exchange their roles via an intracluster umbrella inversion of CH_3^+ through a transition state with D_{3h} symmetry. Indeed, ab initio calculations predict a low barrier for this motion (V_b ∼ 550 cm^{-1}). The carbon atom moves by as much as ∼0.7 Å while crossing the inversion barrier, explaining the relatively small magnitude of the inversion splitting. The value for the ground-state splitting between symmetric (s) and antisymmetric (a) components of the inversion doublet was estimated from the relative intensities of the a−a and s−s bands of the ν_3 transition as $\delta = 3.5 \pm 2$ cm^{-1}, in agreement with the values obtained from the width of the unresolved ν_1 band ($\delta < 7$ cm^{-1}) and theoretical considerations based on reasonable one-dimensional double-minimum potentials ($0.1 < \delta < 5$ cm^{-1}). An interesting aspect of the intracluster tunneling motion in Ar−CH_3^+−Ar is its similarity to the nucleophilic S_N2 displacement reaction of the isoelectronic [Cl−CH_3−Cl]$^-$ system, which is also predicted to proceed on a double-minimum potential via a Walden inversion barrier (see section IV.B.1).[292,293]

In contrast to Ar−CH_3^+−Ar, ab initio calculations for He−CH_3^+−He and Ne−CH_3^+−Ne yield equilibrium geometries with D_{3h} symmetry.[106] Apparently, the double-minimum potential in Rg−CH_3^+−Rg trimers occurs only for larger Rg atoms, where the

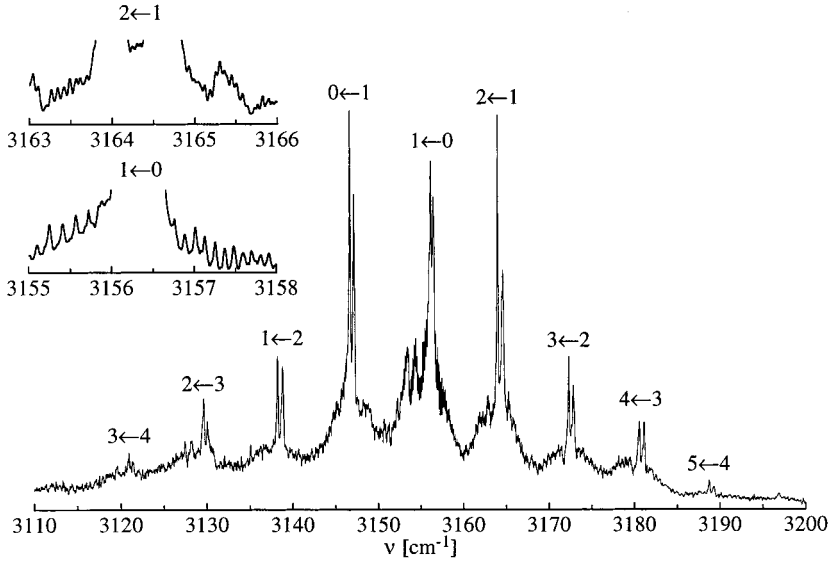

Figure 18. IRPD spectrum of the ν_3 band of Ar−CH_3^+−Ar recorded in the CH_3^+−Ar fragment channel (Reprinted with permission from ref 105. Copyright 1998 American Institute of Physics). The splitting of the Q branches of this perpendicular transition ($\Delta K = \pm 1$) is attributed to inversion tunneling of CH_3^+ within the Ar−CH_3^+−Ar trimer. The insets demonstrate that the spacings in the P and R branches are $4B$ for $K = 1 \leftarrow 0$ and $2B$ for $K = 2 \leftarrow 1$, as expected for an inverting C_{3v} molecule with three equivalent protons.

intermolecular bond to the first ligand is strong enough to cause a substantial angular deformation of the CH_3^+ ion. As the weak interactions in CH_3^+−He and CH_3^+−Ne are mainly based on induction, the effects on geometry and charge distribution of CH_3^+ are small. Consequently, the attractive (mainly induction) and repulsive forces between the CH_3^+ ion and the Rg ligands are comparable in CH_3^+−Rg and Rg−CH_3^+−Rg. Because three-body interactions are small, the binding energy to the second Rg ligand is only slightly smaller than that to the first one, leading to somewhat smaller changes in the CH_3^+ properties upon sequential complexation (e.g., D_e = 959 vs 745 cm^{-1}, R_e = 2.1347 vs 2.2322 Å, Δr_e = −0.0019 vs −0.0015 Å, $\Delta\nu_3^{calc}$ = 16.6 vs 14.0 cm^{-1} for CH_3^+−Ne vs Ne−CH_3^+−Ne).[106] The ν_3 spectrum of Ne−CH_3^+−Ne confirms the results of the ab initio calculations (no experimental data exist for He−CH_3^+−He). Observed nuclear spin statistical weights indicate that Ne−CH_3^+−Ne has inversion symmetry with two equivalent Ne atoms. The absence of inversion tunneling splittings are compatible with a D_{3h} equilibrium structure. In addition, the intermolecular bonds in the trimer are only slightly longer than in the dimer (R_{cm} = 2.34 vs 2.30 Å) and the incremental ν_3 blue shifts are similar ($\Delta\nu_3^{exp}$ = 9.9 vs 11.6 cm^{-1}).[106]

Significantly, the IR spectra of related ionic trimers of the type AH^+−Rg_2 recorded so far are not rotationally resolved, despite the use of laser radiation with sufficiently narrow bandwidth (e.g., A = CO, N_2, SiO; Rg = Ne, Ar).[95,96,99,101,123] Broadening may arise in these cases either from a shorter upper-state lifetime due to fast intracomplex vibrational energy redistribution or vibrational predissociation or from inhomogeneous effects, such as overlapping transitions from sequence hot bands or multiple isomers. In the Rg−CH_3^+−Rg trimers (Rg = Ne, Ar), the coupling between the ν_3 mode and other inter- and intramolecular degrees of freedom is weak, leading to long lifetimes and narrow line widths.

The CH_3^+, NH_3^+, and H_3O^+ ions have zero, one, and two electrons in the $2p_z$ orbital of their central atom. Thus, comparison between complexes of these ions and neutral ligands enables the systematic investigation of the electrophilic character of this orbital as a function of its occupancy. In CH_3^+, this orbital is vacant and very electrophilic, leading to the formation of a strong p bond to Ar, which donates significant electron density into the orbital. The much weaker bond to the second Ar ligand suggests that its electrophilic character is already greatly reduced by this partial charge transfer. If one or two electrons occupy this orbital, its electrophilic and reactive character is further reduced. As a consequence, NH_3^+−Ar and H_3O^+−Ar clearly prefer proton-bound rather than p-bound equilibrium structures, a conclusion reached from both ab initio calculations and rotationally resolved IRPD spectra.[253]

Interestingly, the coarse rotational structure in the ν_3 IRPD spectrum of the CH_3^+−Ar_3 tetramer resembles the K substructure of the corresponding CH_3^+−Ar_2 transition (Figure 18).[105] An equilibrium geometry with two axial (p-bound) and one off-axial (proton-bound) Ar atoms cannot give rise to the observed spectral features unless the complex is assumed to be nonrigid. According to the ab initio calculations for the CH_3^+−Ar dimer, the energies for the vertex-bound local minimum and the side-bound transition state are similar, indicating that the barrier for internal rotation of CH_3^+ around its C_3 axis is small. If in CH_3^+−Ar_3 this barrier is comparable to or smaller than the A rotational constant of CH_3^+−Ar_2 (~5 cm^{-1}), the latter will undergo (nearly) free internal rotation within the CH_3^+−Ar_3 complex. Thus, the observed spectral features may correspond to $\Delta k_{int} = \pm 1$ transitions between different internal rotor states giving rise to a band contour similar to the CH_3^+−Ar_2 trimer band. The presence of two off-axial (proton-bound) Ar atoms would seem to quench this internal motion, as no such structure is observed in the ν_3 band of CH_3^+−Ar_4. An alternative CH_3^+−Ar_3 geometry, with the third Ar atom lying on the C_3 axis, would also give rise a spectrum with a coarse structure similar to that of CH_3^+−Ar_2, as both complexes would have comparable *A* rotational constants. However, the axial site is expected to be less favorable as the charge of the cluster is mainly localized on the CH_3^+ moiety. It is not clear whether the inversion motion present in CH_3^+−Ar_2 is quenched by the addition of subsequent Ar atoms.

c. CH_3^+−H_2 (=CH_5^+). According to ab initio calculations,[294,295] the equilibrium geometry of protonated methane, CH_5^+, can be best described as an eclipsed CH_3^+−H_2 dimer with C_s symmetry, with the H_2 moiety bound in a T-shaped fashion to the $2p_z$ orbital of a pyramidal CH_3^+ ion at an intermolecular separation of 1.1 Å. This geometry is analogous to the CH_3^+−Rg structures discussed above, and the bond strength of CH_3^+−H_2 (42.5 kcal/mol)[294] lies between those of CH_3^+−Ar (11 kcal/mol)[284] and CH_3^+−Kr (48 kcal/mol).[291] The CH_3^+−H_2 dimer features a nonclassical three-center two-electron (3c−2e) bond typical for carbocations.[296] However, the barrier for internal H_2 rotation around the C_3 axis of CH_3^+ via the staggered configuration was calculated to be rather small (<35 cm^{-1}).[294] In addition, the protons of the H_2 and CH_3^+ moieties can be exchanged via a low-lying transition state with C_{2v} symmetry (barrier < 280 cm^{-1}).[294] As a consequence of the low barriers for complete proton scrambling (which become even lower when zero-point effects are taken into account),[295] CH_5^+ is an extremely fluxional molecule with five statistically equivalent protons and the concept of molecular structure becomes problematic.[297] Interestingly, dynamical ab initio path integral calculations based on the Car−Parrinello approach suggest that, although CH_5^+ is highly fluxional (even at 5 K), rapid proton exchange is a concerted process and the probability of finding CH_5^+ in a configuration similar to the CH_3^+−H_2 equilibrium structure is rather high.[296,298] The MW and IR spectra of CH_5^+ were predicted based upon the calculated low barriers for proton exchange using the molecular symmetry group G_{240} (120 equivalent minima) and shown to be quite irregular and very sensitive to the detailed shape of the PES.[299−301]

Recently, the first spectrum of CH_5^+ has been reported.[140] A rotation−vibration−tunneling spec-

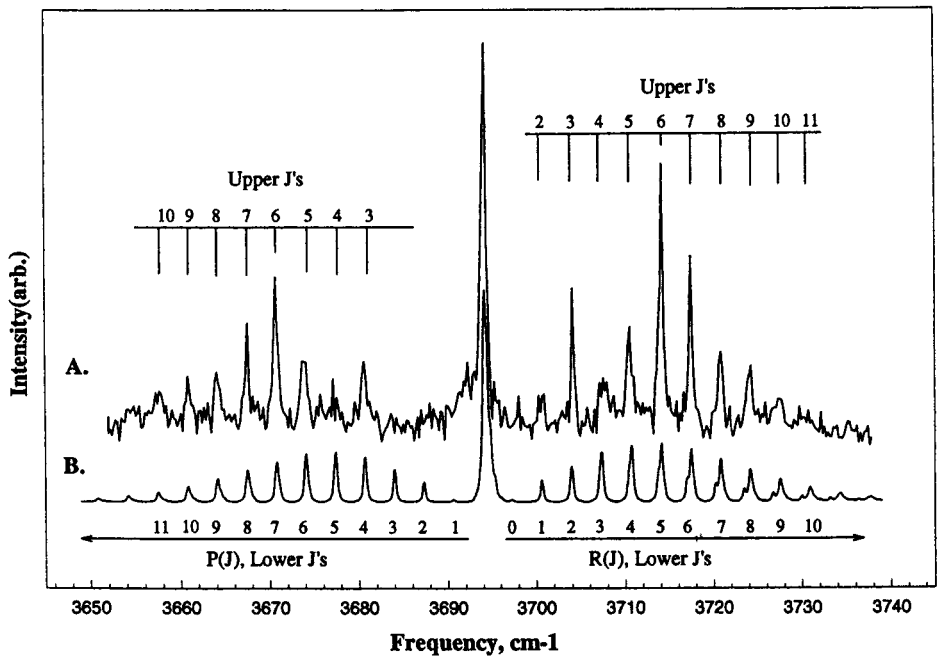

Figure 19. Multiphoton IRPD spectrum of the H−H stretch vibration of $SiH_3^+-H_2$ (A) along with a simulation (B) at T = 90 K (Reprinted with permission from ref 141. Copyright 1995 American Institute of Physics). The spectrum was analyzed assuming free internal rotation of H_2 around the intermolecular C_3 axis.

trum in the region of the C−H stretching modes was obtained by direct absorption in a liquid-N_2-cooled positive column discharge cell containing a H_2-dominated H_2/CH_4 plasma. Over 900 lines between 2770 and 3150 cm^{-1} were attributed to CH_5^+ based upon indirect arguments, including plasma chemistry, Doppler profile, and the subtraction of the known transitions of CH_n^+ (n = 0−3). The spectrum of CH_5^+ is extremely rich and does not show any obvious regularity, in agreement with the theoretical predictions for this very floppy ion. Although assignment of rotational lines has still not been accomplished, the center of the band at 2950 cm^{-1} approximately agrees with the CH_5^+ absorption in the $CH_5^+-H_2$ dimer[302] and ab initio calculations.[295] In accordance with the high PA of CH_4, the C−H stretch potential is reasonably well defined, leading to the appearance of a localized C−H stretch absorption band. Future efforts toward assigning the spectrum of this fundamental ion may include (i) spectra of CH_5^+ in superfluid He droplets to reduce spectral congestion, (ii) spectra in the MW region, and (iii) spectra of deuterated species.[298,301] In addition, Coulomb explosion imaging techniques were suggested to elucidate the ground-state structure of CH_5^+.[298] Some conclusions about CH_5^+ were derived from spectra of CH_5^+ complexed with other ligands (e.g., Ar, H_2, CH_4, N_2; section III.A.2.f).[138,274,302,303]

2. $SiH_3^+-(H_2)_{1,2}$

The closed-shell SiH_3^+ ion is similar to CH_3^+ and possesses a planar D_{3h} structure.[304] Ab initio calculations and spectroscopic data show that the global minimum structure of SiH_5^+ can be viewed as a $SiH_3^+-H_2$ dimer, with the H_2 molecule attached to the $3p_z$ orbital of Si in a T-shaped configuration forming a nonclassical 3c−2e bond.[141,305] Although this structure is topologically analogous to the equilibrium structure of CH_5^+ (section III.B.1.c), there are qualitative differences between SiH_5^+ and CH_5^+, owing to the much weaker interaction of the H_2 molecule with SiH_3^+ ($-\Delta H° \sim 14$ kcal/mol, $R_e = 1.87$ Å)[305,306] compared to CH_3^+ ($-\Delta H° \sim 42$ kcal/mol, $R_e = 1.10$ Å).[294,295] First, the barrier for internal H_2 rotation around the C_3 axis via the staggered transition state is much smaller (<1 vs <35 cm^{-1}).[294,305] Second, while the barrier for proton exchange between the H_2 ligand and CH_3^+ via a C_{2v} transition state is calculated to be very low (<300 cm^{-1}) facilitating rapid proton scrambling,[294] the barrier in $SiH_3^+-H_2$ is much higher (~9500 cm^{-1}) and lies above the dissociation threshold.[305] As a consequence, the 3c−2e bond is localized in $SiH_3^+-H_2$,[307] in contrast to $CH_3^+-H_2$.

The spectrum of SiH_5^+ was investigated in the region of the H−H stretch vibration by means of multiphoton IRPD spectroscopy.[141] The $SiH_3^+-H_2$ complexes were produced in a $SiH_4/He/H_2$ corona discharge. As the binding energy of the $SiH_3^+-H_2$ dimer exceeds the H−H stretch frequency, a multiphoton scheme was employed to resonantly dissociate the complex into SiH_3^+ and H_2 fragments. Tunable IR light (generated by difference frequency mixing in a $LiNbO_3$ crystal) was scanned to excite rovibrational levels of the H−H stretch fundamental. Subsequently, multiple quanta from a tunable CO_2 laser were used to drive the excited dimers over the dissociation threshold. The rotational structure of the observed transition is characteristic for a near prolate symmetric top (Figure 19), compatible with the calculated $SiH_3^+-H_2$ equilibrium geometry assuming free internal rotation of the H_2 unit around the C_3 axis of SiH_3^+ and no scrambling between protons of the H_2 and SiH_3^+ moieties (molecular symmetry group G_{12}). The formation of the $SiH_3^+-H_2$ dimer leads to an increased H−H separation, as electron

density from the H_2 σ bond is donated into the $3p_z$ orbital. The large red shift in the H−H stretch frequency (−467 cm^{-1}) is consistent with the measured bond enthalpy of 14 kcal/mol.[306]

The equilibrium structure of SiH_7^+ was calculated to have C_2 symmetry, with two equivalent H_2 molecules weakly attached to opposite sides of the $3p_z$ orbital of Si in a T-shaped configuration, i.e., $H_2-SiH_3^+-H_2$.[308,309] Both H_2 molecules can rotate almost freely about the C_3 axis of SiH_3^+ (barrier < 35 cm^{-1}). The intermolecular bonds in the $H_2-SiH_3^+-H_2$ trimer ($-\Delta H° \sim 5$ kcal/mol, $R_e = 2.04$ Å)[306,309] are significantly longer and weaker than in the $SiH_3^+-H_2$ dimer ($-\Delta H° \sim 14$ kcal/mol, $R_e = 1.87$ Å).[305,306] A one-photon IRPD spectrum of SiH_7^+, produced in a high-pressure glow discharge of SiH_4 and H_2, was obtained in the H−H stretch region.[310] Only one band was found between 3500 and 4200 cm^{-1}, and its rotational band contour and vibrational frequency was consistent with the asymmetric (out-of-phase) H−H stretch vibration of a $H_2-SiH_3^+-H_2$ trimer with intermolecular separations of ∼2.0 Å. The complexation-induced red shift of the H−H stretch frequency is much smaller in the trimer (−295 cm^{-1}) than in the dimer (−476 cm^{-1}), in accordance with the significantly weaker intermolecular bonds. This is in contrast to the symmetric $Rg-CH_3^+-Rg$ trimers (Rg = He, Ne), where the interactions in the dimer and trimer are similar. The symmetric $H_2-SiH_3^+-H_2$ structure of SiH_7^+ differs also qualitatively from that of CH_7^+, which is best described as a weakly bound $CH_5^+-H_2$ dimer (section III.A.2.f).

3. $C_6H_6^+$–Ne,Ar,Kr

The $^2E_{1g}$ electronic ground state of the benzene cation complexed with Rg atoms (Ne, Ar, Kr) has been characterized by using a novel technique based on high Rydberg spectroscopy.[142−144] The scheme involves using a pulsed laser to prepare neutral C_6H_6-Rg complexes in specific rovibrational levels of the S_1 state. These electronically excited neutrals are subsequently excited by a second tunable laser to high Rydberg levels ($40 < n < 120$) that are then field ionized in the extraction region of a time-of-flight MS. The resulting Rydberg spectrum is transformed into a cation spectrum using an automated cross-correlation ionization energy procedure (CRIES). The procedure entails cross-correlating the experimental spectrum with a theoretical spectrum generated using two adjustable parameters, the ionization energy and the quantum defect. The CRIES spectra, which exhibit full rotational resolution, were analyzed in terms of a rigid symmetric top Hamiltonian that included phenomenological spin−orbit and Coriolis coupling terms.

The data indicate that the neutral and ionic clusters share a common structure, with the Rg atom situated above the ring (C_{6v} symmetry). However, ionization induces a significant shortening of the intermolecular bond. For example, $C_6H_6^+-Ar$ has an intermolecular bond length of 3.513 Å compared to 3.581 Å in the neutral complex. Ionization also increases the intermolecular well depth (by around 170 cm^{-1} for Rg = Ar) due to the additional charge-induced dipole interaction. One interesting observation is that the heavier Rg atoms (Ar, Kr)[143] induce significant spin−orbit coupling (which has not been observed for bare $C_6H_6^+$ and $C_6H_6^+-Ne$).[142,163] For $C_6H_6^+-Ar$ and $C_6H_6^+-Kr$, the coupling constant was determined as 0.51 and 2.89 cm^{-1}, respectively.[143] The origin of the spin−orbit coupling is uncertain at this stage, although an exchange mechanism has been deemed most likely. A more detailed discussion of $C_6H_6^+-Rg$ complexes can be found in the article by Neusser in this issue.

C. Miscellaneous

1. N_2^+–He_n

Complexes of the N_2^+ cation and He atoms have been probed by exciting the strong $B\ ^2\Sigma_u^+ \leftarrow X\ ^2\Sigma_g^+$ (0−0) transition in the near UV (at 390 nm).[90,146] The N_2^+-He complex has significance because of the many studies devoted to the dynamics of $N_2^+ + He$ collisions. Various groups have focused on collision-induced vibrational relaxation,[311,312] collisional quenching from both the A and B electronic states,[313−315] and rotational energy transfer.[316] Of particular note are collisional studies focused on the rotational alignment of N_2^+ drifting under the influence of an electric field in He buffer gas where it was observed that the rotational angular momentum was preferentially aligned perpendicular to the electric field.[317] The alignment comes about because the N_2^+-He potential has an anisotropic, roughly ellipsoidal, repulsive core so that a parallel alignment results in a larger scattering cross section than a perpendicular one.

Spectroscopic studies on the N_2^+-He complex were preceded by accurate MCSCF−CI ab initio calculations of the N_2^+-He PES.[209] Besides featuring the anisotropic repulsive core expected from the collisional alignment studies, the calculated surface exhibits a minimum of −139.4 cm^{-1} in a configuration where the N−N bond is tilted by 45° with respect to the N_2^+-He bond. The well depth for the interaction is relatively insensitive to the orientation of the N_2^+-He and N−N bonds, and there is only a small effective barrier (∼7 cm^{-1}) to internal rotation. The ab initio surface was used to variationally determine rovibrational energy levels which were fitted to a free internal rotor energy expression

$$E(n\nu_s,j,l) = n\nu_s + Bj(j+1) + C_n l(l+1) \quad (2)$$

with $B = 1.879$ cm^{-1}, $\nu_s = 55.231$ cm^{-1}, $2\nu_s = 83.404$ cm^{-1}, $3\nu_s = 92.491$ cm^{-1}, $C_0 = 0.477$ cm^{-1}, $C_1 = 0.370$ cm^{-1}, $C_2 = 0.254$ cm^{-1}. The first term of the energy expression takes into account the N_2^+-He stretch vibration, the second term the internal rotation of the N_2^+ (angular momentum $\hat{j}$), and the third term the end-over-end rotation (angular momentum $\hat{l}$) of the complex.

The N_2^+-He $B \leftarrow X$ electronic spectrum bears a coarse resemblance to the free N_2^+ $B \leftarrow X$ spectrum providing evidence that N_2^+-He has a free internal rotor structure in both the X and B electronic states (thereby supporting the ab initio calculations).[90,146] Exciting the $B \leftarrow X$ transition of the core leads to

transitions with $\Delta j = \pm 1$ and $\Delta l = 0$. The spectrum is almost unshifted from the one of N_2^+ (shift <1 cm^{-1}), showing that the binding energy of the He atom (D_0) is practically the same in the X and B electronic states. The absence of bands associated with excitation of the N_2^+-He stretching vibration constitutes further evidence for similar X and B state potentials. Transitions from $j'' = 7$ but not $j'' = 8$ are observable, suggesting that complexes with $j'' > 7$ are above the dissociation threshold. The derived binding energy lies between 101 and 130 cm^{-1}, a range that almost brackets the theoretical value, $D_0 \sim 98$ cm^{-1}.[209] Features reminiscent of the P and R branch transitions of N_2^+ are observable in the $N_2^+-He_n$ clusters up to $N_2^+-He_6$, suggesting that free internal rotation of the N_2^+ core persists for the larger species.[318]

Surprisingly, the N_2^+-He spectrum contains a hot band involving the N−N stretching vibration, shifted by $\sim$195 cm^{-1} to higher energy from the B ← X origin. Some fraction of the N_2^+-He complexes possessing more than 2200 cm^{-1} of internal energy survive the $\sim$100 μs passage from the ion source to the laser interaction region, despite the fact that only ca. 100 cm^{-1} is required to rupture the N_2^+-He bond.[145,318] By measuring the ratio of the intensities of the hot and origin bands while the flight time between the ion source and the laser interaction region was varied, a vibrational predissociation lifetime of 220 $\pm$ 30 μs was determined. This corresponds to roughly 4×10^9 N−N vibrational periods! Such a long lifetime may seem surprising but is supported by calculations that yield lifetimes in the 120−4260 μs range.[319,320]

2. N_4^+

The N_4^+ molecular complex has long been known as a constituent of nitrogen plasmas[321] and is believed to play a role in stratospheric chemistry. Thermochemical[322] and collision-induced dissociation[323,324] studies show that the energy required for dissociation into N_2 ($X\ ^1\Sigma_g^+$) and N_2^+ ($X\ ^2\Sigma_u^+$) is around 1.1 eV, making it one of the more strongly bound ions discussed in this review. Prior to gas-phase spectroscopic characterization, ab initio,[325,326] electron spin resonance (ESR),[327] and IR matrix[328] studies suggested that N_4^+ has a linear, centrosymmetric $^2\Sigma_u^+$ ground-state structure, with two equivalent N_2 units held together by a central bond that is relatively weak compared to the two terminal N−N bonds. The neon matrix ESR results show that the unpaired electron is located primarily on the inner nitrogen atoms.[327]

The rotationally resolved IR band of the ν_3 asymmetric stretching vibration has been recorded by tunable diode laser spectroscopy in a continuous supersonic slit expansion of pure N_2 crossed by electrons.[111,147] The spectrum confirms earlier notions of the N_4^+ structure: it is consistent with a centrosymmetric linear molecule and exhibits the expected J_{odd}/J_{even} intensity ratio of 5:4. From an analysis of transitions with up to $J = 35$, the band origin and rotational and distortion constants were determined.[111,147] The spectroscopically derived harmonic stretching force constant for the central bond ($k_s = 80$ N/m) confirms that N_4^+ is indeed a relatively strongly bound complex.

The experimental rotational constants and band origin are in excellent agreement with the latest theoretical study, in which a six-dimensional potential-energy function was generated and used in full-dimensional variational calculations to determine the $J = 0$, 1 rovibrational states of the ion.[278] Terminal and central N−N bond lengths are predicted to be 1.110 and 2.005 Å, respectively. The full-dimensional calculations should be useful in guiding future gas-phase spectroscopic searches for combination bands that involve the lower frequency bending and stretching vibrations.

3. Ar_3^+

The ground-state rotational constants of the $^{40}Ar_3^+$ and $^{36}Ar_3^+$ ions were obtained by rotational depletion coherence spectroscopy (RDCS, section II) in a triple-quadrupole mass spectrometer (QMS).[119] Ar_3^+ ions were produced by bombarding solid argon with 8 keV Ar atoms and mass selected in a first QMS. Subsequently, they were irradiated in a second QMS (acting as an ion guide) by linearly polarized pump and probe laser pulses ($\lambda = 532$ nm) with a pulse width of 20 ps. At time t_0, the pump pulse excites a strong parallel transition of Ar_3^+ ($^2\Sigma_g^+ \leftarrow {}^2\Sigma_u^+$).[329,330] Ions with transition moments parallel to the pump laser polarization (Z axis) absorb and undergo fast dissociation leading to a depletion of parent ions with parallel alignment. Remaining are parent ions with perpendicular orientation (XY plane). The ions of this coherently aligned ensemble continue to rotate in random directions with a thermal distribution of rotational periods, thereby destroying the alignment produced at t_0. However, the alignment perpendicular to the Z axis recovers at certain time periods due to the quantization of molecular rotation and the coherent preparation at t_0. These recurrences are probed by the second laser pulse, which is polarized along the Y axis and fired at $t = \Delta t + t_0$. The photofragment ions are filtered by a third QMS and monitored as a function of the delay time, Δt. The observed recurrence times are related to the rotational constant of the ions. Every alternate rotational level is missing, consistent with centrosymmetric structures of $^{40}Ar_3^+$ and $^{36}Ar_3^+$ ($D_{\infty h}$). The experimental Ar−Ar bond length of 2.65 $\pm$ 0.3 Å is in good agreement with theoretical values.[330,331]

IV. Anion Complexes

Rotationally resolved spectra have been obtained for a handful of anion complexes using similar techniques to the ones employed for cation complexes (direct diode laser absorption in a discharge cell and IRPD spectroscopy of complexes formed in a supersonic expansion). While photoelectron spectroscopy (including ZEKE spectroscopy) has been employed to characterize a diverse range of anion complexes (including O^--Ar_n,[83] H^--NH_3,[332] Cl^--Ar,[333] I^--Xe,[334] I^--CH_3I,[335] Cl^--CH_3CN,[336] Br^--CH_3CN,[336] I^--CH_3CN,[336] I^--CO_2 [337]), spectra have not yet been obtained with rotational resolution. The formation and characteristics of delicate dipole-bound anion complexes in which the excess electron is weakly

attached to the complex by virtue of electrostatic interactions have also been subject to extensive studies.[46,338,339] More comprehensive discussions of anion complexes and clusters can be found in refs 20, 45, 340, and 341 and in the article by Schermann in this issue.

A. Proton-Bound Complexes

1. FHF^- and $ClHCl^-$

Diode laser absorption spectra have been recorded for the strongly bound FHF^-,[22] FDF^-,[154] and $ClHCl^-$ [155] bihalide anions formed in a cooled hollow cathode discharge cell. These ions have structures such that the intermediate proton is shared between two equivalent halide anions to form a linear complex and are analogous to symmetric proton-bound cations such as $ArHAr^+$ or $N_2HN_2^+$ (section III.A.1). For FHF^-, the three fundamental frequencies have been determined through measurement of the ν_1, ν_2, and $\nu_1 + \nu_3 - \nu_1$ bands in the 1300 cm^{-1} region and the $\nu_1 + \nu_3$ band at 1848 cm^{-1}. For $ClHCl^-$, the ν_3 band was observed at 723 cm^{-1}. The strength of the intermolecular hydrogen bonds ($D_0 \sim 16\,000$ cm^{-1} for $F^-{-}HF$),[342] short bond lengths ($r_e(F{-}F) = 2.28$ Å, $r_e(Cl{-}Cl) = 3.15$ Å), and large stretching force constants ($k_s = 400$ N/m for FHF^- and 109 N/m for $ClHCl^-$) are evidence for a high degree of covalent binding. The stability of the bihalide ions is further emphasized by the fact that ionic salts such as KHF_2 and $NaHF_2$ have been observed and characterized using neutron diffraction.[343]

The trends noted earlier for the proton-bound cations (section III.A) are carried to an extreme in the symmetrical bihalide ions. The frequency of the proton vibration undergoes a massive drop from 3959 cm^{-1} in HF to 1331 cm^{-1} in FHF^- and ends up being close to the ν_2 bending vibrational frequency (1286 cm^{-1}). Interestingly, stretching vibrational excitation of the intermediate proton in FHF^- and $ClHCl^-$ slightly lengthens and weakens the intermolecular bond. This behavior contrasts with that observed in asymmetric proton-bound cation and anion complexes, where excitation of the shared proton results in a more effective interaction with the lower PA ligand, causing a contraction and strengthening of the intermolecular bond. The larger bihalide anions ($BrHBr^-$, IHI^-) have not yet been observed in gas-phase studies, although their vibrational absorptions have been characterized in matrix isolation studies.[344] It is found that the frequencies of all three vibrational modes, along with the dissociation energy, decrease going down the periodic table.[342,345]

2. $Br^-{-}C_2H_2$

Few rotationally resolved spectra have been obtained for asymmetric proton-bound anions. One example is the linear hydrogen-bonded $Br^-{-}C_2H_2$ complex for which the ν_3 band (asymmetric C−H stretch) was recorded using IRPD spectroscopy.[118] The rotational structure has been analyzed to provide quantitative information on the intermolecular bond lengths in the ground and ν_3 states. Assuming an undistorted C_2H_2 monomer, the vibrationally averaged distances between the intermediate proton and Br^- in the ground and ν_3 states are 2.45 and 2.41 Å, respectively. The 0.04 Å bond contraction accompanying stretching excitation of the shared proton is similar in magnitude to the one observed for comparable cation complexes (section III.A). Interestingly, the rotational structure has an onset at $J' = 28$, indicating that lower J' levels lie below the dissociation threshold, a situation that is analogous to the one observed for $N_2H^+{-}Ar$ (section III.A.1, Figure 6). From the sum of the vibrational and rotational energies for the lowest dissociating level, the dissociation energy of $Br^-{-}C_2H_2$ was estimated as $D_0 = 3020 \pm 3$ cm^{-1}. Currently, this is perhaps the most accurately determined binding energy for an anion complex. On the basis of vibrationally resolved IRPD spectra, it was concluded that the $Cl^-{-}C_2H_2$ and $I^-{-}C_2H_2$ complexes also have linear proton-bound structures.[346,347]

3. $I^-{-}CH_3$

Spectra of the $I^-{-}CH_3$ and $I^-{-}CH_3Ar$ complexes in the C−H stretch region have been obtained using IRPD spectroscopy in a time-of-flight mass spectrometer.[117] The $I^-{-}CH_3$ system is relatively weakly bound: an upper limit of 900 cm^{-1} for the dissociation energy was deduced from the photoelectron spectrum. At least two band systems are observed in the IRPD spectrum, one of which is a perpendicular band that displays resolved $\Delta K = \pm 1$ Q branches. On the basis of the Q branch spacings and the shifts in the C−H stretch bands relative to those of CH_3, the complex was deduced to have a proton-bound $I^-{-}HCH_2$ structure, in accordance with ab initio calculations.[117] Curiously, the Q branch spacing is similar in the $I^-{-}CH_3$ and $I^-{-}CH_3Ar$ spectra, suggesting either that the Ar atom lies on the symmetry axis (an $Ar{-}I^-{-}CH_3$ structure) or that it is very loosely attached and the $I^-{-}CH_3$ unit undergoes free internal rotation. It is also interesting to note that $I^-{-}CH_3Ar$ photodissociates to yield primarily $I^-{-}Ar$ fragments, even though Ar is expected to bind less strongly than CH_3 to I^-. This nonstatistical fragmentation may arise from poor coupling between the excited C−H stretch modes and the $I^-{-}Ar$ bond, as might be expected for a linear $Ar{-}I^-{-}CH_3$ structure where the Ar and CH_3 units are bound to opposite sides of the heavy I^- core.

4. $X^-{-}H_2O$ (X = Cl, Br, I)

A number of IRPD studies have been conducted on the hydrated halide anions (e.g., $Cl^-{-}H_2O$,[158,348] $Br^-{-}H_2O$,[349] $I^-{-}H_2O$[115,350,351]). Spectra of the halide anion−water complexes are important for their role in understanding aqueous solvation of the halide anions. Ab initio calculations demonstrate that the dimers prefer planar C_s structures, in which one of the water protons is bonded to the halide ion with the other dangling free.[158,350,352−354] The nature of the $X^-{-}H_2O$ bond progressively changes as the halide ion becomes larger. High-pressure mass spectrometry studies show that the strength of the $X^-{-}H_2O$ bond diminishes with the size of the halide ion ($-\Delta H°$ = 23.3, 13.1, 12.6, 10.2 kcal/mol for X = F, Cl, Br,

I).[355] This weakening of the hydrogen bond is accompanied by a progressive deviation of the equilibrium X−H−O angle (θ) away from linearity (θ = 177°, 169°, 165°, 149° for X = F, Cl, Br, I)[349,353,354] and a reduction in the barrier for exchange of the bonded and nonbonded protons (7.7, 1.3, 0.2 kcal/mol for X = F, Cl, I).[350,353,354] As for the proton-bound cation complexes discussed in section III.A, formation of the hydrogen bond leads to partial delocalization of the shared proton. This is reflected by an increase in the hydrogen-bonded O−H bond length and a decrease in its vibrational frequency. Both of these effects become progressively less pronounced with increasing halide size (R_{O-H} = 1.055, 0.992, 0.987 Å for X = F, Cl, Br).[349,353,354]

In the case of Cl^--H_2O[158] and Br^--H_2O,[348,349] the IRPD spectra are broadened as the dissociation energy exceeds the photon energy, so that the spectra reflect the absorption contributions of hot complexes. Sharper IRPD spectra have been obtained by coating the complexes with Ar atoms that dissociate more readily following single IR photon absorption.[348,351,356] The vibrationally resolved spectra provide important qualitative information on dimer structures. Bands corresponding to free and bound proton stretches are observed, consistent with asymmetric solvation structures in which a single proton is attached to the halide (as predicted by the calculations). The I^-H_2O spectrum also features bands associated with bound and free O−H stretches, again providing evidence for an asymmetric C_s solvation structure.[115,350] The bands are somewhat sharper than the ones of Cl^-H_2O and Br^-H_2O, as the photon energy is sufficient to fragment cold complexes. Curiously, the bound O−H stretch band consists of a quartet (spacing ~28 cm^{-1}) that collapses to a doublet when a spy (Ar or N_2) is attached.[115] The band's substructure has been postulated as being due to tunneling through the C_{2v} transition state and/or the presence of complexes containing *ortho* and *para* H_2O.[115,350] Conclusions from the vibrationally resolved studies are supported by spectra of I^-−HDO, where K substructure is observed in the free O−H stretch band (in complexes in which the deuteron is hydrogen bonded).[115] The band has the form expected for a mainly perpendicular transition of a complex where the D atom is hydrogen bonded to the I^-. Analysis of the spectrum indicates that the rotational temperature is ~15 K and that the A constant is slightly smaller than the one expected from the ab initio geometry (15 cm^{-1} compared to 16.3 cm^{-1}).

B. S_N2 Complexes

1. Cl^-–CH_3Br

A mid-IRPD spectrum of the Cl^-CH_3Br complex has been recorded with resolution of K structure in the perpendicular ν_4 band (degenerate C−H stretch mode), by monitoring the production of Br^- photofragments (Figure 20).[116] The spacing of the K structure (10 cm^{-1}) is close to twice the *A* rotational constant of CH_3Br, consistent with a linear disposition of the heavy atoms. The Cl^-CH_3Br complex is the entrance channel complex for the exothermic Cl^- + $CH_3Br \rightarrow ClCH_3 + Br^-$ S_N2 exchange reaction. Such reactions have been postulated to occur over a double-minimum potential with a central barrier (Figure 21).[292,357−359] The spectroscopic studies provide strong evidence for the existence of a double-minimum potential. If the complexes are manufactured from a source of Cl^- and CH_3Br to form reactant-like Cl^-CH_3Br complexes, a structured spectrum is observed resulting from photoactivated complexes with sufficient energy to cross the central barrier and proceed on to become products. On the other hand, the spectrum of product-like Br^-−CH_3Cl complexes (formed from Br^- and CH_3Cl) is essentially structureless and results from photodissociation of hot complexes, as 3 μm photons do not provide cold complexes with sufficient energy to exit the well. The spectrum shown in Figure 20 is analogous to the one of the $Ar-CH_3^+-Ar$ complex (which is isoelectronic with the $ClCH_3Cl^-$ S_N2 complex) where both K and J structure were resolved (section III.B.1.b, Figure 18).

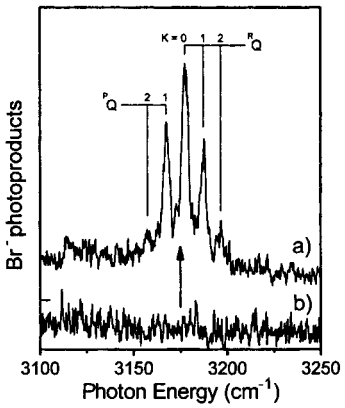

Figure 20. IRPD spectra of (a) the Cl^-CH_3Br complex and (b) Br^-CH_3Cl obtained by detection of Br^- reaction products (Reprinted with permission from ref 116. Copyright 1999 American Chemcial Society). The arrow shows the orgin of the Cl^-CH_3Br complex located in the IRPD spectrum of $Cl^-CH_3Br-Ar_3$. Labels indicate the lower *K* assignment of the structure to Q branches of a perpendicular transition.

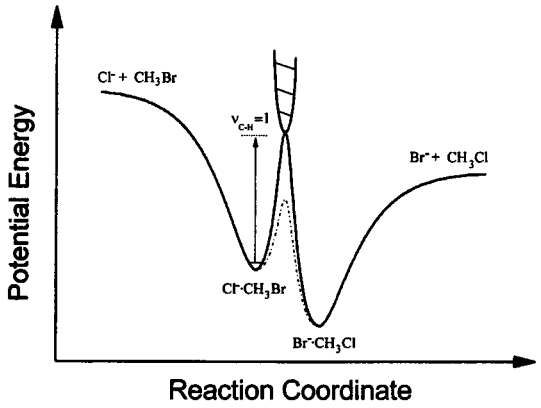

Figure 21. Schematic potential energy curve for the Cl^- + $CH_3Br \rightarrow ClCH_3 + Br^-$ exchange reaction (Reprinted with permission from ref 116. Copyright 1999 American Chemical Society). The ab initio value for the reaction barrier[367,368] is shown by the solid line, while the value extracted from thermal decomposition[369] of Cl^-CH_3Br is shown in by the dotted line.

V. Outlook

The high-resolution spectroscopic study of ionic complexes has developed into an active field with explorations of molecular ionic complexes in the MW, mid-IR, and VIS/UV parts of the spectrum. While spectroscopic studies of ionic complexes have lagged corresponding work on neutral van der Waals molecules, it is likely that the situation will be readdressed. A particularly encouraging sign is that some complexes (e.g., OCH^+-Ar) have now been studied using several different techniques (IRPD, direct IR absorption, FTMW). Future developments will involve the continued application of proven techniques to uncharacterized cation and anion complexes. One direction is toward larger systems in order to follow the microsolvation process. Currently, the largest complexes for which rotationally resolved spectra have been obtained are $CH_3CNH^+-H_2$, $Ar-CH_3^+-Ar$, and $H_9O_4^+$. Existing rotationally resolved IRPD studies have often been limited to rather small complexes due to the bandwidth of the OPO light sources commonly employed ($\sim$0.02 cm^{-1}). By using color center or diode lasers, rotationally resolved IRPD spectra may be obtainable for much larger complexes, although homogeneous lifetime broadening could be a limiting factor. In this regard the recent application of direct absorption techniques in slit jet plasmas is encouraging. In addition, the scope of PD studies (in the IR, VIS, UV) can be extended. One possible approach involves a double-resonance strategy where the high resolution of MW spectroscopy is combined with the high sensitivity of PD to gather spectra of mass-selected ionic complexes. In addition, the application of ZEKE and high Rydberg spectroscopy to obtain rotationally resolved spectra of ionic complexes (with geometries similar to their neutral precursors) appears to be feasible.

A better understanding of PESs will result from complementary studies on complexes in different spectral regions. Currently there are relatively few MW studies of cooled ionic systems, although experience with H_3^+-Ar and OCH^+-Ar has demonstrated their feasibility. Molecular constants derived from IRPD studies should provide effective guides for MW investigations. Future studies will undoubtedly refine our understanding of the interaction potential by directly probing intermolecular vibrational bands in the far IR spectral region (100−500 cm^{-1}). For many interesting complexes (e.g., H_5^+, $N_2H_7^+$, F^--H_2O, Na^+-H_2O), IRPD strategies are ineffective in providing rotationally resolved spectra, either because the dissociation thresholds lie above optically accessible states or because of homogeneous lifetime broadening. For such systems, direct absorption approaches (FTMW, direct IR absorption, cavity ring down) appear to be more appropriate.

Developments in ion sources can also be expected to extend the range of complexes and the quality of spectra. This is the realm of the tinkerer! With a few exceptions, the existing ion sources create the ionic complexes by either electron impact, electrical discharge, or laser ablation in a supersonic expansion. Another promising means for formation of charged complexes is by electrospray, an approach that has been used recently to generate transition-metal-containing complexes for spectroscopic interrogation.[360,361]

Parallel to further advances in high-resolution spectroscopy of ionic complexes, significant progress is expected in the next few years in the development of high-quality ab initio PESs. In contrast to most neutral complexes, for ionic dimers the deformation of the monomer units upon complexation is significant and cannot be neglected in deriving PESs with experimental accuracy. Consequently, the calculation of full-dimensional PESs at high levels of theory are required, and such calculations with subsequent solution of the rovibrational problem are presently feasible for ionic dimers with a few degrees of freedom (e.g., N_2CO^+,[362] O_2^+-He,[363] N_4^+,[278] H_2^+-He[210,215]). It is hoped that advances in theoretical chemistry and computer resources make such calculations possible for larger systems.

VI. Acknowledgments

The studies in Basel have been financed by the Swiss National Science Foundation (No. 20-36153.92, 20-41768.94, 20-49104.96, 20-055285.98). E.J.B. thanks the Australian Research Council and the University of Melbourne for financial support.

VII. Abbreviations

CRIES	cross-correlation ionization energy spectroscopy
DMA	distributed multipole analysis
ESR	electron spin resonance
FTMW	Fourier transform microwave
IR	infrared
IRPD	infrared photodissociation
LIF	laser-induced fluorescence
MATI	mass-analyzed threshold ionization
MCA	methyl cation affinity
MW	microwave
MS	mass spectrometer
OPO	optical parametric oscillator
PA	proton affinity
PD	photodissociation
PES	potential energy surface, photoelectron spectroscopy
PIE	photoionization efficiency
PFI	pulsed field ionization
QMS	quadrupole mass spectrometer
RDCS	rotational depletion coherence spectroscopy
REMPI	resonance-enhanced multiphoton ionization
Rg	rare gas
RKR	Rydberg−Klein−Rees
VIS	visible
UV	ultraviolet
ZEKE	zero kinetic energy photoelectron spectroscopy

VIII. References

(1) Levy, D. *Adv. Chem. Phys.* **1981**, *47*, 323.
(2) Legon, A. C.; Millen, D. J. *Chem. Rev.* **1986**, *86*, 635.
(3) Miller, R. E. *J. Phys. Chem.* **1986**, *90*, 3301.
(4) Nesbitt, D. J. *Chem. Rev.* **1988**, *88*, 843.
(5) Bernstein, E. R. *Atomic and Molecular Clusters*; Elsevier: Oxford, 1990.
(6) Cohen, R. C.; Saykally, R. J. *J. Phys. Chem.* **1992**, *96*, 1024.
(7) Heaven, M. C. *Annu. Rev. Phys. Chem.* **1992**, *42*, 283.
(8) Saykally, R. J.; Blake, G. A. *Science* **1993**, *259*, 1570.
(9) Nesbitt, D. J. *Annu. Rev. Phys. Chem.* **1994**, *45*, 367.
(10) Leopold, K. R.; Fraser, G. T.; Novick, S. E.; Klemperer, W. *Chem. Rev.* **1994**, *94*, 1807.

(11) Felker, P. M.; Maxton, P. M.; Schaeffer, M. W. *Chem. Rev.* **1994**, *94*, 1787.
(12) Buck, U. *J. Phys. Chem.* **1994**, *98*, 5190.
(13) Elrod, M. J.; Saykally, R. J. *Chem. Rev.* **1994**, *94*, 1975.
(14) Suhm, M. A.; Nesbitt, D. J. *Chem. Soc. Rev.* **1995**, *24*, 45.
(15) Kleinermanns, K.; Gerhards, M.; Schmitt, M. *Ber. Bunsen-Ges. Phys. Chem.* **1997**, *101*, 1785.
(16) Quack, M.; Suhm, M. A. *Adv. Mol. Vib. Col. Dyn.* **1998**, *3*, 205.
(17) Buck, U. *Adv. Mol. Vib. Col. Dyn.* **1998**, *3*, 127.
(18) Zwier, T. S. *Adv. Mol. Vib. Col. Dyn.* **1998**, *3*, 249.
(19) Novick, S. Bibliography of Rotational Spectra of Weakly Bound Complexes. Electronic updates are available on the web at http://www.wesleyan.edu/chem/faculty/novick/vdw.html, 2000.
(20) Castleman, A. W.; Keesee, R. G. *Chem. Rev.* **1986**, *86*, 589.
(21) Bogey, M.; Bolvin, H.; Demuynck, C.; Destombes, J. L. *Phys. Rev. Lett.* **1987**, *58*, 988.
(22) Kawaguchi, K.; Hirota, E. *J. Chem. Phys.* **1987**, *87*, 6838.
(23) Yeh, C. S.; Pilgrim, J. S.; Willey, K. F.; Robbins, D. L.; Duncan, M. A. *Int. Rev. Phys. Chem.* **1994**, *13*, 231.
(24) Ray, U.; Jarrold, M. F. In *Advances in metal and semiconductor clusters*; Duncan, M. A., Ed.; JAI: Greenwich, 1993; Vol. 1.
(25) Lessen, D. E.; Asher, R. L.; Brucat, P. J. In *Advances in metal and semiconductor clusters*; Duncan, M. A., Ed.; JAI: Greenwich, 1993; Vol. 1.
(26) Duncan, M. A. *Annu. Rev. Phys. Chem.* **1997**, *48*, 69.
(27) Lisy, J. M. *Int. Rev. Phys. Chem.* **1997**, *16*, 267.
(28) Kleiber, P. D.; Chen, J. *Int. Rev. Phys. Chem.* **1998**, *17*, 1.
(29) Lisy, J. M. In *Cluster Ions*; Ng, C.-Y., Baer, T., Powis, I., Eds.; Wiley: New York, 1993.
(30) Farrar, J. M. In *Cluster Ions*; Ng, C.-Y., Baer, T., Powis, I., Eds.; Wiley: New York, 1993.
(31) Crofton, M. W.; Price, J. M.; Lee, Y. T. In *Clusters of Atoms and Molecules II*; Haberland, H., Ed.; Springer: Berlin, 1994; Vol. 56.
(32) Ebata, T.; Fujii, A.; Mikami, N. *Int. Rev. Phys. Chem.* **1998**, *17*, 331.
(33) Maier, J. P. *Ion and cluster ion spectroscopy and structure*; Elsevier: Amsterdam, 1989.
(34) Bieske, E. J.; Maier, J. P. *Chem. Rev.* **1993**, *93*, 2603.
(35) Bieske, E. J. *J. Chem. Soc., Faraday Trans.* **1995**, *91*, 1.
(36) Müller-Dethlefs, K.; Dopfer, O.; Wright, T. G. *Chem. Rev.* **1994**, *94*, 1845.
(37) Neusser, H. J.; Krause, H. *Chem. Rev.* **1994**, *94*, 1845.
(38) Zhang, X.; Knee, J. L. *Faraday Discuss.* **1994**, *97*, 299.
(39) Schlag, E. W. *ZEKE Spectroscopy*; Cambridge University Press: Cambridge, 1998.
(40) Hillier, I. H. In *Molecular Interactions*; Ratajczah, H., Orville-Thomas, W. J., Eds.; Wiley: New York, 1981; Vol. 2.
(41) Rao, C. N. R.; Pradeep, T. *Chem. Soc. Rev.* **1991**, *20*, 477.
(42) Tomoda, S.; Kimura, K. In *Photoionization and Photodissociation of Small Molecules and Clusters*; Ng, C. Y., Ed.; World Scientific: Singapore, 1992.
(43) Castleman, A. W. In *Clusters of Atoms and Molecules II*; Haberland, H., Ed.; Springer: Berlin, 1994; Vol. 56.
(44) Castleman, A. W.; Wei, S. *Annu. Rev. Phys. Chem.* **1994**, *45*, 685.
(45) Castleman, A. W.; Bowen, K. H. *J. Phys. Chem.* **1996**, *100*, 12911.
(46) Hendricks, J. H.; De Clercq, H. L.; Lyapustina, S. A.; Fancher, C. A.; Lippa, T. P.; Collins, J. M.; Arnold, S. T.; Lee, G. H.; Bowen, K. H. *Front. Sci. Ser.* **1996**, *16*, 321.
(47) Brutschy, B. *Chem. Rev.* **1992**, *92*, 1567.
(48) Lifshitz, C. In *Cluster Ions*; Ng, C.-Y., Baer, T., Powis, I., Eds.; Wiley: New York, 1993.
(49) Garvey, J. F.; Herron, W. J.; Vaidyanathan, G. *Chem. Rev.* **1994**, *94*, 1999.
(50) Bowen, R. D. *Acc. Chem. Res.* **1991**, *24*, 364.
(51) Garvey, J. F.; Peifer, W. R.; Coolbaugh, M. T. *Acc. Chem. Res.* **1991**, *24*, 48.
(52) Armentrout, P. B.; Baer, T. *J. Phys. Chem.* **1996**, *100*, 12866.
(53) Ferguson, E. E.; Arnold, F. *Acc. Chem. Res.* **1981**, *14*, 327.
(54) Smith, D. *Chem. Rev.* **1992**, *92*, 1473.
(55) Herbst, E.; Klemperer, W. *Astrophys. J.* **1973**, *185*, 505.
(56) Zundel, G. In *The Hydrogen Bond-Recent Developments in Theory and Experiments. II Structure and Spectroscopy*; Schuster, P., Zundel, G., Sandorfy, C., Eds.; North-Holland: Amsterdam, 1976.
(57) Pimentel, G. C.; McClellan, A. L. *The Hydrogen Bond*; Freeman: London, 1960.
(58) Vinograd, S. N.; Linnell, R. H. *Hydrogen Bonding*; Van Nostrand: New York, 1971.
(59) Marcus, Y. *Ion solvation*; Wiley: New York, 1985.
(60) Le Roy, R. J.; Carley, J. S. *Adv. Chem. Phys.* **1980**, *42*, 353.
(61) Hutson, J. M. In *Adv. Mol. Dyn. Col. Dyn.*; JAI Press Inc.: Greenwich, CT, 1991; Vol. 1.
(62) Hutson, J. M. *J. Chem. Phys.* **1992**, *96*, 6752.
(63) Nesbitt, D. J.; Naaman, R. *J. Chem. Phys.* **1989**, *91*, 3801.
(64) van der Avoird, A.; Wormer, P. E. S.; Moszynski, R. *Chem. Rev.* **1994**, *94*, 1931.
(65) van der Avoird, A.; Wormer, P. E. S.; Moszynski, R. In *Molecular Interactions*; Scheiner, S., Ed.; Wiley: New York, 1997.
(66) Randall, R. W.; Ibbotson, J. B.; Howard, B. J. *J. Chem. Phys.* **1994**, *100*, 7042.
(67) Hutson, J. M.; Thornley, A. E. *J. Chem. Phys.* **1994**, *100*, 2505.
(68) Bacic, Z.; Miller, R. E. *J. Phys. Chem.* **1996**, *100*, 12945.
(69) Hutson, J. M. *Annu. Rev. Phys. Chem.* **1990**, *41*, 123.
(70) Elrod, M. J.; Saykally, R. J.; Cooper, A. R.; Hutson, J. M. *Mol. Phys.* **1994**, *81*, 579.
(71) Hutson, J. M. *J. Phys. Chem.* **1992**, *96*, 4237.
(72) Fellers, R. S.; Leforestier, C.; Braly, L. B.; Brown, M. G.; Saykally, R. J. *Science* **1999**, *284*, 945.
(73) Kebarle, P. In *Ion−Molecule Reactions*; Franklin, J. L., Ed.; Plenum: New York, 1972.
(74) Castleman, A. W.; Märk, T. D. *Adv. At. Mol. Phys.* **1985**, *20*, 65.
(75) Keesee, R. G.; Castleman, A. W., Jr. *J. Phys. Chem. Ref. Data* **1986**, *15*, 1011.
(76) Shi, Z.; Ford, J. V.; Wei, S.; Castleman, A. W. *J. Chem. Phys.* **1994**, *99*, 8009.
(77) Wei, S.; Tzeng, W. B.; Castleman, A. W. *J. Chem. Phys.* **1990**, *92*, 332.
(78) Wei, S.; Castleman, A. W. *Int. J. Mass Spectrom. Ion Processes* **1994**, *131*, 233.
(79) Klots, C. E. *J. Chem. Phys.* **1985**, *83*, 5834.
(80) Klots, C. E. *Z. Phys. D* **1987**, *5*, 83.
(81) Klots, C. E. *Z. Phys. D* **1991**, *21*, 335.
(82) Yourshaw, I.; Zhao, Y.; Neumark, D. M. *J. Chem. Phys.* **1996**, *105*, 351.
(83) Arnold, S. T.; Hendricks, J. H.; Bowen, K. H. *J. Chem. Phys.* **1995**, *102*, 39.
(84) Okumura, M.; Yeh, L. I.; Lee, Y. T. *J. Chem. Phys.* **1985**, *83*, 3705.
(85) Okumura, M.; Yeh, L. I.; Myers, J. D.; Lee, Y. T. *J. Chem. Phys.* **1986**, *85*, 2328.
(86) Yeh, L. I.; Okumura, M.; Myers, J. D.; Price, J. M.; Lee, Y. T. *J. Chem. Phys.* **1989**, *91*, 7319.
(87) Price, J. M.; Crofton, M. W.; Lee, Y. T. *J. Chem. Phys.* **1989**, *91*, 2749.
(88) Okumura, M.; Yeh, L. I.; Myers, J. D.; Lee, Y. T. *J. Phys. Chem.* **1990**, *94*, 3416.
(89) Yeh, L. I.; Lee, Y. T.; Hougen, J. T. *J. Mol. Spectrosc.* **1994**, *164*, 473.
(90) Bieske, E. J.; Soliva, A. S.; Welker, M.; Maier, J. P. *J. Chem. Phys.* **1990**, *93*, 4477.
(91) Willey, K. F.; Yeh, C. S.; Robbins, D. L.; Pilgrim, J. S.; Duncan, M. A. *J. Chem. Phys.* **1992**, *97*, 8886.
(92) Ding, L. N.; Young, M. A.; Kleiber, P. D.; Stwalley, W. C.; Lyyra, A. M. *J. Phys. Chem.* **1993**, *97*, 2181.
(93) Scurlock, C. T.; Pullins, S. H.; Reddic, J. E.; Duncan, M. A. *J. Chem. Phys.* **1996**, *104*, 4591.
(94) Nizkorodov, S. A.; Maier, J. P.; Bieske, E. J. *J. Chem. Phys.* **1995**, *103*, 1297.
(95) Nizkorodov, S. A.; Dopfer, O.; Meuwly, M.; Maier, J. P.; Bieske, E. J. *J. Chem. Phys.* **1996**, *105*, 1770.
(96) Nizkorodov, S. A.; Dopfer, O.; Ruchti, T.; Meuwly, M.; Maier, J. P.; Bieske, E. J. *J. Phys. Chem.* **1995**, *99*, 17118.
(97) Bieske, E. J.; Nizkorodov, S. A.; Bennett, F. R.; Maier, J. P. *J. Chem. Phys.* **1995**, *102*, 5152.
(98) Meuwly, M.; Nizkorodov, S. A.; Maier, J. P.; Bieske, E. J. *J. Chem. Phys.* **1996**, *104*, 3876.
(99) Nizkorodov, S. A.; Meuwly, M.; Maier, J. P.; Dopfer, O.; Bieske, E. J. *J. Chem. Phys.* **1998**, *108*, 8964.
(100) Nizkorodov, S. A.; Spinelli, Y.; Bieske, E. J.; Maier, J. P.; Dopfer, O. *Chem. Phys. Lett.* **1997**, *265*, 303.
(101) Olkhov, R. V.; Nizkorodov, S. A.; Dopfer, O. *Chem. Phys.* **1998**, *239*, 393.
(102) Roth, D.; Nizkorodov, S. A.; Maier, J. P.; Dopfer, O. *J. Chem. Phys.* **1998**, *109*, 3841.
(103) Dopfer, O.; Roth, D.; Maier, J. P. *Chem. Phys. Lett.* **1999**, *310*, 201.
(104) Dopfer, O.; Nizkorodov, S. A.; Olkhov, R. V.; Maier, J. P.; Harada, K. *J. Phys. Chem. A* **1998**, *102*, 10017.
(105) Olkhov, R. V.; Nizkorodov, S. A.; Dopfer, O. *J. Chem. Phys.* **1998**, *108*, 10046.
(106) Dopfer, O.; Olkhov, R. V.; Maier, J. P. *J. Chem. Phys.* **2000**, *112*, 2176.
(107) Ohshima, Y.; Endo, Y. *Chem. Phys. Lett.* **1996**, *256*, 635.
(108) Ohshima, Y.; Sumiyoshi, Y.; Endo, Y. *J. Chem. Phys.* **1997**, *106*, 2977.
(109) Carrington, A.; Gammie, D. I.; Shaw, A. M.; Taylor, S. M.; Hutson, J. M. *Chem. Phys. Lett.* **1996**, *260*, 395.
(110) Carrington, A. *Science* **1996**, *274*, 1327.
(111) Ruchti, T.; Speck, T.; Connelly, J. P.; Bieske, E. J.; Linnartz, H.; Maier, J. P. *J. Chem. Phys.* **1996**, *105*, 2591.
(112) Linnartz, H.; Speck, T.; Maier, J. P. *Chem. Phys. Lett.* **1998**, *288*, 504.
(113) Speck, T.; Linnartz, H.; Maier, J. P. *J. Chem. Phys.* **1997**, *107*, 8706.

(114) Ruchti, T.; Rohrbacher, A.; Speck, T.; Connelly, J. P.; Bieske, E. J.; Maier, J. P. *Chem. Phys.* **1996**, *209*, 169.
(115) Bailey, C. G.; Kim, J.; Dessent, C. E. H.; Johnson, M. A. *Chem. Phys. Lett.* **1997**, *269*, 122.
(116) Ayotte, P.; Kim, J.; Kelley, J. A.; Nielsen, S. B.; Johnson, M. A. *J. Am. Chem. Soc.* **1999**, *121*, 6950.
(117) Nielsen, S. B.; Ayotte, P.; Kelley, J. A.; Weddle, G. H.; Johnson, M. A. *J. Chem. Phys.* **1999**, *111*, 10464.
(118) Wild, D. A.; Milley, P. J.; Loh, Z.; Wolynec, P.; Weiser, P. S.; Bieske, E. J. *J. Chem. Phys.* **2000**, *113*, 1075.
(119) Magnera, T. F.; Sammond, D. M.; Michl, J. *Chem. Phys. Lett.* **1993**, *211*, 378.
(120) Rodham, D. A.; Blake, G. A. *Chem. Phys. Lett.* **1997**, *264*, 522.
(121) Wang, K.; Rodham, D. A.; McKoy, V.; Blake, G. A. *J. Chem. Phys.* **1998**, *108*, 4817.
(122) Nizkorodov, S. A.; Maier, J. P.; Bieske, E. J. *J. Chem. Phys.* **1995**, *102*, 5570.
(123) Dopfer, O.; Olkhov, R. V.; Maier, J. P. *J. Phys. Chem. A* **1999**, *103*, 2982.
(124) Botschwina, P.; Oswald, R.; Linnartz, H.; Verdes, D. *J. Chem. Phys.* **2000**, *113*, 2736.
(125) Verdes, D.; Linnartz, H.; Maier, J. P.; Botschwina, P.; Oswald, R.; Rosmus, P.; Knowles, P. J. *J. Chem. Phys.* **1999**, *111*, 8400.
(126) Nizkorodov, S. A. Ph.D. Thesis, University of Basel, 1997.
(127) Olkhov, R. V.; Nizkorodov, S. A.; Dopfer, O. *J. Chem. Phys.* **1997**, *107*, 8229.
(128) Dopfer, O.; Roth, D.; Olkhov, R. V.; Maier, J. P. *J. Chem. Phys.* **1999**, *110*, 11911.
(129) Carrington, A.; Shaw, A. M.; Taylor, S. M. *J. Chem. Soc., Faraday Trans.* **1995**, *91*, 3725.
(130) Bogey, M.; Bolvin, H.; Demuynck, C.; Destombes, J. L.; Van Eijck, B. P. *J. Chem. Phys.* **1988**, *88*, 4120.
(131) Demuynck, C. *J. Mol. Spectrosc.* **1994**, *168*, 215.
(132) Bailleux, S.; Bogey, M.; Bolvin, H.; Civis, S.; Cordonnier, M.; Krupnov, A. F.; Tretyakov, M. Y.; Walters, A.; Coudert, L. H. *J. Mol. Spectrosc.* **1998**, *190*, 130.
(133) Dopfer, O.; Nizkorodov, S. A.; Meuwly, M.; Bieske, E. J.; Maier, J. P. *Chem. Phys. Lett.* **1996**, *260*, 545.
(134) Bieske, E. J.; Nizkorodov, S. A.; Dopfer, O.; Maier, J. P.; Stickland, R. J.; Cotterell, B. J.; Howard, B. J. *Chem. Phys. Lett.* **1996**, *250*, 266.
(135) Dopfer, O.; Nizkorodov, S. A.; Meuwly, M.; Bieske, E. J.; Maier, J. P. *Int. J. Mass Spectrom. Ion Processes* **1997**, *167−168*, 637.
(136) Lakin, N. M.; Dopfer, O.; Howard, B. J.; Maier, J. P. *Mol. Phys.* **2000**, *98*, 81.
(137) Price, J. M.; Crofton, M. W.; Lee, Y. T. *J. Phys. Chem.* **1991**, *95*, 2182.
(138) Boo, D. W.; Lee, Y. T. *J. Chem. Phys.* **1995**, *103*, 520.
(139) Olkhov, R. V.; Nizkorodov, S. A.; Dopfer, O. *J. Chem. Phys.* **1999**, *110*, 9527.
(140) White, E. T.; Tang, J.; Oka, T. *Science* **1999**, *284*, 135.
(141) Boo, D. W.; Lee, Y. T. *J. Chem. Phys.* **1995**, *103*, 514.
(142) Siglow, K.; Neuhauser, R.; Neusser, H. J. *Chem. Phys. Lett.* **1998**, *293*, 19.
(143) Siglow, K.; Neuhauser, R.; Neusser, H. J. *J. Chem. Phys.* **1999**, *110*, 5589.
(144) Neuhauser, R.; Siglow, K.; Neusser, H. J. *Phys. Rev. Lett.* **1998**, *80*, 5089.
(145) Bieske, E. J.; Soliva, A. S.; Friedmann, A.; Maier, J. P. *J. Chem. Phys.* **1992**, *96*, 4035.
(146) Bieske, E. J.; Soliva, A. S.; Friedmann, A.; Maier, J. P. *J. Chem. Phys.* **1992**, *96*, 28.
(147) Speck, T.; Ruchti, T.; Linnartz, H.; Maier, J. P. *J. Mol. Spectrosc.* **1997**, *185*, 425.
(148) Agreiter, J. K.; Knight, A. M.; Duncan, M. A. *Chem. Phys. Lett.* **1999**, *313*, 162.
(149) Pullins, S. H.; Reddic, J. E.; France, M. R.; Duncan, M. A. *J. Chem. Phys.* **1998**, *108*, 2725.
(150) France, M. R.; Pullins, S. H.; Duncan, M. A. *J. Chem. Phys.* **1998**, *108*, 7049.
(151) France, M. R.; Pullins, S. H.; Duncan, M. A. *J. Chem. Phys.* **1998**, *109*, 8842.
(152) Chen, J.; Cheng, Y. C.; Kleiber, P. D. *J. Chem. Phys.* **1997**, *106*, 3884.
(153) Bellert, D.; Buthelezi, T.; Brucat, P. J. *Chem. Phys. Lett.* **1998**, *290*, 317.
(154) Kawaguchi, K.; Hirota, E. *J. Mol. Struct.* **1995**, *352/353*, 389.
(155) Kawaguchi, K. *J. Chem. Phys.* **1988**, *88*, 4186.
(156) Mikami, N.; Sasaki, T.; Sato, S. *Chem. Phys. Lett.* **1991**, *180*, 431.
(157) Johnson, M. A.; Lineberger, W. C. In *Techniques for the Study of Ion−Molecule Reactions*; Farrar, J. M., Saunders, W. H. J., Eds.; Wiley:, 1988; Vol. XX.
(158) Choi, J.-H.; Kuwata, K. T.; Cao, Y.-B.; Okumura, M. *J. Phys. Chem.* **1998**, *102*, 503.
(159) Müller-Dethlefs, K.; Schlag, E. W. *Annu. Rev. Phys. Chem.* **1991**, *42*, 109.
(160) Zhu, L.; Johnson, P. M. *J. Chem. Phys.* **1991**, *94*, 5769.
(161) Müller-Dethlefs, K.; Schlag, E. W. S. *Angew. Chem., Int. Ed. Engl.* **1998**, *37*, 1346.
(162) A regularly updated list of papers describing ZEKE and MATI studies is available on the Internet (http://eos.phys.chemie.tu-muenchen.de/zeke/zekelist.html).
(163) Neuhauser, R. G.; Siglow, K.; Neusser, H. J. *J. Chem. Phys.* **1997**, *106*, 896.
(164) Kennedy, R.; Miller, T. A. *J. Chem. Phys.* **1986**, *85*, 2326.
(165) Dimauro, L. F.; Heaven, M.; Miller, T. M. *Chem. Phys. Lett.* **1984**, *104*, 526.
(166) Letokhov, V. S. *Laser Photoionization Spectroscopy*; Academic: New York, 1987.
(167) Fuke, K.; Yoshiuchi, H.; Kaya, K.; Achiba, Y.; Sato, K.; Kimura, K. *Chem. Phys. Lett.* **1984**, *108*, 179.
(168) Gonohe, N.; Abe, H.; Mikami, N.; Ito, M. *J. Phys. Chem.* **1985**, *89*, 3642.
(169) Dopfer, O.; Melf, M.; Müller-Dethlefs, K. *Chem. Phys.* **1996**, *207*, 437.
(170) Fujii, A.; Sawamura, T.; Tanabe, S.; Ebata, T.; Mikami, N. *Chem. Phys. Lett.* **1994**, *225*, 104.
(171) Pino, T.; Boudin, N.; Brechignac, P. *J. Chem. Phys.* **1999**, *111*, 7337.
(172) Bieske, E. J.; McKay, R. I.; Bennett, F. R.; Knight, A. E. W. *J. Chem. Phys.* **1990**, *92*, 4620.
(173) Scheiner, S. *Molecular Interactions*; Wiley: New York, 1997.
(174) Lias, S. G.; Barmess, J. E.; Liebman, J. F.; Holmes, J. L.; Levin, R. D.; Mallard, W. G. *J. Phys. Chem. Ref. Data Suppl.* **1988**, *17*, 1.
(175) Bieske, E. J.; Nizkorodov, S. A.; Bennett, F.; Maier, J. P. *Int. J. Mass Spectrom. Ion Processes* **1995**, *150*, 167.
(176) Kabbadj, Y.; Huet, T. R.; Rehfuss, B. D.; Gabrys, C. M.; Oka, T. *J. Mol. Spectrosc.* **1994**, *163*, 180.
(177) Fraser, G. T.; Pine, A. S. *J. Chem. Phys.* **1989**, *91*, 3319.
(178) Peterson, K. I.; Klemperer, W. *J. Chem. Phys.* **1984**, *81*, 3842.
(179) Leopold, K. R.; Fraser, G. T.; Lin, F. J.; Nelson, D. D.; Klemperer, W. *J. Chem. Phys.* **1984**, *81*, 4922.
(180) Meuwly, M.; Bemish, R. J. *J. Chem. Phys.* **1997**, *106*, 8672.
(181) Meuwly, M. *J. Chem. Phys.* **1999**, *111*, 2633.
(182) Hiraoka, K.; Salujia, P. P. S.; Kebarla, P. *Can. J. Chem.* **1979**, *57*, 2159.
(183) Kolbuszewski, M. *Chem. Phys. Lett.* **1995**, *244*, 39.
(184) Gudeman, C. S.; Begemann, M. H.; Pfaff, J.; Saykally, R. J. *Phys. Rev. Lett.* **1983**, *50*, 727.
(185) Nowek, A.; Leszczynski, J. *J. Chem. Phys.* **1996**, *105*, 6388.
(186) Meuwly, M. *J. Chem. Phys.* **1999**, *110*, 4347.
(187) Fehsenfeld, F. C.; Dunkin, D. B.; Ferguson, E. E. *Astrophys. J.* **1974**, *188*, 43.
(188) Hiraoka, K.; Kebarle, P. *J. Chem. Phys.* **1975**, *63*, 1688.
(189) Dixon, D. A.; Komornicki, A.; Kraemer, W. P. *J. Chem. Phys.* **1984**, *81*, 3603.
(190) Ma, L. M.; Smith, B. J.; Pople, J. A.; Radom, L. *J. Am. Chem. Soc.* **1991**, *113*, 7903.
(191) Talbi, D.; Pauzat, F. *Astron. Astrophys.* **1987**, *181*, 394.
(192) Talbi, D.; Pauzat, F. *Astron. Astrophys.* **1990**, *229*, 253.
(193) Maluendes, S. A.; McLean, A. D.; Herbst, E. *Astrophys. J.* **1992**, *397*, 477.
(194) Radom, L. *Int. J. Mass Spectrom. Ion Processes* **1992**, *118/119*, 339.
(195) Amano, T.; Warner, H. E. *Astrophys. J.* **1989**, *342*, L99.
(196) Fox, A.; Wlodek, S.; Hopkinson, A. C.; Lien, M. H.; Sylvain, M.; Rodriquez, C.; Bohme, D. K. *J. Phys. Chem.* **1989**, *93*, 1549.
(197) Yamaguchi, Y.; Schaefer, H. F., III. *J. Chem. Phys.* **1995**, *102*, 5327.
(198) Warner, H. E.; Fox, A.; Amano, T.; Bohme, D. K. *J. Chem. Phys.* **1989**, *91*, 5310.
(199) Olkhov, R. V.; Dopfer, O. *Chem. Phys. Lett.* **1999**, *314*, 215.
(200) Qian, H.-B.; Low, S. J.; Seccombe, D.; Howard, B. J. *J. Chem. Phys.* **1997**, *107*, 7651.
(201) Hughes, J. M.; von Nagy-Felsobuki, E. I. *J. Phys. Chem.* **1997**, *A101*, 3995.
(202) Meuwly, M.; Maier, J. P.; Rosmus, P. *J. Chem. Phys.* **1998**, *109*, 3850.
(203) Chalasinski, G.; Klos, J.; Cybulski, M.; Szczesniak, M. *Collect. Czech. Chem. Commun.* **1998**, *63*, 1473.
(204) Schinke, R. *Photodissociation Dynamics*; Cambridge Univeristy Press: Cambridge, 1993.
(205) Ewing, G. E. *J. Phys. Chem.* **1987**, *91*, 4662.
(206) McLaughlin, D. R.; Thompson, D. L. *J. Chem. Phys.* **1979**, *70*, 2748.
(207) Joseph, T.; Sathyamurthy, N. *J. Chem. Phys.* **1987**, *86*, 704.
(208) Miller, S.; Tennyson, J. *J. Chem. Phys.* **1987**, *87*, 6648.
(209) Miller, S.; Tennyson, J.; Follmeg, B.; Rosmus, P.; Werner, H. *J. Chem. Phys.* **1988**, *89*, 2178.
(210) Spirko, V.; Kraemer, W. P. *J. Mol. Spectrosc.* **1995**, *172*, 265.
(211) Falcetta, M. F.; Siska, P. E. *Mol. Phys.* **1996**, *88*, 647.
(212) Jurek, M.; Spirko, V.; Kraemer, W. P. *J. Mol. Spectrosc.* **1997**, *182*, 364.
(213) Kraemer, W. P.; Jurek, M.; Spirko, V. *J. Mol. Spectrosc.* **1998**, *187*, 206.

(214) Falcetta, M. F.; Siska, P. E. *Mol. Phys.* **1999**, *97*, 117.
(215) Meuwly, M.; Hutson, J. M. *J. Chem. Phys.* **1999**, *110*, 2418.
(216) Hunter, G.; Pritchard, H. O. *J. Chem. Phys.* **1967**, *46*, 2153.
(217) Dinelli, B. M.; Sueur, C. R. L.; Tennyson, J.; Amos, R. D. *Chem. Phys. Lett.* **1995**, *232*, 295.
(218) Kabbadj, Y.; Huet, T. R.; Uy, D.; Oka, T. *J. Mol. Spectrosc.* **1996**, *175*, 277.
(219) Simandiras, E. D.; Gaw, J. F.; Handy, N. C. *Chem. Phys. Lett.* **1987**, *141*, 166.
(220) Hobza, P.; Zahradnik, R.; Smith, D. *Chem. Phys. Lett.* **1993**, *208*, 497.
(221) Beyer, M.; Savchenko, E. V.; Niedner-Schatteburg, G.; Bondybey, V. E. *J. Chem. Phys.* **1999**, *110*, 11950.
(222) Hiraoka, K.; Mori, T. *J. Chem. Phys.* **1989**, *91*, 4821.
(223) Escribano, R.; Bunker, P. R. *Chem. Phys. Lett.* **1988**, *143*, 439.
(224) Schwarz, H. A. *J. Chem. Phys.* **1977**, *67*, 5525.
(225) Jiang, J. C.; Wang, Y. S.; Chang, H. C.; Lin, S. H.; Lee, Y. T.; Niedner-Schatteburg, G.; Chang, H. C. *J. Am. Chem. Soc.* **2000**, *122*, 1398.
(226) Meot-Ner, M.; Field, F. H. *J. Am. Chem. Soc.* **1977**, *99*, 998.
(227) Lau, Y. K.; Ikuta, S.; Kebarle, P. *J. Am. Chem. Soc.* **1982**, *104*, 1462.
(228) Magnera, T. F.; David, D. E.; J., M. *Chem. Phys. Lett.* **1991**, *182*, 363.
(229) Yamabe, S.; Minato, T.; Hirao, K. *J. Chem. Phys.* **1984**, *80*, 1576.
(230) Frisch, M. J.; Del Bene, J. E.; Binkley, J. S.; Schaefer, H. F., III. *J. Chem. Phys.* **1986**, *84*, 2279.
(231) Lee, E. P. F.; Dyke, Michl, J. *Mol. Phys.* **1991**, *73*, 375.
(232) Xie, Y. M.; Remington, R. B.; Schaefer, H. F., III. *J. Chem. Phys.* **1994**, *101*, 4878.
(233) Ojamäe, L.; Shavitt, I.; Singer, S. J. *Int. J. Quantum Chem.: Quantum Chem. Symp.* **1995**, *29*, 657.
(234) Klein, S.; Kochanski, E.; Strich, A.; Sadlej, A. J. *J. Phys. Chem. A* **1997**, *101*, 4799.
(235) Valeev, E. F.; Schaefer, H. F., III. *J. Chem. Phys.* **1998**, *108*, 7197.
(236) Wales, D. J. *J. Chem. Phys.* **1999**, *110*, 10403.
(237) Wales, D. J. *J. Chem. Phys.* **1999**, *111*, 8429.
(238) Tuckerman, M. E.; Marx, D.; Klein, M. L.; Parrinello, M. *Science* **1997**, *275*, 817.
(239) Wei, D.; Salahub, D. R. *J. Chem. Phys.* **1997**, *106*, 6086.
(240) Cheng, H. P.; Krause, J. L. *J. Chem. Phys.* **1997**, *107*, 8461.
(241) Cheng, H. P. *J. Phys. Chem. A* **1998**, *102*, 6201.
(242) Marx, D.; Tuckerman, M. E.; Hutter, J.; Parrinello, M. *Nature* **1999**, *397*, 601.
(243) Yang, X.; Castleman, A. W. *J. Am. Chem. Soc.* **1989**, *111*, 6845.
(244) Conway, B. E.; Bockris, J. O. M.; Linton, H. *J. Chem. Phys.* **1956**, *24*, 834.
(245) Agmon, N. *Chem. Phys. Lett.* **1995**, *244*, 456.
(246) Stearn, A. E.; Eyring, H. *J. Chem. Phys.* **1937**, *5*, 113.
(247) Bernal, J. D.; Fowler, R. H. *J. Chem. Phys.* **1933**, *8*, 515.
(248) Eigen, M. *Angew. Chem., Int. Ed. Engl.* **1964**, *3*, 1.
(249) Meuwly, M.; Nizkorodov, S. A.; Bieske, E. J.; Maier, J. P.; Dopfer, O. *Chem. Phys. Lett.* **1997**, *270*, 252.
(250) Lakin, N. M.; Dopfer, O.; Meuwly, M.; Howard, B. J.; Maier, J. P. *Mol. Phys.* **2000**, *98*, 63.
(251) Crofton, M. W.; Oka, T. *J. Chem. Phys.* **1983**, *79*, 3157.
(252) Crofton, M. W.; Oka, T. *J. Chem. Phys.* **1987**, *86*, 5983.
(253) Dopfer, O. et al. Unpublished rotationally resolved IR spectra and ab initio calculations of NH_3^+-Rg and H_3O^+-Rg dimers.
(254) Dopfer, O. et al. Unpublished results.
(255) Read, J. P.; Buckingham, A. D. *Chem. Phys. Lett.* **1997**, *270*, 245.
(256) Randall, R. W.; Ibbotson, J. B.; Howard, B. J. *J. Chem. Phys.* **1994**, *100*, 7051.
(257) Brooks, M. D.; Hughes, D. J.; Howard, B. J. *J. Chem. Phys.* **1996**, *104*, 4391.
(258) Brooks, M. D.; Hughes, D. J.; Howard, B. J. *J. Chem. Phys.* **1996**, *107*, 2738.
(259) Miller, R. E.; Heijman, G. A.; Wormer, P. E. S.; van der Avoird, A.; Moszynski, R. *J. Chem. Phys.* **1999**, *110*, 5651.
(260) Pak, I.; Roth, D. A.; Hepp, M.; Winnewisser, G.; Scouteris, D.; Howard, B. J.; Yamada, K. M. T. *Z. Naturforsch.* **1998**, *53a*, 7725.
(261) Heijman, G. A.; Wormer, P. E. S.; van der Avoird, A.; Miller, R. E.; Moszynski, R. *J. Chem. Phys* **1999**, *110*, 5639.
(262) Urban, R. D.; Jörissen, L. G.; Matsumoto, Y.; Takami, M. *J. Chem. Phys.* **1995**, *103*, 3960.
(263) Gao, D.; Liangjin, C.; Zhiru, L.; Fu-Ming, T.; Yuh-Kang, P. *Chem. Phys. Lett.* **1997**, *277*, 483.
(264) Heijman, G. A.; Korona, T.; Moszynski, R.; Wormer, P. E. S.; van der Avoird, A. *J. Chem. Phys* **1997**, *107*, 902.
(265) Schwarz, H. A. *J. Chem. Phys.* **1980**, *72*, 284.
(266) Ichihashi, M.; Yamabe, J.; Murai, K.; Nonose, S.; Hirao, K.; Kondow, T. *J. Phys. Chem.* **1996**, *100*, 10050.
(267) Hirao, K.; Fujikawa, T.; Konishi, H.; Yamabe, S. *Chem. Phys. Lett.* **1984**, *104*, 184.
(268) Lifshitz, C.; Louage, F. *J. Phys. Chem.* **1989**, *93*, 5633.
(269) Castleman, A. W., Jr.; Tzeng, W. B.; Wei, S.; Morgan, S. *Faraday Trans.* **1990**, *86*, 2417.
(270) Tang, I. N.; Castleman, A. W., Jr. *J. Chem. Phys.* **1975**, *62*, 4576.
(271) Pudzianowski, A. T. *J. Chem. Phys.* **1995**, *102*, 8029.
(272) Platts, J. A.; Laidig, K. E. *J. Phys. Chem.* **1995**, *99*, 6487.
(273) Hiraoka, K.; Kudaka, I.; Yamabe, S. *Chem. Phys. Lett.* **1991**, *184*, 271.
(274) Boo, D. W.; Liu, Z. F.; Suits, A. G.; Tse, J. S.; Lee, Y. T. *Science* **1995**, *269*, 57.
(275) Kim, S.-J.; Schreiner, P. R.; von Rague Schleyer, P.; Schaefer, H. F., III. *J. Phys. Chem.* **1993**, *97*, 12232.
(276) Yamaguchi, Y.; Gaw, J. F.; Schaefer, H. F., III. *J. Chem. Phys.* **1983**, *78*, 4074.
(277) Hirao, K.; Yamabe, S. *Chem. Phys. Lett.* **1981**, *79*, 279.
(278) Leonard, C.; Rosmus, P.; Carter, S.; Handy, N. C. *J. Phys. Chem. A* **1999**, *103*, 1846.
(279) Meot-Ner, M. *J. Am. Chem. Soc.* **1984**, *106*, 1257.
(280) Dopfer, O.; Olkhov, R. V.; Roth, D.; Maier, J. P. *Chem. Phys. Lett.* **1998**, *296*, 585.
(281) Nizkorodov, S. A.; Roth, D.; Olkhov, R. V.; Maier, J. P.; Dopfer, O. *Chem. Phys. Lett.* **1997**, *278*, 26.
(282) Le Roy, R. J.; Davies, M. R.; Lam, M. E. *J. Phys. Chem.* **1991**, *95*, 2167.
(283) Miller, R. E. *Acc. Chem. Res.* **1990**, *23*, 10.
(284) Hiraoka, K.; Kudaka, I.; Yamabe, S. *Chem. Phys. Lett.* **1991**, *178*, 103.
(285) Crofton, M. W.; Kreiner, W. A.; Jagod, M.-F.; Rehfuss, B. D.; Oka, T. *J. Chem. Phys.* **1985**, *83*, 3702.
(286) Crofton, M. W.; Jagod, M.-F.; Rehfuss, B. D.; Kreiner, W. A.; Oka, T. *J. Chem. Phys.* **1988**, *88*, 666.
(287) Cunje, A.; Rodriquez, C. F.; Bohme, D. K.; Hopkinson, A. C. *J. Phys. Chem. A* **1998**, *102*, 478.
(288) Brupbacher, T.; Makarewicz, J.; Bauder, A. *J. Chem. Phys.* **1994**, *101*, 9736.
(289) Fiacco, D. L.; Kirchner, B.; Burns, W. A.; Leopold, K. R. *J. Mol. Spectrosc.* **1998**, *191*, 389.
(290) Drucker, S.; Cooksy, A. L.; Klemperer, W. *J. Chem. Phys.* **1993**, *98*, 5158.
(291) Hovey, J. K.; McMahon, T. B. *J. Phys. Chem.* **1987**, *91*, 4560.
(292) Olmstead, W. N.; Brauman, J. I. *J. Am. Chem. Soc.* **1977**, *99*, 4219.
(293) Hase, W. L.; Wang, H.; Peslherbe, G. H. In *Advances in Gas-Phase Ion Chemistry*; Adams, N. G., Babcock, L. M., Eds.; JAI: Greenwich, 1998; Vol. 3.
(294) Müller, H.; Kutzelnigg, W.; Noga, J.; Klopper, W. *J. Chem. Phys.* **1997**, *106*, 1863.
(295) Schreiner, P. R.; Kim, S.-J.; Schaefer, H. F., III.; von Rague Schleyer, P. *J. Chem. Phys.* **1993**, *99*, 3716.
(296) Marx, D.; Parrinello, M. *Nature* **1995**, *375*, 216.
(297) Scuseria, G. E. *Nature* **1993**, *366*, 512.
(298) Marx, D.; Parrinello, M. *Science* **1999**, *284*, 59.
(299) Bunker, P. R. *J. Mol. Spectrosc.* **1996**, *176*, 297.
(300) Kolbuszewski, M.; Bunker, P. R. *J. Chem. Phys.* **1996**, *105*, 3649.
(301) East, A. L. L.; Kolbuszewski, M.; Bunker, P. R. *J. Phys. Chem. A* **1997**, *101*, 6746.
(302) Boo, D. W.; Lee, Y. T. *Chem. Phys. Lett.* **1993**, *211*, 358.
(303) Boo, D. W.; Lee, Y. T. *Int. J. Mass. Spectrom. Ion Processes* **1996**, *159*, 209.
(304) Smith, D. M.; Martineau, P. M.; Davies, P. B. *J. Chem. Phys.* **1992**, *96*, 1741.
(305) Hu, C. H.; Shen, M.; Schaefer, H. F., III. *Chem. Phys. Lett.* **1992**, *190*, 543.
(306) Hiraoka, K.; Katsuragawa, J.; Minamitsu, A. *Chem. Phys. Lett.* **1997**, *267*, 580.
(307) Gong, X. G.; Guenzburger, D.; Saitovitch, E. B. *Chem. Phys. Lett.* **1997**, *275*, 392.
(308) Liu, R.; Zhou, X. *J. Phys. Chem.* **1993**, *97*, 9555.
(309) Hu, C.-H.; Schreiner, P. R.; von Rague Schleyer, P.; Schaefer, H. F., III. *J. Phys. Chem.* **1994**, *98*, 5040.
(310) Cao, Y. B.; Choi, J. H.; Haas, B. M.; Johnson, M. S.; Okumura, M. *J. Phys. Chem.* **1993**, *97*, 5215.
(311) Kriegel, M.; Richter, R.; Lindinger, W.; Barbier, L.; Ferguson, E. E. *J. Chem. Phys.* **1987**, *88*, 213.
(312) Zenevich, V. A.; Freysinger, W.; Pogrebnya, S. K.; Lindinger, W.; Dmitrieva, I. K.; Porshnev, P. I.; Tosi, P. *J. Chem. Phys.* **1991**, *94*, 7972.
(313) Katayama, D. H.; Miller, T. A.; Bondybey, V. E. *J. Chem. Phys.* **1980**, *72*, 5469.
(314) Katayama, D. H.; Dentamaro, A. V. *J. Chem. Phys.* **1989**, *91*, 4571.
(315) Tellinghuisen, J. B.; Winkler, C. A.; Freeman, C. G.; McEwan, M. J.; Phillips, L. F. *J. Chem. Soc., Faraday Trans.* **1972**, *68*, 835.
(316) Duncan, M. A.; Bierbaum, V. M.; Ellison, G. B.; Leone, S. R. *J. Chem. Phys.* **1983**, *79*, 5448.
(317) Dressler, R.; Meyer, H.; Leone, S. R. *J. Chem. Phys.* **1987**, *87*, 6029.
(318) Bieske, E. J.; Nizkorodov, S. A.; Friedmann, A.; Maier, J. P. *Int. J. Mass. Spectrom. Ion. Processes* **1994**, *135*, 19.

(319) Berning, A.; Werner, H. *J. Chem. Phys.* **1994**, *100*, 1953.
(320) Buchachenko, A. A.; Baisogolov, A. Y.; Stepanov, N. F. *Chem. Phys. Lett.* **1994**, *220*, 93.
(321) Payzant, J. D.; Kebarle, P. *J. Chem. Phys.* **1970**, *53*, 4723.
(322) Hiraoka, K.; Nakajima, G. *J. Chem. Phys.* **1988**, *88*, 7709.
(323) Schulz, R. H.; Armetrout, P. B. *Int. J. Mass Spectrom. Ion Processes* **1991**, *107*, 29.
(324) Schulz, R. H.; Armentrout, P. B. *J. Chem. Phys.* **1992**, *96*, 1046.
(325) Sohlberg, K.; Futrell, J.; Szalewicz, K. *J. Chem. Phys.* **1991**, *94*, 6500.
(326) Kemister, G.; Peel, J. B. *Org. Mass. Spectrosc.* **1993**, *28*, 311.
(327) Knight, L. B.; Johannessen, K. D.; Cobranchi, C. B.; Earl, E. A.; Feller, D.; Davidson, E. R. *J. Chem. Phys.* **1987**, *87*, 885.
(328) Thompson, W. E.; Jacox, M. E. *J. Chem. Phys.* **1990**, *93*, 3856.
(329) Levinger, N. E.; Ray, D.; Murray, K. K.; Mullin, A. S.; Schulz, C. P.; Lineberger, W. C. *J. Chem. Phys.* **1988**, *89*, 71.
(330) Ikegami, T.; Kondow, T.; Iwata, S. *J. Chem. Phys.* **1993**, *98*, 3038.
(331) Gadea, F. X.; Savrda, J.; Paidarova, I. *Chem. Phys. Lett.* **1994**, *223*, 369.
(332) Snodgrass, J. T.; Coe, J. V.; Freidhoff, C. B.; McHugh, K. M.; Bowen, K. H. *Faraday Discuss. Chem. Soc.* **1988**, *86*, 241.
(333) Lenzer, T.; Yourshaw, I.; Furlanetto, M. R.; Reiser, G.; Neumark, D. M. *J. Chem. Phys.* **1999**, *110*, 9578.
(334) Lenzer, T.; Furlanetto, M. R.; Asmis, K. R.; Neumark, D. M. *J. Chem. Phys.* **1998**, *109*, 10754.
(335) Arnold, C. C.; Neumark, D. M.; Cyr, D. M.; Johnson, M. A. *J. Phys. Chem.* **1995**, *99*, 1633.
(336) Markovich, G.; Perera, L.; Berkowitz, M. L.; Cheshnovsky, O. *J. Chem. Phys.* **1996**, *105*, 2675.
(337) Arnold, D. W.; Bradforth, S. E.; Kim, E. H.; Neumark, D. M. *J. Chem. Phys.* **1995**, *102*, 39.
(338) Desfrancois, C.; Baillon, B.; Schermann, J. P.; Arnold, S. T.; Hendricks, J. H.; Bowen, K. H. *Phys. Rev. Lett.* **1994**, *72*, 48.
(339) Desfrancois, C.; Abdoul-Carime, H.; Khelifa, N.; Schermann, J. P. *J. Chim. Phys. Phys.-Chim. Biol.* **1995**, *92*, 409.
(340) Haberland, H.; Bowen, K. H. *Springer Ser. Chem. Phys.* **1994**, *56*, 134.
(341) Dessent, C. E. H.; Johnson, M. A.; Becker, I.; Cheshnovsky, O. *Adv. Chem. Phys.* **1999**, *106*, 265.
(342) Wenthold, P. G.; Squires, R. R. *J. Phys. Chem.* **1995**, *99*, 2002.
(343) Evans, J. C.; Lo, G. Y.-S. *J. Phys. Chem.* **1966**, *70*, 11.
(344) Lugez, C. L.; Jacox, M. E.; Thompson, W. E. *J. Chem. Phys.* **1996**, *105*, 3901.
(345) Caldwell, G.; Kebarle, P. *Can. J. Chem.* **1985**, *63*, 1399.
(346) Weiser, P. S.; Wild, D. A.; Bieske, E. J. *Chem. Phys. Lett.* **1998**, *299*, 303.
(347) Weiser, P. S.; Wild, D. A.; Bieske, E. J. *J. Chem. Phys.* **1999**, *110*, 9443.
(348) Ayotte, P.; Weddle, G. H.; Kim, J.; Johnson, M. A. *J. Am. Chem. Soc.* **1998**, *120*, 12361.
(349) Ayotte, P.; Bailey, C. G.; Weddle, G. H.; Johnson, M. A. *J. Phys. Chem.* **1998**, *102*, 3067.
(350) Johnson, M.; Kuwata, K.; Wong, C.; Okumura, M. *Chem. Phys. Lett.* **1996**, *260*, 551.
(351) Ayotte, P.; Weddle, G. H.; Kim, J.; Kelley, J.; Johnson, M. A. *J. Phys. Chem.* **1999**, *103*, 443.
(352) Combariza, J. E.; Kestner, N. R.; Jortner, J. *J. Chem. Phys.* **1994**, *100*, 2851.
(353) Xantheas, S. S.; Dunning, T. *J. Phys. Chem.* **1994**, *98*, 13489.
(354) Xantheas, S. S. *J. Phys. Chem.* **1996**, *100*, 9703.
(355) Arshadi, M.; Yamdagni, R.; Kebarle, P. *J. Phys. Chem.* **1970**, *74*, 1475.
(356) Ayotte, P.; Weddle, G. H.; Kim, J.; Johnson, M. A. *Chem. Phys.* **1998**, *239*, 485.
(357) Shaik, S. S.; Schlegel, H. B.; Wolfe, S. *Theoretical Aspects of Physical Chemsitry*; John Wiley and Sons Inc.: New York, 1992.
(358) Vigginiano, A. A.; Morris, R. A.; Paschkewitz, J. S.; Paulson, J. F. *J. Am. Chem. Soc.* **1992**, *114*, 10477.
(359) Graul, S. T.; Bowers, M. T. *J. Am. Chem. Soc.* **1994**, *116*, 3875.
(360) Spence, T. G.; Burns, T. D.; Posey, L. A. *J. Phys. Chem. A* **1997**, *101*, 139.
(361) Spence, T. G.; Trotter, B. T.; Burns, T. D.; Posey, L. A. *J. Phys. Chem. A* **1998**, *102*, 6101.
(362) Hochlaf, M.; Leonard, C.; Ferguson, E. E.; Rosmus, P.; Reinsch, E. A.; Carter, S.; Handy, N. C. *J. Chem. Phys.* **1999**, *111*, 4948.
(363) Schmelz, T.; Reinsch, E.-A.; Rosmus, P. *J. Phys. Chem.* **1995**, *99*, 15580.
(364) Dopfer, O. Habilitation Thesis, University of Basel, 1999.
(365) Hunter, E. P. L.; Lias, S. G. *J. Phys. Chem. Ref. Data* **1998**, *27*, 413.
(366) Israelachvili, J. *Intermolecular and Surface Forces*; Academic Press: London, 1992.
(367) Li, C.; Ross, P.; Szulejko, J. E.; McMahon, T. B. *J. Am. Chem. Soc.* **1996**, *118*, 9360.
(368) Hu, W. P.; Truhlar, D. G. *J. Am. Chem. Soc.* **1995**, *117*, 10726.
(369) Seely, J. V.; Morris, R. A.; Viggiano, A. A.; Wang, H.; Hase, W. L. *J. Am. Chem. Soc.* **1997**, *119*, 577.

CR990064W